NiS/CuO Heterostructure Integrated on Nickel Foam as Cathode Electrode for Electrocatalytic Water Splitting

Tamirat Bekele Delesa

A Thesis Submitted to the Department of Materials Science and Engineering

School of Mechanical, Chemical, and Materials Engineering

Presented in Partial Fulfillment of the Requirement for the Degree of Master's in Materials Science and Engineering

Office of Graduate Studies

Adama Science and Technology University

June, 2023

Adama, Ethiopia

NiS/CuO Heterostructure Integrated on Nickel Foam as Cathode Electrode for Electrocatalytic Water Splitting

Tamirat Bekele Delesa

Advisor: Dinsefa Mensur Andoshe (PhD, Asso. Prof.)

Co-Advisor: Osman Ahmed Zelekew (PhD, Asso. Prof.)

A Thesis Submitted to the Department of Materials Science and Engineering

School of Mechanical, Chemical, and Materials Engineering

Presented in Partial Fulfillment of the Requirement for the Degree of Master's in Materials Science and Engineering

Office of Graduate Studies

Adama Science and Technology University

June, 2023

Adama, Ethiopia

Declaration

I hereby declare that this Master Thesis entitled “NiS/CuO Heterostructure Integrated on Nickel Foam as Cathode Electrode for Electrocatalytic Water Splitting” is my original work. That is, this thesis has not been presented as part of any other university program to obtain an academic degree, diploma, or certificate. All the sources and materials used in this thesis have been appropriately acknowledged by citing them.

Tamirat Bekele Delesa	_____	26/06/2023
Name of student	Signature	Date

Recommendation of Advisor

I/we, the advisor(s) of this thesis, hereby certify that I/we have read the revised version of the thesis entitled "NiS/CuO Heterostructure Integrated on Nickel Foam as Cathode Electrode for Electrocatalytic Water Splitting" prepared under my/our guidance by Tamirat Bekele Delesa submitted in partial fulfillment of the requirements for the degree of Masters of Science in Materials Science and Engineering. Therefore, I/we recommend the submission of a revised version of the thesis to the department following the applicable procedures.

Dinsefa Mensur Andoshe (PhD)	_____	26/06/2023
Major Advisor/Supervisor	Signature	Date
Osman Ahmed Zelekew (PhD)	_____	26/06/2023
Co-advisor/Co-supervisor	Signature	Date

Approval

I/we, the advisors of the thesis entitled “NiS/CuO Heterostructure Integrated on Nickel Foam as Cathode Electrode for Electrocatalytic Water Splitting” and developed by Tamirat Bekele Delesa, hereby certify that the recommendation and suggestions made by the board of examiners are appropriately incorporated into the final version of the thesis.

Dinsefa Mensur Andoshe (PhD)	_____	26/06/2023
Major Advisor/Supervisor	Signature	Date
Osman Ahmed Zelekew (PhD)	_____	26/06/2023
Co-advisor/ Co-supervisor	Signature	Date

Approval of Board of Reviewers

We, the undersigned, members of the Board of Examiners of the thesis by Tamirat Bekele Delesa have read and evaluated the thesis "NiS/CuO Heterostructure Integrated on Nickel Foam as Cathode Electrode for Electrocatalytic Water Splitting" and the candidate was evaluated during an open defense session. This is, therefore, to certify that the thesis is accepted for partial fulfillment of the requirement of the degree of Master of Science in Materials Science and Engineering.

Fetene Fufa Bakare (PhD)	_____	26/06/2023
Chairperson	Signature	Date
Tadele Hunde Wondimu (PhD)	_____	26/06/2023
Internal Examiner	Signature	Date
Sintayehu Nibret Tiruneh (PhD)	_____	26/06/2023
External Examiner	Signature	Date

Finally, approval and acceptance of the thesis is contingent upon the submission of its final copy to the Office of Postgraduate Studies (OPGS) through the Department Graduate Council (DGC) and School Graduate Committee (SGC).

_____	_____	_____
Department Head	Signature	Date
_____	_____	_____
School Dean	Signature	Date
_____	_____	_____
Office of Postgraduate Studies, Dean	Signature	Date

ACKNOWLEDGEMENT

First and foremost, I would like to express my profound gratitude to the Almighty for granting me strength, wisdom, and perseverance throughout this research journey. It is through the grace of God that I have been able to overcome obstacles, find inspiration, and remain steadfast in my pursuit of knowledge. I would like to extend my deepest appreciation to my supervisor, Dr. Dinsefa Mensur Andoshe, for his unwavering commitment to academic excellence. His insightful feedback, constructive criticism, and dedication to mentorship have greatly shaped the outcome of this work. I am truly grateful for his guidance and mentorship throughout this thesis. I would like to express my deepest gratitude and appreciation to my co-Advisor, Dr. Osman Ahmed Zelekew, and Dr. Lemma Teshome Tufa and his esteemed team at Chungnam National University for their invaluable support throughout my thesis, including their contributions to the characterization process. I would also like to acknowledge the contributions of the faculty members, colleagues, and peers who have engaged in meaningful discussions, shared their knowledge, and offered support throughout this research journey. Their diverse perspectives and collaborative spirit have broadened my understanding and enriched the development of this thesis. My heartfelt thanks go to my family and friends for their unwavering support, love, and encouragement throughout this endeavor. Their belief in my abilities, patience during challenging times, and understanding of the sacrifices required for this project has been a constant source of motivation. I am deeply grateful for their presence in my life. Last, but certainly, not least, I am deeply indebted to the Department of Material Science and Engineering and Adama Science and Technology University for providing me with a full scholarship, necessary resources, facilities, and research opportunities.

Table of Contents

LIST OF TABLES

LIST OF FIGURES

LIST OF ACRONYMS

Cdl	Double-layer Capacitance
CE	Counter electrode
CV	Cyclic Voltammetry
DFT	Density Functional Theory
DI	Deionized
ECSA	Electrochemically Active Surface Area
EIS	Electrochemical Impedance Spectroscopy
eV	Electron Voltage
FTO	Fluorine doped Tin Oxide
HER	Hydrogen Evolution Reaction
LSV	Linear Sweep Voltammetry
n	Number of transferred electrons in the electrode reaction
NF	Nickel Foam Electrode
OER	Oxygen Evolution Reaction
pH	Potential of Hydrogen
RE	Reference electrode
SEM	Scanning Electron Microscope
SHE	Standard Hydrogen Electrode
WE	Working electrode
XRD	X-ray Diffraction
η	Overpotential
ΔG	Gibbs Free Energy Change

ABSTRACT

Developing clean and renewable energy resources has become a crucial global concern due to the combined challenges of energy scarcity and environmental pollution. The widespread production of hydrogen, which is regarded as the energy carrier of the future, still faces economic challenges. To address this, there is a need for low-cost synthetic designs to create electrocatalysts that can facilitate the hydrogen evolution reaction (HER). In this study, a simple and efficient electrochemical deposition method was used to directly fabricate a series of NiS/CuO heterostructures and its individual components copper oxide (CuO) and NiS sulfide (CuS) as low-cost catalysts for HER on a nickel foam (NF) substrate. SEM and XRD were utilized to examine the morphology, and structure of the prepared electrodes. The X-ray diffraction analysis confirmed the formation of the NiS/CuO heterostructure. In addition, electrochemical methods such as cyclic voltammetry (CV), linear sweep voltammetry (LSV), electrochemical impedance spectroscopy (EIS), and chronoamperometry were employed to modify the nickel foam and investigate the HER. This heterostructure promoted efficient charge transport and exhibited a synergistic electrocatalytic effect that facilitated the HER in acidic and alkaline medium. The optimized heterostructure obtained through 200s and 600s long two-step electrodepositions (CNS_{600}), shows HER activity at 10 $mAcm^{-2}$ with overpotential of 260 mV in acidic medium and 170 mV in alkaline medium. CNS_{600} demonstrates an impressive ability to generate hydrogen (H_2) continuously, maintaining its catalytic activity for a minimum of 8 hours in an acidic environment and 18 hours in a basic environment. The remarkable electrocatalytic performance of NiS/CuO/NF can be attributed to the synergistic interaction between NiS and CuO, the presence of a large active surface area, and the high electrical conductivity of the electrode. These desirable characteristics are achieved through the binder-free synthesis method utilized in its fabrication. Based on these advantages, including the rapid and straightforward electrode preparation, the proposed electrode is well-suited to serve as a non-noble metal cathode electrode in HER process.

Keywords: *Electrocatalysis, Heterostructures, NiS/CuO, Hydrogen evolution reaction, Electrochemical deposition*

CHAPTER ONE

1. Introduction

1.1 Background of the study

As the consumption of traditional fossil fuels continues to rise and environmental issues caused by greenhouse gas emissions become more prominent, there are concerns about the future viability of energy sources. The energy demand has been increasing steadily over the past century due to population growth and global development. It is expected that energy demand will continue to increase from 16 Terawatts (TW) in 2010 to 23 TW in 2030, and possibly even up to 30 TW in 2050. (Lewis & Nocera, 2006). Traditional energy sources like coal, oil, and natural gas made up 80% of worldwide energy consumption, whereas renewable sources such as solar photovoltaic, wind, biopower, and hydropower accounted for only 20%(Hassall & van den Belt, 2017). The depletion of fossil fuels is happening rapidly as we continue to depend heavily on them, causing harmful environmental impacts such as global warming. The increasing use of fossil fuels has brought about various challenges such as energy scarcity, air pollution, and global warming (De Luna et al., 2019; Dresselhaus & Thomas, 2001; Hou, Zhuang, & Feng, 2017; Zou & Zhang, 2015). This has led to a push for the development of sustainable and environmentally friendly alternative energy sources.

Developing eco-friendly and sustainable fuels is a critical objective in the scientific arena. Consequently, there have been numerous attempts to harness renewable energy sources such as solar, wind, and hydroelectric power (Seh et al., 2017). Out of the different forms of clean energy studied, hydrogen (H_2) is considered one of the most environmentally friendly options, and its high heating value makes it suitable for various applications. With a heating value of 141.9 MJ per kilogram, H_2 provides nearly three times more energy than regular gasoline, which only offers 47.5 MJ (Nikolaidis & Poullikkas, 2017). There is a consensus that hydrogen is the most appropriate and eco-friendly energy source to substitute non-renewable fossil fuels, mainly because of its exceptional energy conversion efficiency, higher specific energy density (120 vs. 44 MJ kg^{-1}) compared to gasoline, absence of carbon dioxide emissions, and compatibility with the environment (X. Li, Hao, Abudula, & Guan, 2016; W. Wang, Xu, Xu, Zhou, & Shao, 2020; Z. Zong et al., 2019). Currently, there are two predominant ways of producing H_2: steam methane reforming and water electrolysis (Sengeni Anantharaj et al., 2016). Apart from generating H_2, steam reforming also generates CO_2, which is harmful to the environment and reduces the

effectiveness of the cell. As a result, water electrolysis is a more practical means of providing H_2 on a large scale. Given that water is the only starting molecule and a byproduct in the hydrogen economy cycle, where the combustion of H_2 generates energy and regenerates water simultaneously, electrochemical water splitting, or water electrolysis, is seen as a clean, efficient, and sustainable alternative for substituting fossil (Gray, 2009).

The most recent developments in electrocatalytic HER using less expensive and abundant on-Earth nanoparticles are discussed, with a focus on low-cost and non-platinum electrocatalysts based on transition metals, metal alloys, core-shell structures, transition metal oxides, carbides, nitrides, phosphides, dichalcogenides, borides, and metal-free composite catalysts (J. Zhu, Hu, Zhao, Lee, & Wong, 2019). Transition Metal Oxides (TMOs) are widely used in electrocatalysis because of their cost-effective, stable, accessible, and environmentally benign characteristics (J. Zhu et al., 2019). However, the intrinsically low electrical conductivity, sluggish reaction kinetics, limited adsorption sites for H, and inappropriate H-binding energy of most TMOs are the barriers to attaining high electrocatalytic properties (Ghosh & Basu, 2018; Gong & Dai, 2015; Phuruangrat, Ham, Hong, Thongtem, & Lee, 2010). Various strategies have been proposed, such as decreasing the sizes of the structure, creating material to be porous structures, integrating TMOs with conductive carbon supports, introducing surface defects or O-vacancies, and doping other atoms (J. Chen et al., 2016; Haque et al., 2019; Luo et al., 2016; Shu, Kang, Jin, Yue, & Shen, 2017; M. Q. Yang, Wang, Wu, & Ho, 2018; T. Zheng et al., 2017).

Co and Ni-based electrodes have been extensively studied thus far among the transitional metal oxides, primarily due to their remarkable stability and superior electrocatalytic activity (L. Yu et al., 2017). Nevertheless, there have been studies exploring the potential of CuO nanoparticles as a bi-functional electrocatalyst due to their abundance, non-toxic nature, and improved redox properties. Notably, (Huan et al., 2017) recently proposed that an electrocatalyst based on copper oxide nano-dendrites exhibited a remarkably low overpotential in a 1 M NaOH solution, indicating high efficiency for water oxidation. As reported by (Tahira, Ibupoto, Willander, & Nur, 2019), Co_3O_4-CuO nanocomposites were synthesized using the dip-coating method demonstrating notable efficiency in the hydrogen evolution reaction. Although Co_3O_4 and CuO materials individually exhibited limited activity in the HER, the Co_3O_4-CuO nanocomposites achieved a remarkably low overpotential. The deficient catalytic performance of copper oxides is attributed to their poor electrical conductivity, necessitating higher overpotentials to attain substantial catalytic current densities (Sabir, Pervaiz, Khosa, & Sohail, 2023). To enhance the HER

activities of copper oxides, a strategy involving the combination of reduced graphene oxide, a porous network of metal-organic framework (MOF), and three-dimensional copper foam is employed (Ye & Wen, 2018). Therefore, combining an electrocatalyst that demonstrates activity in the HER with CuO represents a promising approach to achieving high-performance results.

Recently, metal oxide-metal sulfide composite electrocatalysts have gained attention as a promising alternative due to their unique properties and synergistic effects.(Shit, Bolar, Murmu, & Kuila, 2021) successfully synthesized MoS_2/Fe_2O_3 heterostructure electrocatalysts on NF using a straightforward electrochemical deposition approach. These hybrid electrocatalysts demonstrated remarkable HER activity, with a low overpotential of 80 mV at a current density of 10 mA/cm² and a Tafel slope of 46 mV/dec. (Khan et al., 2019) developed the NiO/NiS electrocatalyst with highly efficient, stable, cost-effective, and low overpotential oxygen evolution electrocatalyst in alkaline medium. In an investigation carried out by (T. Li et al., 2017), they successfully fabricated binder-free Co_3O_4/CoS_2 nanoneedle films that exhibited exceptional catalytic performance in the HER. The remarkable HER performance achieved can be attributed to the synergistic effect resulting from the excellent electrochemical integration, as well as the unique structure of the nanoneedle films, which provide a facile charge transfer pathway for HER. Additionally, the Co_3O_4/CoS_2 interfaces were found to possess abundant active sites, further contributing to the enhanced catalytic activity.

Building upon the aforementioned observations, this study focuses on the electrochemical deposition of NiS/CuO heterostructures onto NF using a two-step process. Extensive investigations were conducted to examine the impact of the incorporation of NiS on the physicochemical properties and electrocatalysis efficiency of the heterostructures. The results obtained from Tafel and Nyquist plot analyses provided valuable insights into the alterations in substrate adsorption-desorption, charge transfer efficiency, and kinetic aspects of the involved reactions due to the heterostructures. The successful integration of CuO with NiS exhibited a synergistic effect, significantly enhancing the electrocatalytic activity of the heterostructure

1.2 Statement of the problem

Electrocatalysis for hydrogen evolution is a critical field of research that aims to develop efficient and sustainable methods for the production of hydrogen gas (Anwar, Khan, Zhang, & Djire, 2021). However, several challenges and limitations persist in this area, hindering its widespread implementation and practical application. These challenges include high

overpotential requirements, low catalytic activity, limited stability, and reliance on costly and scarce noble metal catalysts (Y. Li et al., 2020). The high overpotential necessary for the hydrogen evolution reaction (HER) in electrocatalysis leads to increased energy consumption and reduced efficiency, thus constraining the feasibility of the process. Additionally, the low catalytic activity of current electrocatalysts necessitates the use of large amounts of catalyst material, further increasing costs and impeding scalability. Moreover, the limited stability of electrocatalysts under harsh reaction conditions affects their long-term performance, durability, and reliability.

Platinum group metal-based catalysts have long been acknowledged as the most efficient catalysts for hydrogen evolution reaction (HER)(C. Li & Baek, 2019). However, their widespread use in large-scale hydrogen production is hindered by their high cost and scarcity. To achieve a hydrogen-based economy, it is crucial to reduce the reliance on noble metals and instead utilize abundant and non-noble metal alternatives that exhibit exceptional catalytic performance and durability. Nonetheless, non-noble catalysts suffer from challenges such as high overpotential and low activity, which hinder efficient HER. In recent years, several electrocatalysts have been developed to enhance HER performance, and CuO has emerged as a promising alternative due to its cost-effectiveness and abundance(Sabir et al., 2023). Nevertheless, CuO exhibits poor conductivity and stability in harsh reaction conditions. To overcome this limitation, a composite electrocatalyst comprising CuO and NiS has been proposed as a potential solution. The incorporation of NiS into CuO is expected to improve the conductivity and stability of the resulting composite electrocatalyst, leading to enhanced HER performance.

1.3 General objective

The general objective of this study is NiS/CuO Heterostructure Integrated on NF as Cathode Electrode for Electrocatalytic Water Splitting

1.4 Specific objectives

The specific objectives of this study are:

- ✓ Synthesize and characterize the NiS/CuO heterostructure electrocatalyst.
- ✓ Investigate the electrocatalytic activity of the heterostructure electrocatalyst for HER.
- ✓ Compare the HER performance of the NiS/CuO heterostructure electrocatalyst with that of pure CuO, NiS

- ✓ Analyze the mechanism of the HER process on the NiS/CuO heterostructure electrocatalyst using electrochemical techniques.

1.5 Significance of the study

This study is highly significant for sustainable energy production as it focuses on developing efficient and sustainable methods for hydrogen gas production through electrochemical hydrogen evolution. By addressing current electrocatalyst limitations and proposing innovative solutions, this research contributes to the transition towards a clean and renewable energy future, diminishing dependence on fossil fuels and mitigating environmental consequences. Additionally, the study tackles economic challenges associated with large-scale hydrogen production by exploring alternative catalyst materials and design strategies, intending to reduce expenses and enhance scalability. The research also enhances our fundamental understanding of the hydrogen evolution reaction, leading to the development of improved catalyst materials, optimized electrode structures, and enhanced reaction conditions. These technological advancements have broader implications in electrochemistry and catalysis beyond hydrogen evolution, impacting various fields and applications.

1.6 Scope of the study

This research covers the investigation of HER performance of an electrocatalyst consisting of CuO and NiS, which was fabricated utilizing the electrochemical deposition technique. The study will involve the synthesis of the heterostructure electrocatalyst, its structural and morphological characterization, and its electrochemical evaluation using different techniques, including LSV, Tafel slope analysis for HER kinetics and mechanism determination, EIS for charge transfer kinetics analysis, and Chronoamperometry for stability testing. Additionally, the study will explore how synergistic effect affects the HER performance of the hybrid electrocatalyst.

CHAPTER TWO

2. Literature Review

2.1 Global energy status

Implementing sustainable energy sources is one of the biggest challenges facing the globe today. The rate at which the world's population is expanding is unsustainable for the available fuel sources. Additionally, the detrimental effects of using nonrenewable energy sources on the planet are increasing at an unsustainable rate. Finally, the disparity in the availability of energy resources that results in energy-poor places should be taken into account. Around the world, liquids, natural gas, and coal make up more than 70% of the energy consumed. The technologies used to manufacture these fuels, however, have been developed over a long period. Making a procedure effective enough to take the place of these dependable fuel sources requires time and money. The rising energy demand depicted in Figure 2.1 as well as carbon dioxide emissions in gigatons.

(a) (b)

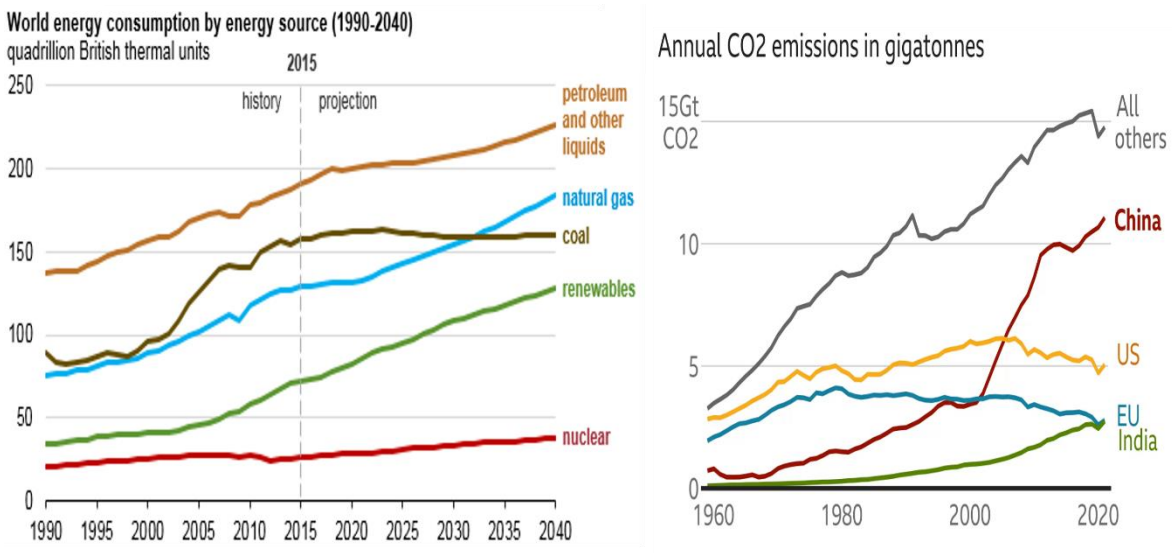

Figure 2.1 a) Global energy demand trend vs energy supply resources (Doman, 2017), and b) Global carbon dioxide emissions(Rincon, 2021).

However, throughout the past few decades, two crucial reasons have driven the development of alternative fuels. The first is the wildly unequal rate of fossil fuel production and consumption. Fossil fuels will run out within a few decades as a result of the rising demand. The second is the effects of burning fossil fuels on the ecosystem. Burning these fuels releases greenhouse gases, specifically carbon dioxide. Because it is

plentiful, takes a long time to decompose, and can trap heat in the atmosphere, carbon dioxide has a particularly negative impact(Bockris & Appleby, 1972).

These various challenges indicate the necessity for an alternative fuel source that satisfies the following conditions: it should be renewable, have low emissions to facilitate comprehensive lifecycle analysis, be efficient and plentiful enough to cater to the increasing global energy demands, and must be easily accessible across all regions of the world. To achieve this, a range of energy sources will be utilized. Among these options, hydrogen has emerged as a potential alternative (Dincer & Acar, 2018).

2.2 Hydrogen Prospects

With its use in numerous industries, including oil refining and various chemical production processes like ammonia and methanol, it is predicted that demand for hydrogen would rise(Scholz, 1993). Additionally, increased interest in green energy and stronger government pollution laws are predicted to increase hydrogen generation. Particularly, the use of hydrogen as a clean-burning fuel can help reduce dependency on fossil fuels and boost emissions reduction. (Nwogu, Alkali, & Gobina, 2015; Veziro & Barbir, 1992). However, steam reformation, which emits a significant amount of carbon dioxide, is currently the most used method for creating hydrogen. The use of hydrogen as an environmentally friendly alternative is not feasible under the existing approach, which takes into account the entire lifecycle of the process and results in emissions that are almost identical to those from burning fossil fuels(Cammack, Frey, & Robson, 2001; Jain, 2009). In response to rising worldwide demand and environmental concerns, new hydrogen production techniques are being developed as well as a diversified market. Water electrolysis or water splitting is the method that is most in demand for making hydrogen(Nwogu et al., 2015).

2.3 Water Electrolysis

The three primary pathways for splitting water are electrolysis (using electricity), thermolysis (using heat), and photolysis (solar)(Albonetti, Perathoner, & Quadrelli, 2019). To replace the present CO_2-generating technologies for manufacturing hydrogen, water electrolysis has emerged as a significant contender. When water is electrolyzed, an electrical current is applied, and a charge transfer reaction occurs at the electrode-solution interface, converting the electrical energy to the chemical. Simply simple, water electrolysis separates water into oxygen and hydrogen. As a result, the sole by-product is oxygen,

making this process a zero-emission one(Albonetti et al., 2019). The overall governing equation is:

$$H_2O \rightarrow H_2 + 1/2O_2,\ \Delta G^0 = +237.2\ kJ/mol \quad (2.1)$$

In acidic solution:

$$\text{Cathode: } 2H^+ + 2e^- \rightarrow H_2 \quad (2.2)$$

$$\text{Anode: } H_2O \rightarrow 1/2O_2 + 2H^+ + 2e^- \quad (2.3)$$

In alkaline solution:

$$\text{Cathode: } 2H_2O + 2e^- \rightarrow H_2 + 2OH \quad (2.4)$$

$$\text{Anode: } 2OH^- \rightarrow 1/2O_2 + H_2O + 2e^- \quad (2.5)$$

The energy needed to produce hydrogen is not easily explained. The Gibbs free energy shift for this reaction is substantial, measuring ΔG^0 = +237 kJ/mol. Through the Nernst equation, this equates to E^0 = 1.23V(Curie, 2013; Mishra, Basu, Shetti, Reddy, & Aminabhavi, 2019). The present power consumption for water electrolysis would put a burden on the system and again reduce the environmental benefits. Utilizing newly enhanced renewable energy sources including wind, solar, hydroelectricity, biomass, and geothermal energy might serve as an alternative to grid-supplied electricity. One of these sources would be the possibility to supplement water electrolysis regionally, which is another benefit(Albonetti et al., 2019). Lowering the energy barrier to split water, storing hydrogen, reducing the cost of specialized materials to conduct this process, scaling up production, and overall basic scientific discoveries at each stage are some of the biggest issues facing scientists today(Pant & Gupta, 2008).

2.4 Fundamentals of Hydrogen Evolution Reaction

HER is a multi-step process with the two-electron transfer taking place on the cathode surface via two different mechanisms with three possible reactions(Huang et al., 2021; Xiumin Li et al., 2016; Morales-Guio, Stern, & Hu, 2014). The first step is the Volmer reaction (eqn. 2.6 and 2.7), where a proton reacts with an electron to generate an adsorbed hydrogen atom (H*) on the electrode material surface (M). The proton sources are the

hydronium cation (H_3O^+) and the water molecule in acidic and alkaline electrolytes, respectively. Subsequently, the H_2 formation may occur via the Heyrovsky reaction (eq. 2.8 and 2.9) or the Tafel reaction (eqn. 2.10), or both. In the Heyrovsky step, another proton diffuses to the H* and then reacts with a second electron to produce H_2. During the Tafel step, two hydrogen atoms (H*) located nearby come together on the electrode surface, resulting in the generation of H_2 (Gileadi, 2011). The overall HER can be written as:

(1) electrochemical hydrogen adsorption (Volmer reaction) (eq. 2.6 and 2.7)

$$H_3O^+ + M + e^- \rightarrow M - H^* + H_2O \text{ (acidic medium)} \quad 2.6$$

$$H_2O + M + e^- \rightarrow M - H^* + OH^- \text{ (alkaline medium)} \quad 2.7$$

(2) electrochemical desorption (Heyrovsky reaction) (eq. 2.8 and 2.9)

$$H^+ + e^- + M - H^* \rightarrow H_2 + M \text{ (acidic medium)} \quad 2.8$$

$$H_2O + e^- + M - H^* \rightarrow H_2 + OH^- + M \text{ (alkaline medium)} \quad 2.9$$

or

(3) chemical desorption (Tafel reaction) (eq. 2.10)

$$2M - H^* \rightarrow H_2 + 2M \text{ (both acidic and alkaline mediums)} \quad 2.10$$

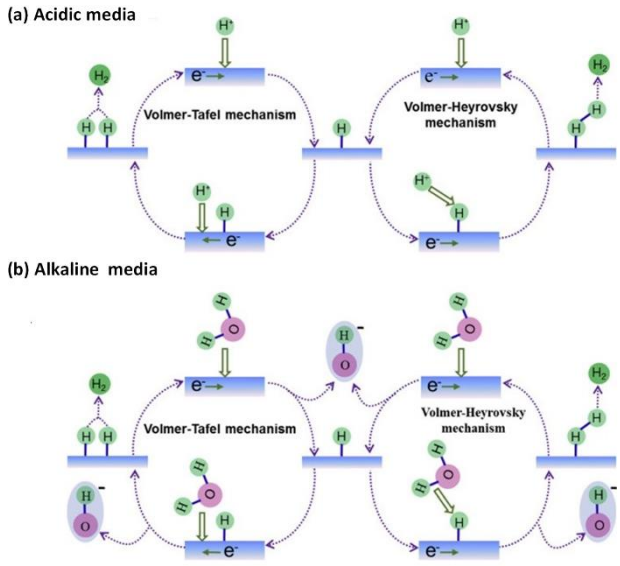

Figure 2.2 Diagrammatic representation of HER in (a) alkaline and (b) acidic medium(Sahoo, Bisoi, Huang, Tsai, & Lee, 2021).

2.5 Measurements Criteria for Catalytic Activity

2.5.1 Over Potential

The thermodynamic equilibrium potentials in any electrolytes for the water splitting are 0 and 1.23 V (both versus RHE: reversible hydrogen electrode) for catalyzing HER and OER, respectively. However, because of those inherent kinetic obstacles, a practical process requires an additional potential, typically known as the overpotential and represented by the symbol η (Sengeni Anantharaj et al., 2016; Y. Guo et al., 2019; Sinha, Kim, & Robertson, 2021). Three different types of overpotentials, namely the activation overpotential, concentration overpotential, and resistance overpotential, are present throughout the water-splitting process. An appropriate electrode material can significantly lower the activation overpotential, an inherent feature of the electrocatalyst (J. Wang et al., 2020). The overpotential is often determined from the polarization curve produced by charting the current density vs the overpotential for a particular current density. The greater performance of the electrocatalyst is shown by the lower value of the overpotential at the same current density (J. Wang et al., 2020).

2.5.2 Tafel Slope and exchange current density

The Tafel equation enables the determination of two significant kinetic properties, namely the Tafel slope and exchange current density (Roger, Shipman, & Symes, 2017; Sinha et al., 2021; J. Wang et al., 2020).

$$\eta = a + b \log j \qquad 2.11$$

The letters η stand for overpotential, b for Tafel slope, and j for current density. The reaction mechanism and potential kinetic rate of the electrocatalyst may both be inferred from the Tafel slope. The lower value of the Tafel slope indicates that a smaller overpotential is required to increase the same current density, which predicts a quicker charge transfer kinetic. Exchange current density (j_0), which reflects the intrinsic rate of the electron transfer between an analyte in solution and the electrode under equilibrium conditions and is only correlated to the catalyst materials, electrolyte, and temperature is the corresponding value of j calculated from the Tafel equation when the value of η is equal to zero.

In other words, the more exchange current density there is, the more active the water-splitting catalyst will be. An effective electrocatalyst for water electrolysis typically has a low overpotential, a small Tafel slope, and a high exchange current density, to put it briefly (J. Wang et al., 2020).

2.5.3 Turn Over Frequency

Turnover frequency (TOF), which may be used to determine each catalytic active site's intrinsic activity under certain reaction circumstances, is defined as the number of molecules that react at each accessible catalytic site each time (Zou & Zhang, 2015). Eq. (2.12) can be utilized to calculate the TOF.

$$\mathrm{TOF} = {}^{jA}/_{\alpha Fn} \qquad 2.12$$

According to the LSV, j represents the appropriate current density at a specified overpotential in this equation. 'α and A' stands for the electron number of the catalyst (electrons mol^{-1}) and the surface area of the working electrode. n is the number of moles (mol) of covered metal atoms on the electrode, which may be calculated by dividing the mass (g) by the molality (g mol^{-1}). F stands for the Faraday constant, which is equal to 96 485.3 C mol^{-1} under the standard situation.

2.5.4 Stability

To evaluate a catalyst's capacity to continue acting over a lengthy period, stability is used as another very significant characteristic. Galvanostatic or potentiostat electrolysis measurement and cyclic voltammetry (CV) or linear sweep voltammogram (LSV) are two straightforward electrochemical methods that may be used to describe and assess the catalytic stability, respectively (Zou & Zhang, 2015). Galvanostatic or potentiostatic electrolysis measurements are conducted to observe the change in potential or current density over time while maintaining a constant current density. Typically, a standard current density of 10 mA cm^{-2} is utilized as a benchmark to evaluate the catalytic stability.

2.6 Metal Oxide as HER Catalyst

Transition metal oxides (TMOs) have gained significant popularity in the field of electrocatalysis due to their affordable, stable, readily available, and environmentally friendly properties. Among various classes of electrocatalysts, TMOs are currently regarded as the most promising for HER (J. Zhu et al., 2019). There have been six reported categories of metal oxide-based electrocatalysts for HER. The aforementioned group encompasses various types of electrocatalysts for the hydrogen evolution reaction (HER), including single transition metal oxides, spinel oxides, perovskite oxides, metal (oxy)hydroxides, specifically structured metal oxides, and oxide-containing hybrids (Y. Zhu et al., 2020).

2.6.1 Single transition metal oxides

Among the various metal oxides, single transition metal oxides such as NiO, CoO, TiO_2, Ti_2O_3, MoO_3, MoO_2, WO_3, WO_2, MnO_2, and CeO_2 have emerged as the primary contenders in the field of electrocatalysis for applications related HER. These oxides have undergone extensive investigation and have been evaluated through diverse approaches to assess their potential as HER electrocatalysts (Y. Zhu et al., 2020). Modifying the intrinsic catalytic activity of stoichiometric oxides has been a widely recognized and effective approach to enhancing their electronic structure, conductivity, and hydrogen adsorption energies. Among these methods, the introduction of oxygen vacancies (OVs) has emerged as a popular and successful technique for achieving such modifications (D. Chen, Chen, Baiyee, Shao, & Ciucci, 2015; Ji, Bi, Zhang, Cao, & Zhao, 2020; K. Zhu, Shi, Zhu, & Yang, 2020). Y. Li et al. successfully developed a highly efficient HER electrocatalyst for acidic media by preparing oxygen-deficient $WO_{2.9}$ through a simple thermal treatment (**Fig. 2.3a**). The tailored structure of $WO_{2.9}$ demonstrated remarkable improvements in acidic HER activity, with a lower overpotential (η_{10}) of 70 mV and a steeper Tafel slope of 50 mV dec^{-1} compared to pristine WO_3 (**Fig. 2.3b & c**) (Y. H. Li et al., 2015). According to first-principles simulations, WO_3 exhibits characteristics of a degenerate semiconductor with favorable hydrogen adsorption-free energy and good conductivity. This behavior can be attributed to the presence of gap states generated by oxygen vacancies (OVs).

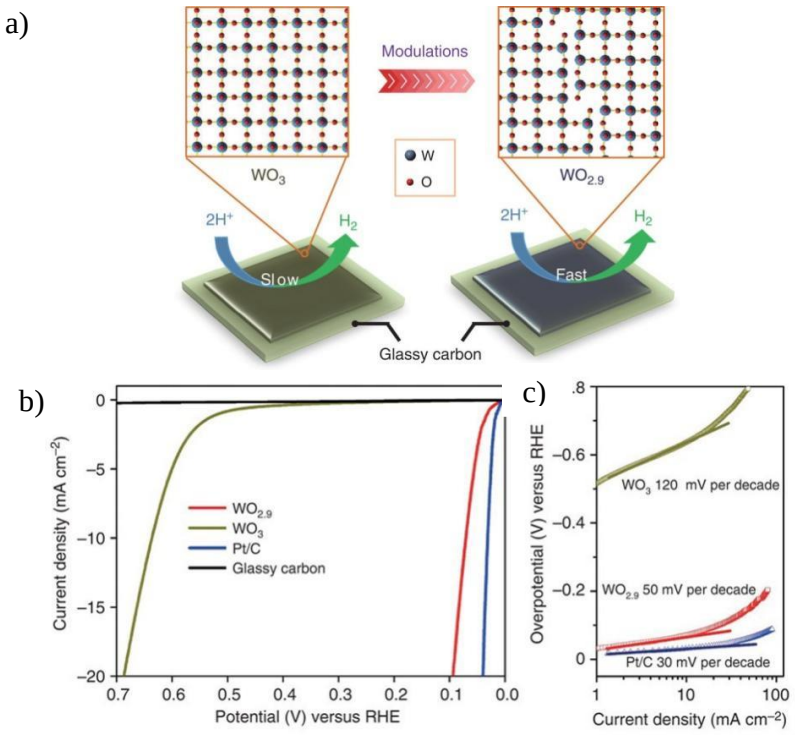

Figure 2.3 (a) Reaction mechanism of electrocatalytic H_2 evolution for WO_3 and $WO_{2.9}$ (b) HER polarization curves and (c) Tafel plots of different catalysts in 0.5 M H_2SO_4

By modifying the electronic structures through the incorporation of foreign non-metal heteroatoms such as nitrogen (N), fluorine (F), or sulfur (S), there is a possibility of enhancing the performance of the alkaline HER (Xingxing Yu et al., 2020; L. Zhang et al., 2018; C. Zhong et al., 2020). Zhang et al. employed nitrogen (N) atoms to modify the electrochemical adsorption sites on the surface of NiO in order to enhance the alkaline HER activity (L. Zhang et al., 2018). In a recent study, Zhong et al. described the utilization of halogen F anion doping to enhance the alkaline HER activity of CoO. Theoretical and experimental findings suggest that surface charge redistribution following N modification enables the simultaneous facilitation of initial water dissociation, hydrogen adsorption on low coordinated oxygen (LCO) sites, and OH desorption on nickel sites. This collective effect accelerates the overall process of hydrogen evolution (C. Zhong et al., 2020). The introduction of fluorine (F) anions at O^{2-} sites enables the creation of favorable conditions for HER. This F^- anion doping induces charge redistribution in nearby cobalt (Co) sites, facilitating water dissociation and weakening hydrogen adsorption. Moreover, hetero-non-metal doping not only has an electrical effect but also allows for the adjustment of the crystallinity of metal oxides. In a related context, Yu et al. made an intriguing discovery

that the addition of electronegative sulfur (S) to crystalline cobalt oxide could lead to structural disorder (Xingxing Yu et al., 2020). When compared to its crystalline counterpart, the S-CoO_x catalyst exhibits a higher catalytic activity for both HER and OER in alkaline media. This increased activity is attributed to the presence of more abundant defect sites and reduced oxygen coordination caused by the disorder in the S-CoO_x structure. By introducing hetero non-metal atoms (such as nitrogen, fluorine, phosphorus, or sulfur), the HER performance of transition metal oxides can be significantly and easily improved in both acidic and alkaline conditions.

2.6.2 Spinel oxides

In spinel-type metal oxides, the formula AB_2O_4 is commonly observed. In this formula, A represents a divalent transition metal ion situated at a tetrahedral position, while B represents a trivalent transition metal ion located at an octahedral site (**Fig. 2.4a**)(Y. Zhu et al., 2020). A and B locations in the spine structure can be occupied by the same elements (e.g., Co_3O_4) or by different elements (e.g., $NiCo_2O_4$). Spinel oxides have gained a lot of interest for a variety of applications in oxygen electrocatalysis (Ye Zhou et al., 2019), photocatalysis (Kudo & Miseki, 2009), lithium batteries (Lee et al., 2020), supercapacitors (Lee et al., 2020), etc. because of their straightforward manufacturing process, economical nature, and the ability to tailor their composition according to specific requirements. Co_3O_4 stands out as the most commonly studied spinel oxide, particularly in the context of alkaline HER electrocatalysis. Numerous efforts have been dedicated to developing effective Co_3O_4-based HER electrocatalysts suitable for use in alkaline environments (Y. Zhu et al., 2020). Zhu et al. successfully fabricated hollow microtube arrays of Co_3O_4 (Co_3O_4-MTA) with a hierarchical porosity using an electrochemical sacrificial template technique (**Fig. 2.4b**) (Wei et al., 2022). With hollow interiors and porous shells, Co_3O_4-MTA displays exceptional alkaline activity for HER with low onset overpotentials and large current densities **(Fig.2.4c)**. In a recent publication, Xiao et al. employed a plasma-assisted method to introduce phosphorus (P) atoms into the in situ-generated oxygen vacancies of Co_3O_4, aiming to enhance HER activity (Wei et al., 2022).In addition to Co_3O_4, other AB_2O_4 spinel oxides with other A and B elements, such as $NiCo_2O_4$, have also been thoroughly explored in HER electrocatalysis (X. Gao et al., 2016; L. Huang et al., 2019; D. Liu et al., 2018; S. Peng et al., 2018). Through a thermally driven conversion method, Gao et al. successfully produced hierarchical $NiCo_2O_4$ hollow micro cuboids composed of one-dimensional porous nanowire subunits. The unique three-dimensional hierarchical structures have led to a notable improvement in HER kinetics of $NiCo_2O_4$. Additionally, according to Liu et al., the HER activity of $NiCo_2O_4$ can be significantly influenced by the number of oxygen

vacancies present (D. Liu et al., 2018). Furthermore, numerous other spinel oxides with diverse chemical compositions have been noted, including Ce-$MnCo_2O_4$ (X. Huang et al., 2018), $CuCo_2O_4$ NSs (Pawar et al., 2019), exhibit encouraging HER catalytic activity in alkaline solutions.

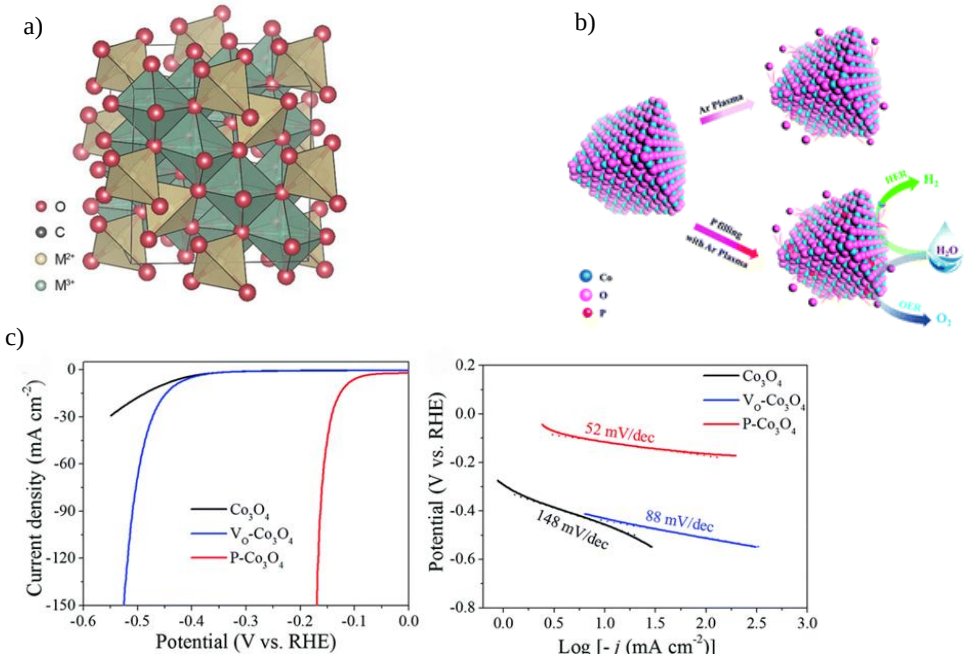

Figure 2.4 (a) General crystal structure of spinel metal oxides. (b) The schematic diagram for the preparation of P-Co_3O_4 and VO-Co_3O_4 by a plasma-assisted approach. (c) HER polarization curves of various catalysts in a 1 M KOH and Tafel slope.

2.6.3 Perovskite oxides

Perovskite oxides, a group of functional metal oxides, exhibit a general formula of ABO_3. In this formula, the A-site cations, which are usually rare-earth or alkaline earth metals, have a 12-fold oxygen coordination, while the B-site cations, typically transition metals, have a 6-fold oxygen coordination (**Fig. 2.5a**) (Y. Zhu et al., 2020). Perovskite oxides have demonstrated notable performance as electrocatalysts for the oxygen evolution reaction (OER). However, the majority of single-phase perovskite oxides suffer from limited intrinsic electrical conductivity and activity, resulting in an inadequate performance for the hydrogen evolution reaction (HER). This limitation hinders the practical application of perovskite oxides in water splitting processes (Si et al., 2022). Various techniques, including doping and defect engineering (R. Zong et al., 2021), surface modification (J. H. Kim et al., 2021), and morphological control (Hua, Li, Sun, et al., 2017), have been

employed to manipulate the surface characteristics, crystal structure, and electronic structure of perovskite oxides. These approaches enable precise control over the properties of perovskite oxides, facilitating their optimization to the electrocatalytic performance.

HER electrocatalysis using perovskite oxides has been relatively overlooked in the past. While there have been initial investigations in the 1990s on the use of $Sr_{1-x}NbO$, which lacks an A-site, as a catalyst for HER in strong acids, the observed HER activity remained quite low (Manoharan & Goodenough, 1990). As an active and stable electrocatalyst for HER in the alkaline medium, Xu et al. reported an A-site praseodymium (Pr)-doped $Pr_{0.5}(Ba_{0.5}Sr_{0.5})_{0.5}Co_{0.8}Fe_{0.2}O_{3-\delta}$($Pr_{0.5}$BSCF) perovskite with cubic structure (Xu et al., 2016). In comparison to the undoped $Ba_{0.5}Sr_{0.5}Co_{0.8}Fe_{0.2}O_3$(BSCF) perovskite, $Pr_{0.5}$ BSCF exhibits a considerable increase in HER catalytic activity with a low overpotential of 237 mV to reach 10 mA cm^{-2} **(Fig.2.5b)**. A little amount of fluorine (F) dopants in $La_{0.5}Ba_{0.25}Sr_{0.25}CoO_3$ upshifts the O 2p-band center and activates the lattice O's redox capacity, which enhances the alkaline HER activity (Hua et al., 2018). By employing a straightforward electrospinning method, perovskite nanorods of $SrNb_{0.1}Co_{0.7}Fe_{0.2}O_3$(SNCF-NR) were successfully synthesized, showcasing favorable hydrogen evolution reaction (HER) performance and stability in the alkaline electrolyte(Y. Zhu et al., 2017). $La_{0.5}(Ba_{0.4}Sr_{0.4}Ca_{0.2})_{0.5}Co_{0.8}Fe_{0.2}O_3$ (LBSCCF) perovskite for HER catalysis was also created using the same technique (Hua, Li, Zhang, Sun, & Luo, 2017). Through the use of colloidal crystal templates, a $LaFeO_3$ perovskite with a 3D ordered microporous (3DOM) structure (3DOM-LF) was created, displaying a roughly fourfold increase in alkaline HER activity compared to its bulk LF counterpart (Dai et al., 2019).

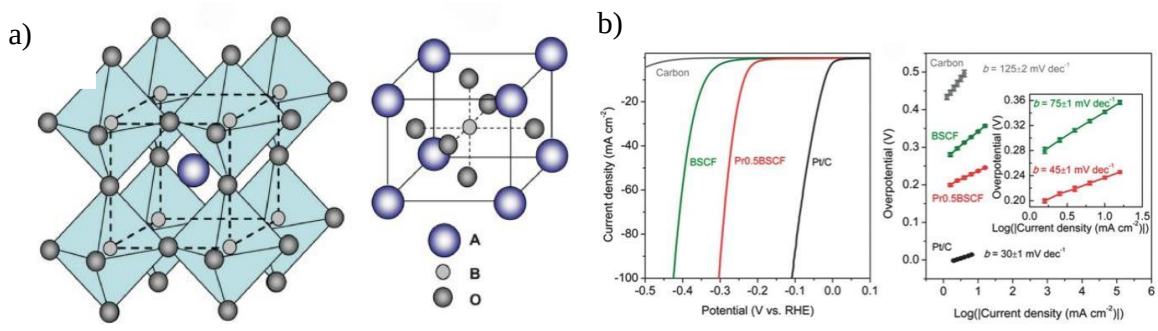

Figure 2.5 (a) The structure of ABO_3 perovskite oxide. (b) HER Polarization curves of various catalysts in a 1 M KOH

2.6.4 Metal (oxy)hydroxides

Transition metal (oxy)hydroxides, including the notable category of layered double hydroxides (LDHs), are a type of layered metal oxide. These materials possess several noteworthy characteristics, such as affordability, a significant specific surface area, excellent stability in alkaline environments, and a distinctive electron distribution (J. S. Kim, Kim, Kim, & Kang, 2018; Yanyong Wang, Yan, El Hankari, Zou, & Wang, 2018). Although unmodified metal (oxy)hydroxides are commonly regarded as promising electrocatalysts for OER, their activity is often restricted for HER due to inefficient hydrogen adsorption energies (X. Wang et al., 2020; J. Zhang et al., 2019). Through a one-pot hydrothermal synthesis, Fe-substituted hierarchical VOOH hollow spheres were successfully produced with varying doping ratios. As synthesized samples emerged as the optimal composition, displaying a low overpotential of 93 mV to achieve a current density of 10 mA cm^{-2} in alkaline environments (**Fig. 2.6a**) (J. Zhang et al., 2019). Chen et al. demonstrated that the hydrogen evolution kinetics can be enhanced by partially substituting ruthenium (Ru) atoms for iron (Fe) atoms in the NiFe- LDH (G. Chen et al., 2018). The Ru-doped NiFeRu-LDH nanosheets exhibit exceptional performance in facilitating HER when placed in a 1 M KOH solution. They exhibit an overpotential of 29 mV at a current density of 10 mA cm^{-2}, which is comparable to the performance of the benchmark Pt/C catalyst (**Fig. 2.6c**). In a separate study, Fan et al. reported a straightforward atmospheric solvothermal method to introduce atomic iridium (Ir) into NiCo-LDH, followed by spontaneous galvanic displacement to create a bifunctional catalyst (G. Chen et al., 2018). The prepared Ir-NiCo LDH demonstrates remarkable catalytic performance, achieve a remarkably low overpotential of 21 mV for the HER at a current density of 10 mA cm^{-2} in a 1 M KOH electrolyte.

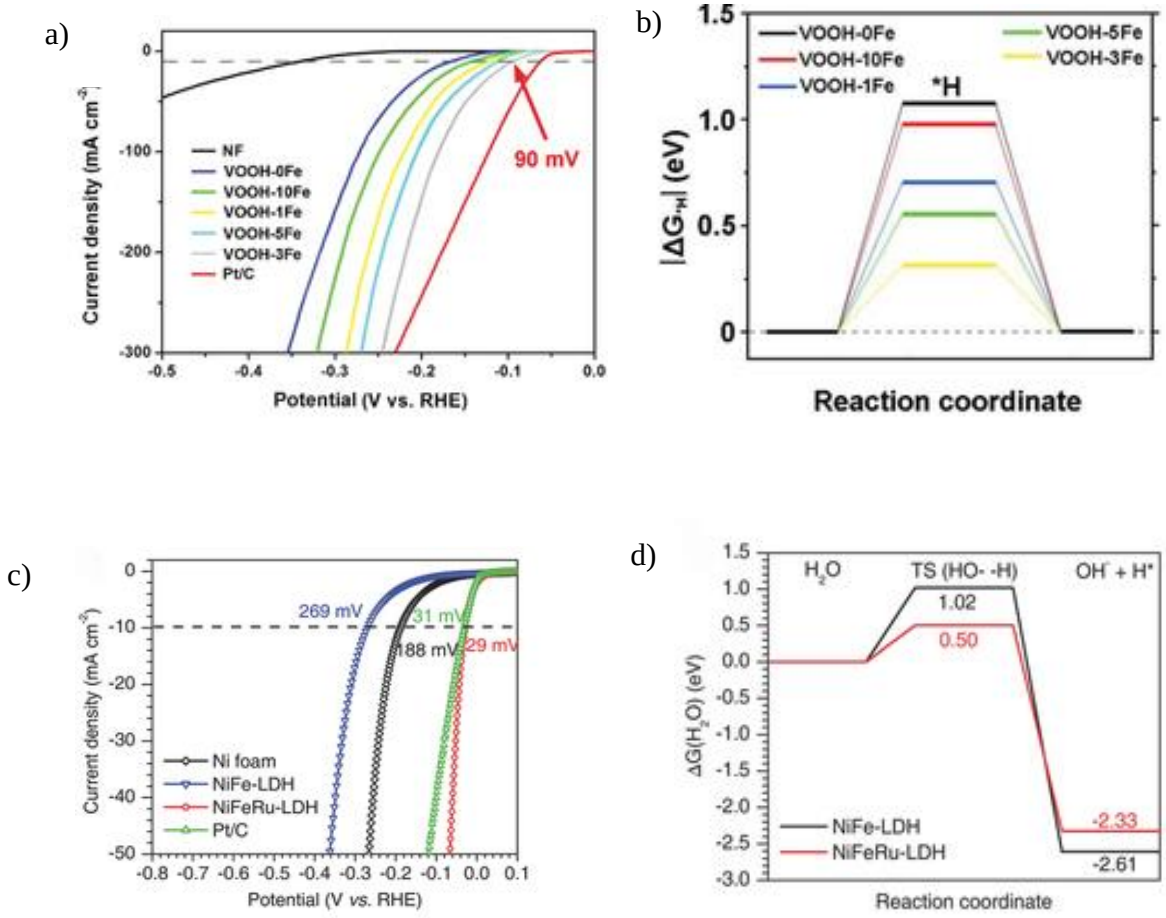

Figure 2.6 (a) HER Polarization curves of various catalysts in 1 M KOH (b) Free energy diagram to illustrate the adsorption of hydrogen. (c) Polarization curves for different catalysts in a 1 M KOH (d) Calculated adsorption-free energy diagrams to depict the Volmer step

2.6.5 Oxide-containing composite

Mixed metal oxides containing two or more oxide components have been explored for HER electrocatalysis due to the anticipated synergistic effects and advantageous properties offered by the combination of multiple components (D. Gao et al., 2019; J. Liu et al., 2018; Lv, Xu, Yang, Huang, & Zhang, 2019). Liu et al. employed a simple wet chemical method to fabricate hybrid porous nanosheet arrays composed of closely interconnected RuO_2 and NiO nanoparticles (J. Liu et al., 2018). The RuO_2/NiO hybrid catalyst exhibited superior alkaline HER activity compared to the conventional Pt catalyst. The researchers found that the enhanced HER performance is attributed to the interfacial synergy between RuO_2 and NiO induced by the applied potential. Specifically, NiO promotes water dissociation, while

the Ru species derived from RuO_2 serves as an active site for hydrogen adsorption and evolution. Lv et al. have also reported a similar phenomenon in mixed metal oxides of $TiO_2/Co_2P_4O_{12}$ (Lv et al., 2019). During the alkaline HER process, it was found that TiO_2 facilitates the surface reduction of $Co_2P_4O_{12}$ to metallic Co, leading to improved performance. The enhanced catalytic activity is attributed to the synergistic interaction among Co, $Co_2P_4O_{12}$, and TiO_2. Recent studies have investigated different mixed metal oxide catalyst systems for alkaline HER, including systems such as Co-Cu-WNW (D. Gao et al., 2019), CuCoONW (Kuang, Han, Wang, Li, & Zheng, 2016), $MoO_2/Fe_{1.89}$ $Mo_{4.11}O_7$ (Hao et al., 2018), NiO/Co_3O_4 (Wei et al., 2019), CoO/Fe_3O_4 (Adamson et al., 2020), $TiO_2/NiCo_2O_4$ (Vadakkekara, Illathvalappil, & Kurungot, 2018), and $Ni_3(VO_4)_2/NiCo_2O$ (Shang, Chi, et al., 2017). The creation of heterostructures is considered a critical approach for enhancing the catalytic performance of materials with tailored activities (Y. Zhu et al., 2020). Heterostructure catalysts possess unique properties that can lead to improved or entirely novel catalytic performance for HER. To enhance the HER catalytic activity of bare metal (hydro)oxides, it is advantageous and effective to incorporate other electroactive materials, such as metals/alloys and metal phosphides/sulfides/selenides/carbides/nitrides, through hybridization (Z. Chen, Duan, Wei, Wang, & Ni, 2019; Kuang et al., 2016).

2.6.5.1 Synergistic effect

Metal (hydro)oxides have demonstrated significant capability as effective promoters of water dissociation (H. Wang et al., 2020). Metal (hydro)oxides play a crucial role in facilitating the Volmer stage of water dissociation during the alkaline HER. To create efficient electrocatalysts for alkaline HER, metal (hydro)oxides can be combined with commonly used HER electrocatalysts. The Markovic group successfully developed a synergistic hybrid catalyst for alkaline HER by combining $Ni(OH)_2$ with Pt (Subbaraman et al., 2011).

To enhance the initial water dissociation and the formation of hydrogen intermediates in alkaline environments, the researchers electrodeposited a water dissociation promoter, specifically Li^+ intercalated $Ni(OH)_2$, onto a Pt surface. By combining noble metal nanoparticles (e.g., Pt NWs) with metal (hydro)oxide complexes (e.g., $SL/Ni(OH)_2$) (Yin et al., 2015), Pt/Co(OH) (Xing, Han, Wang, Li, & Yang, 2017), Ru/(Fe, Ni)(OH) (Xiao et al., 2020), Ru/CoO (J.-X. Guo et al., 2019), Ru/SnO_2 (W. Dong et al., 2020), and Ag/Cu_2O (Song et al., 2019), they created highly effective catalysts for the alkaline HER have been investigated. Cost-effective and efficient alkaline HER electrocatalysts can be developed by combining metal (hydro)oxides with non-noble metal compounds, such as transition metal

sulfides. A notable example is the hybridization of MoS_2 with NiCo-LDH, which was successfully achieved by Hu et al. This MoS_2/NiCo-LDH hybrid exhibited exceptional electrocatalytic performance for the HER in alkaline electrolytes (J. Hu et al., 2017). The MoS_2/NiCo-LDH hybrid demonstrated superior intrinsic activity compared to bare MoS_2, suggesting that the presence of NiCo-LDH acts as a promoter. The interface between MoS_2 and NiCo-LDH in the hybrid structure, benefiting from the favorable heterostructure, enhances the chemisorption of H (on MoS_2) and OH (on LDH). As a result, the water dissociation step and the overall HER catalysis process are significantly accelerated. Other noble metal-free electroactive materials, including Ni-Laser (Ni/NiO) (Ou et al., 2017), Ni/Mn_3O_4 (Xu Li et al., 2016), Ni/LixNiO (K. Lu et al., 2020), CoNSNTs/TiO_2NDs (Feng et al., 2017), $MoNi_4/MoO_2$ (J. Zhang et al., 2017), NiCu/NiFeOx (Yongfang Zhou et al., 2019), Co_9S_8/TiO_2 (Deng et al., 2018), $NiS_2/Ni(OH)_2$ (L. Zhang et al., 2017).

2.6.5.2 Electronic effect

The presence of heterointerfaces in hybrid catalysts enables the tuning of the electronic structure of active catalysts, leading to a favorable hydrogen binding energy. This characteristic contributes to improved catalytic performance in the acid-based HER (H. Wang et al., 2020). In a recent study, Xie et al. developed a hybrid catalyst composed of Pt and WO_3, which exhibited remarkable activity for the acidic HER. The performance of this hybrid catalyst was found to be comparable to that of commercially available Pt/C catalysts. (C. Xie et al., 2020). In-situ Raman spectroscopy and electrochemical impedance spectroscopy were employed by Xie et al. to observe the electrochemically driven phase transition from WO_3 to H_xWO_3. This transition was found to contribute to the promoting mechanism of Pt/WO_3. The Pt/WO_3 hybrid catalyst was discovered to facilitate electron transfer during the HER by providing a hydrogen transfer channel from the in-situ generated $HxWO_3$ to Pt. This, in turn, enhanced the HER kinetics. Similarly, Jiang et al. reported a Pt/MoO_2 heterostructure that exhibited Pt-like HER activity in acidic solutions, with an overpotential of only 20 mV at 10 mA cm^{-2} (Jiang et al., 2020). In addition to Pt metal, various other materials such as polyaniline and metal sulfides have been utilized in the fabrication of heterostructure catalysts for the acidic hydrogen evolution reaction (Z. F. Huang et al., 2019). Wang and colleagues observed that the interaction between WO_3 and polyaniline (PANI) at the d-interfacial level improves the electronic structure of the PANI surface (Z. F. Huang et al., 2019). The WO_3/PANI hybrid catalyst demonstrates excellent electrocatalytic activity for the HER in 0.5 M H_2SO_4, exhibiting a small Tafel slope of 46 mV dec^{-1} and a low overpotential of 74 mV at 10 mA cm^{-2}. Additionally, a self-standing

HER catalyst in acidic conditions has been successfully developed by coating $CuS/NiCo_2O_4$ on carbon fiber paper (CFP) (L An et al., 2015). Surprisingly, the $CuS/NiCo_2O_4$/CFP hybrid catalyst exhibits remarkable durability, maintaining its performance for at least 50 hours in an acidic environment. This exceptional stability can be attributed to the strong electronic coupling within the heterostructure, which mitigates the adverse effects of irreversible dissolution observed in spinel $NiCo_2O_4$ oxide under corrosive acidic conditions. The presence of hetero-interfaces facilitates efficient charge transfer, thereby enhancing the HER process not only in acidic environments but also in alkaline conditions. Taking advantage of these characteristics, Oh et al. developed a bifunctional electrocatalyst for alkaline water electrolysis by constructing a heterostructure using the perovskite oxides $La_{0.5}Sr_{0.5}CoO_3$ (LSC) and $MoSe_2$ (Oh et al., 2019). Due to this electrical effect, an alkaline electrolyzer built with a $MoSe_2$/LSC heterostructure exhibits exceptional stability over 1000 hours at a high current density of 100 mA cm^{-2}. A strong HER electrocatalyst in alkaline environments is suggested in another recent study using a porous nano spindle made of carbon-encapsulated MoO_2-FeP heterojunction (FeP/MoO_2C)(G. Yang et al., 2020). In addition to these catalysts, a number of additional low-cost heterostructure catalysts have been developed as very effective alkaline HER catalysts through interfacial electron transfer, including Ni-FeNP (Ni/γ-Fe_2O_3) (Suryanto, Wang, Hocking, Adamson, & Zhao, 2019), Ni/MoO_2 (Suryanto et al., 2019), Co-P/Co_3O_4 (L. Yang et al., 2018), V-CoP/a-CeO_2 (L. Yang, Liu, & Jiao, 2020), MoS_2/Ni_2O_3H (J. Hu et al., 2020),MoS_2/NiFe-LDH (Islam et al., 2018).

2.6.5.3 Support effect

Hybrid construction not only enables the modulation of electron structure through electron transfer at the hetero-interface but also imparts enhanced properties beneficial for HER electrocatalysis. These include increased surface area for more exposed active sites, improved electronic conductivity, and enhanced mass transfer rates. Wu et al. demonstrated this by synthesizing metallic WO_2-carbon mesoporous nanowires (MWCMNs) through the calcination of inorganic/organic WO_3-ethylenediamine hybrid precursors (**Fig. 2.7a**) (R. Wu, Zhang, Shi, Liu, & Zhang, 2015). Other hybrid catalysts with functional carbon components, such as WO_3-x/CNFs (J. Chen et al., 2016), WO_3/NPRGO (G. Hu et al., 2019),WO_2/C_3N_4 (S.-S. Lu et al., 2019), and $NiCo_2O_4$/rGO (Askari & Salarizadeh, 2019), have also been reported. Aside from functional carbon, a few other substances with a large surface area, such as MOF, can be combined with metal oxides to form promising HER electrocatalysts. Recently, Zeng et al. prepared Co_3O_4@Co-MOF using a one-pot

hydrothermal technique, making it an effective electrocatalyst for general water splitting **(Fig.2.67c)** (S. Zheng et al., 2019). Co_3O_4@Co-MOF hybrid has strong catalytic activity because the evenly dispersed Co_3O_4 nanocubes supported on a high-surface-area Co-MOF allow the full usage of electrocatalyst active sites.

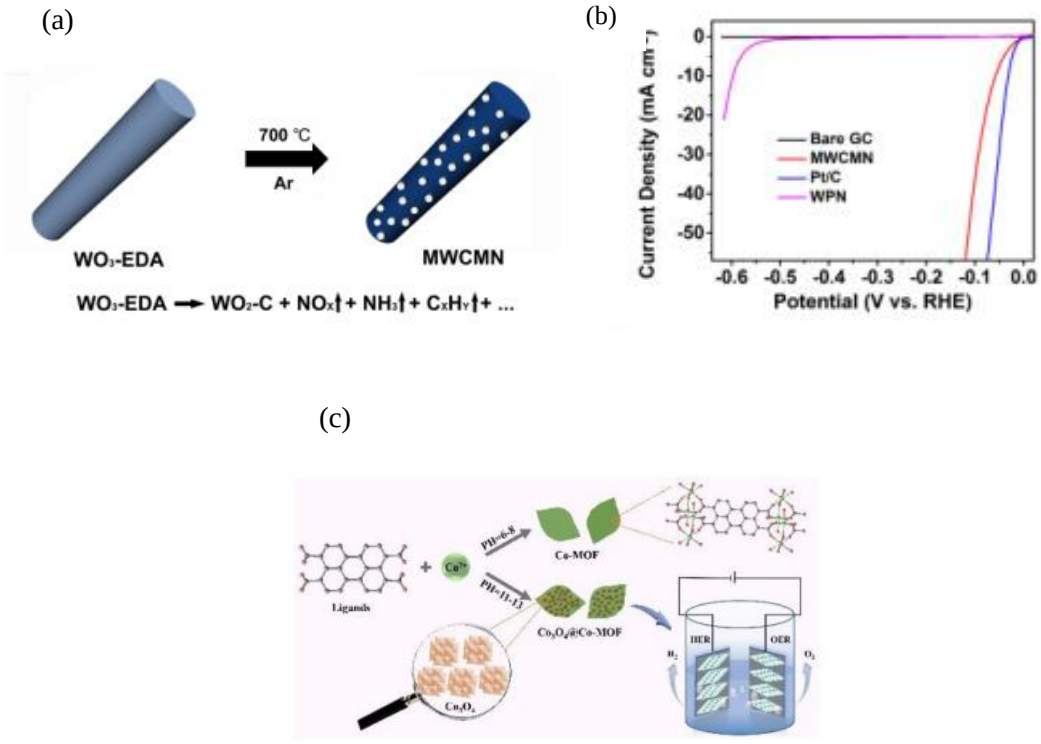

Figure 2.7 (a) Synthetic schematic diagram of MWCMNs. (b) HER polarization curves of different catalysts in 0.5 M H_2SO_4 (c) Schematic of the fabrication of the Co-MOF and Co_3O_4/Co-MOF hybrid.

2.7 Synthesis and Fabrication Methods of Metal Oxide-containing hybrids

Metal oxide-containing hybrid electrocatalysts have emerged as a promising category of materials for HER owing to their exceptional catalytic activity, stability, and tunability. These materials are created by integrating metal oxides with other substances such as carbon, graphene, and metal sulfides, resulting in hybrid structures that exhibit enhanced electrocatalytic performance. Various fabrication methods have been employed to produce metal oxide-containing hybrid electrocatalysts for HER.

2.7.1 Solvothermal and Hydrothermal synthesis

The fabrication of metal oxide-containing hybrid electrocatalysts for HER often involves the utilization of hydrothermal and solvothermal synthetic methods. Solvothermal synthesis entails the reaction between metal precursors and solvents at elevated temperatures and pressures, leading to the formation of metal oxide nanoparticles with precise control over their size and morphology. These nanoparticles are subsequently combined with other materials to create hybrid structures. A hydrothermal synthesis is a similar approach, where metal precursors react with water under elevated temperatures and pressures to generate the desired metal oxide nanoparticles.

Through the utilization of a hydrothermal technique, Khan et al successfully synthesized heterostructures comprising nickel oxide/nickel sulfide (NiO/NiS), along with their constituents, nickel oxide (NiO) and nickel sulfide (NiS) (Khan et al., 2019). These materials were examined as affordable electrocatalysts for the electrochemical water-splitting process. S. Li et al. employed a hydrothermal method to synthesize a $CoFe_2O_4$/N-doped carbon hybrid electrocatalyst for HER (Shuaijie Li et al., 2021). The authors observed that the hybrid electrocatalyst demonstrated remarkable activity and stability in HER due to the synergistic interaction between $CoFe_2O_4$ and N-doped carbon. In a separate study conducted by Ibupoto et al a MoS_2@NiO heterostructure composite electrocatalyst for HER was synthesized using a hydrothermal method and the MoS_2@NiO heterostructure displayed exceptional HER performance, achieving a low overpotential of 226 mV to achieve a current density of 10 mA/cm² (Ibupoto et al., 2019). A hydrothermal method was employed to fabricate the Co_3O_4/Fe_2O_3@NF electrocatalyst, which exhibited a distinctive thin-wall cell structure. The electrocatalyst demonstrated remarkable electrocatalytic activity for OER in alkaline solution, attributed to the combined influence of Co_3O_4 and Fe_2O_3, along with the conductive three-dimensional structure provided by the NF substrate, resulting in a synergistic effect. The unique thin-wall cell structure and the 3D conductive feature of NF contributed to the excellent performance of the Co_3O_4/Fe_2O_3@NF electrode in OER (Yuying Yang et al., 2021). A highly effective electrocatalyst with a distinctive cavity structure, consisting of a phosphorus-substituted cell-shaped Co_3O_4/NiO heterojunction, was successfully created using a simple hydrothermal reaction followed by a gas phase phosphating strategy (Xu Yu et al., 2023). Similarly, Co_3O_4/NiO composite film was prepared by a simple two-step hydrothermal process and discontinuous annealing (H. Zhao, Meng, Yu, Li, & Liu, 2022).

According to a study conducted by (Sivakumar et al., 2021), the fabrication of a $NiCo/NiO/NiCo_2O_4$ composite was achieved through a solvothermal process employing various solvent ratios. The resulting composite demonstrated an abundance of active edges and exhibited enhanced electrical conductivity compared to its pure counterparts. (J. Huang et al., 2018) report a facile solvothermal pathway for the synthesis of spinel-type $Ni_xFe_{3-x}O_4$ oxides/Ni metal nanocomposites. $Co_9S_8@Co_3O_4/NF$ successfully synthesized a hierarchically porous hybrid heterostructure on Ni foam, which is consisted of Co_9S_8 nanoflakes supported on CoO_4 nanoneedles, via a simple, efficient, and low-temperature step-wise solvothermal method (X. Wang et al., 2022). Another study by Yong Yang et al introduces excellent HER activity, characterized by low overpotential and high durability, which was observed in Co-Mo mixed oxide nanostructures with controlled structures and compositions. These nanostructures included hollow $Co_3O_4/CoMoO_4$ heterostructures and ball-in-ball $CoMoO_4$ nanospheres, which were synthesized via a one-pot solvothermal method and further transformed into hollow structures through thermal treatment (Yong Yang et al., 2016).

2.7.2 Chemical vapor deposition

Chemical vapor deposition (CVD) has undergone continuous advancements and gained significant recognition as a highly dependable and potent method for generating a vast array of ultrathin 2D nanomaterials (S. Zhao, Wang, & Fu, 2019). Typically, the growth of 2D nanomaterials using the CVD technique comprises three fundamental stages. These stages encompass the vaporization and thermal breakdown of precursors, the movement and diffusion of reactants, and finally, the formation and expansion of crystals on the substrate through nucleation and growth processes. In the study conducted by (H. Kang, Youn, Oh, Manavalan, & Jeon, 2020) hybrid catalysts composed of MoS_2 and MoO_2 were synthesized on a carbon cloth (CC) substrate using CVD and annealing techniques. The purpose of this research was to utilize the MoS_2-MoO_2 hybrids to reduce the charge transfer resistance of electrodes and achieve exceptional long-term stability. CVD was also utilized to synthesize nanostructured material consisting of $WS_2/WO_x/C$ membranes and used as catalytic electrodes for electrochemical hydrogen evolution (X. Wang et al., 2017). These membranes possess remarkable characteristics of being both free-standing and flexible. The synthesis process involves a two-step heat treatment of ammonium tetrathiotungstate ($(NH_4)_2WS_4$) and polyacrylonitrile (PAN), which are spin-coated onto graphite foils. Upon exposure to high temperatures (850 °C), the two precursors undergo decomposition, resulting in the formation of WS_2 and carbon species. Additionally, the incorporation of a

small amount of oxygen triggers the growth of $WO_{2.9}$ nanowires. (Mettenbörger et al., 2016) synthesized a Fe_2O_3-TiO_2 hybrid electrocatalyst using CVD that demonstrated high HER activity and stability. Ebbinghaus, 2002 et al. employed $La_{1-x}(Ca, Sr)_xCoO_3$ as substrates and catalysts to grow carbon nanotubes via chemical vapor deposition (CVD)(Ebbinghaus, 2002). Most of the metal oxides reported in the literature for the growth of carbon nanotubes via CVD are Co based oxides, such as $La_{0.5}Sr_{0.5}Co_{0.8}Fe_{0.2}O_3$ (Park et al., 2015), $La_{0.58}Sr_{0.4}Fe_{0.2}Co_{0.8}O_3$(Elumeeva et al., 2016) and $La_{0.6}Sr_{0.4}CoO_3$(Thiele, Colmenarejo, Grobéty, & Züttel, 2009).

2.7.3 Co-precipitation

Co-precipitation has been widely used to synthesize metal oxide-containing hybrids due to its simplicity and cost-effectiveness. (Ng, Kok, & Ong, 2017) proposed a straightforward, scalable, and cost-effective approach to synthesize high-performance cobalt oxide platelets with a hexagonal shape, supported on iron oxides (Fe_3O_4 and α-Fe_2O_3), as electrocatalysts for water electrolysis. Another study involved the synthesis of a NiO/Co_3O_4 nanoparticle decorated on nitrogen-doped carbon through co-precipitation, followed by calcination at 400°C. The resulting composite electrocatalyst demonstrated remarkable electrocatalytic activity, characterized by a low onset potential and high current density (Tahir et al., 2017). Co_3O_4/MnO_2 nanocomposites have been successfully synthesized using a co-precipitation method, resulting in exceptional catalytic performance and enhanced stability (Worku, Ayele, Habtu, & Yemata, 2021). Large-scale synthesis of $ZnFe_2O_4$/TiO_2 nanocomposites has been carried out to create spinel-type ferrite photocatalysts for efficient hydrogen production through water splitting (Draz et al., 2021). A two-step method involving co-precipitation and sulfuration has been employed to directly grow a hierarchical $NiCo_2O_4$/Ni_3S_2 hybrid on NF which enables the creation of the hybrid material with enhanced properties (Du, Wang, Li, & Zhang, 2018). A nanocomposite photocatalyst consisting of CuO and graphitic carbon nitride (g-C_3N_4) was successfully synthesized using the co-precipitation method. This composite exhibited enhanced performance in the photocatalytic process of water splitting, leading to improved efficiency in harnessing solar energy for the generation of hydrogen fuel (Ragupathi, Raja, Panigrahi, & Subramaniam, 2020).

2.7.4 Electrodeposition

Electrodeposition synthesis has emerged as a highly promising method for the fabrication of metal oxide-containing hybrid materials in the field of electrocatalysis for HER (B. Kang, Hussain, Cheng, Peng, & Wang, 2022; Shit et al., 2021). This technique involves

depositing metal oxides onto various substrates, resulting in hybrid materials with enhanced electrocatalytic activity towards HER. The electrodeposition method offers several advantages, including easy control over the amount and size of the deposited materials by adjusting key plating parameters such as deposition time, voltage, and electrolyte concentration (Y. Kim et al., 2023). It provides a rapid and straightforward approach for the controlled synthesis of uniformly dispersed electrocatalysts, eliminating the need for additional capping agents or reductants. Moreover, this technique is simple to implement and can be easily scaled up to larger production volumes. Additionally, electrodeposition allows for precise control over the growth of nanostructures, enabling controlled, patterned, and faceted crystal growth (Kale, Borse, Gomaa Abdelkader Mohamed, & Wang, 2021).

Various research studies have documented the effective utilization of electrodeposition synthesis in the creation of metal oxide-containing hybrid materials for electrocatalysis of HER. One notable example is the fabrication of a MoO_3/Ni-NiO hybrid nanomaterial through a unique sequential electrodeposition approach. This hybrid structure combines amorphous NiO nanosheets with ultrafine Ni and MoO_3 nanoparticles. The resulting MoO_3/Ni-NiO hybrid exhibits remarkable bifunctional activity for both HER and OER, along with long-term durability(Xiaopeng Li et al., 2020). The technique of electrodeposition has been employed to selectively deposit ultrathin flakes of Co_3O_4 nanocrystals onto ZnO nanorods. It has been observed that the quantity of Co_3O_4 deposited on ZnO scaffolds has a more significant impact on the performance of oxygen evolution compared to cases where ZnO scaffolds are absent (H. Wu et al., 2018). In their study, (Shasha Li et al., 2018) successfully synthesized $CoMoO_x$/CoNi foam electrocatalysts for HER on a NF substrate. The synthesis involved a straightforward hydrothermal method followed by electrodeposition. The electrocatalyst produced remarkable performance, showcasing a low overpotential of 82 mV at a current density of 10 mA cm^{-2}, along with exceptional long-term stability. By utilizing a straightforward two-step electrodeposition technique, a MoS_2/Fe_2O_3 heterostructure was directly produced on a nickel foam substrate(Shit et al., 2021). The integration of Fe_2O_3 with MoS_2 in this heterostructure resulted in a synergistic enhancement of its electrocatalytic activity. Furthermore, the binder-free growth on a conductive nickel foam (NF) enabled the heterostructure to achieve a higher catalytic current density. (B. Guo et al., 2018) utilized a one-step electrodeposition technique to synthesize nanoflowers composed of ferric oxide (Fe_3O_4) decorated with cobalt monophosphide (CoP_x) on titanium nitride (TiN) nanoarrays. The resulting Fe_3O_4–CoP_x/TiN hybrid material exhibited remarkable activity for the hydrogen evolution reaction (HER), displaying an onset potential of 50 mV and demonstrating superior stability even

after 100 hours of operation. Furthermore, a self-supported nanowire array consisting of a core/shell structure of Co_3O_4/NiO was prepared by combining hydrothermal synthesis with electro-deposition methods on a nickel foam substrate. The obtained hybrid demonstrated exceptional electrocatalytic activity in facilitating HER, as indicated by a low overpotential and Tafel slope. The enhanced electrocatalytic activity was attributed to the cooperative effect between NiO and Co_3O_4, which led to an increase in active sites and facilitated efficient charge transfer (J. Wu, Li, Huang, & Lin, 2013). Additionally, a different approach involved the direct growth of $NiCo_2O_4$ on a three-dimensional textile and wavy CC substrate using a simple and cost-effective electrodeposition method. This process resulted in distinct morphologies and a high-purity adhesive deposit, providing a robust and stable material for water oxidation on the CC substrate (Albu, Al Abass, & AlOtaibi, 2023).

Table 2-1 Summary of metal oxides and Metal oxide based composite catalysts for HER

Catalysts	Substrate	Loading amount (mg/cm^2)	Electrolyte	η (mV)	I ($mA\ cm^{-2}$)	Tafel slope ($mV\ dec^{-1}$)	Stability	Reference
MoO_{3-x}	ITO	-	0.5M H_2O_4	201	10	90	800 cycle	(W. Zhang, Li, Firby, Al-Hussein, & Elezzabi, 2019)
WO_{3-x}	GC	0.243	0.5M H_2O_4	440	10	30	8hr	(Sharma, Kumar, & Halder, 2019)
$TiO_{1.23}$	Ti foil	-	0.5M H_2O_4	198	10	88	40hr	(Swaminathan, Subbiah, & Singaram, 2016)
S-doped MoO_2 NSs	GC	0.283	0.5M H_2O_4	176	10	42	3000 cycles	(Geng, Liu, Yu, Yang, & Li, 2020)
S-CoO_x	NF	-	KOH	136	10	80	1000 cycle	(Xingxing Yu et al., 2020)
$NiCo_3O_4$NSs	NF	-	KOH	170	10	77	12hr	(Zeng et al., 2018)
Ce-$MnCo_2O_4$	GC	-	KOH	389	10	96	12hr	(X. Huang et al., 2018)
$NiFe_2O_4$	GC		KOH	300	10	125	10hr	(Dalai, Mohanty, Mitra, & Jena, 2019)
MoS_2/Ti_4O_7	GC	0.1962	0.5M H_2O_4	287	10	48	1000 cycle	(J. Zhao et al., 2020)
CoS_2/Co_3O_4	CC	1.25	0.5M H_2O_4	152	10	45	5000s	(T. Li et al., 2017)
$CuS/NiCo_2O_4$	CFP	-	0.5M H_2O_4	72	10	41	50hr	(Li An et al., 2015)
WS_2/WO_3	GC	0.14	0.5M H_2O_4	395	10	50	2000 cycle	(Shang, Rao, et al., 2017)
W-doped MoS_2/MoO_2/CNT	CNT	-	0.5M H_2O_4	62	10	44	16.5hr	(C. Li et al., 2020)
$MoSe_2/MoO_3$	GC	-	0.5M H_2O_4	221	10	56	7000s	(Xia, Wang, Liu, Du, & Ye, 2018)
Cu_2O/Co_3O_4	CNT	-	0.5M H_2O_4	160	10	73	10000s	(Jin & Chen, 2018)
WO_2/C_3N_4	GC	-	0.5M H_2O_4	98	10	94	1000 cycle	(S.-S. Lu et al., 2019)
$NiCo_2O_4$/rGO	GC	-	0.5M H_2O_4	108	10	49	2500s	(Askari & Salarizadeh, 2019)
MoS_2/Co_3O_4	NF		KOH	205	10	98	14hr	(Muthurasu, Maruthapandian, & Kim, 2019)
$MoS_2/Ni(OH)_2$	CC	0.8	KOH	80	10	60	16hr	(B. Zhang et al., 2017)
Co_9S_8/TiO_2	NF	-	KOH	139	10	65	10hr	(Deng et al., 2018)
$CoS_2/Ni(OH)_2$	CC	-	KOH	99	10	118	30hr	(L. Chen et al., 2017)
Ni_3S_2/V_2O_5	NF	2.1	KOH	95	10	108	-	(X. Zhong et al., 2017)
Ni_3S_2/NiO_2	NF	-	KOH	130	10	33	12hr	(Du, Wang, & Zhang, 2018)
$NiS_2/Ni(OH)_2$	Ti	-	KOH	90	10	89	1000 cycle	(L. Zhang et al., 2017)
$Ni_3S_2/Co(OH)_2$	NF	6.1	KOH	72	10	116	20hr	(Z. Wang et al., 2020)
$CuS/Ni(OH)_2$	GC	0.286	KOH	95	10	104	30hr	(S.-Q. Liu et al., 2018)
$NiSe_2@NiO_x$	CFF	5	KOH	132	10	85	24hr	(H. Li et al., 2017)
Cu_3N/CuO	NF	-	KOH	118	10	122	10days	(Panda, Menezes, Zheng, Orthmann, & Driess, 2019)
CoO/Fe_3O_4	CFP	6	KOH	220	10	73	10hr	(Adamson et al., 2020)
Co_3O_4/Fe_3O_4	Si	0.25	KOH	370	10	117	8hr	(Ng et al., 2017)
Co_3O_4/CuO	GC	-	KOH	288	10	65	2000 cycle	(Tahira et al., 2019)
NiO/Co_3O_4	CFP	0.28	KOH	170	10	119	20hr	(Wei et al., 2019)

CHAPTER THREE

3. Materials and Methods

3.1 Chemicals and Materials

Nickel Foam (NF, purity > 99.99%; surface density 346 g/cm^2; and thickness 1 mm) and FTO (purity 99.99%) obtained from MTI Korea Inc, Copper (II) sulfate hexahydrate [$CuSO_4.5H_2O$ 98%, Alpha Chemika, Mumbai, India], Sodium sulfate pentahydrate [$Na_2SO_4.5H_2O$ 98%, Alpha Chemika, Mumbai, India], Nickel Chloride hexahydrate [$NiCl_2.4H_2O$ 98%, LobaChemie, Mumbai, India], Thiourea [CH_4N_2S, HiMedia, Mumbai, India], sulfuric acid (H_2SO_4), [H_2SO_4, Alpha Chemika], and ethanol. All chemicals utilized in the study were of analytical grade and employed without any additional purification steps.

3.2 Electrodeposition of CuO electrocatalyst

The electrodeposition of copper was conducted on a conductive nickel foam substrate in a three-electrode cell using a BioLogic SP300 electrochemical workstation (Won-A-Tech Co. Ltd, South Korea) at room temperature. The same electrodeposition experiments were also carried out on Fluorine-doped tin oxide (FTO) films that were cut into 1 cm × 3 cm pieces for XRD analysis. All HER experiments were performed with the materials on the NF electrode. The deposition process was based on a previously reported method (Roy, Jadhav, Cho, & Seo, 2019). Before the deposition, the NF was cleaned to remove the oxide layer on the surface. The cleaning process involved ultrasonication in ethanol, 1 M HCl solution, and deionized water. After cleaning, the NF was dried and used as the working electrode. A platinum wire and an Ag/AgCl/saturated KCl electrode were used as the counter electrode and reference electrode, respectively. A solution of 0.1 M $CuSO_4.5H_2O$ and 0.1 M of Na_2SO_4 dissolved in 20 mL of deionized water was used as the electrolyte for the electrodeposition process. The deposition was carried out at a potential of -1V vs. Ag/AgCl for 200 seconds. The resulting reddish-brown colored film was washed with ethanol and DI water and dried at 60 °C. The electrodeposited Cu on Ni foam was further calcined at a temperature of 400°C for 2 hours in an air atmosphere.

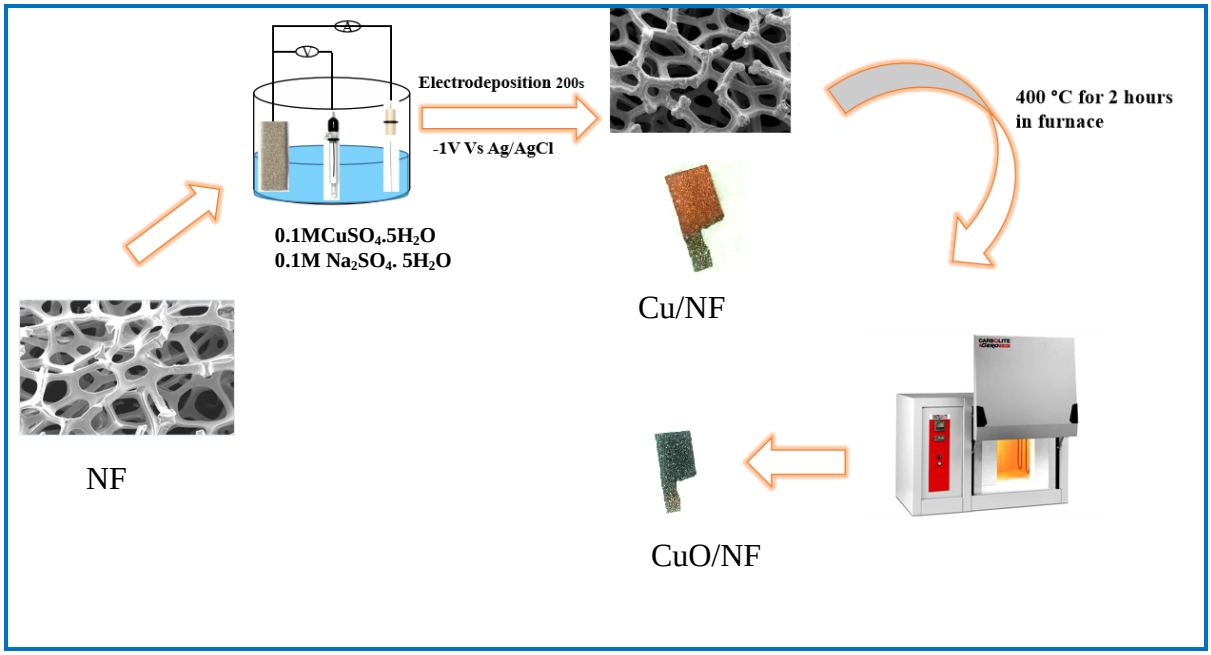

Figure 3.1 Schematic illustration of the fabrication of CuO/NF

3.3 Electrodeposition of Ni-S electrocatalyst

The Ni-S catalysts on NF substrates were synthesized by potentiostatic deposition using a BioLogic SP300 electrochemical workstation (Won-A-Tech Co. Ltd, South Korea) under ambient conditions. The working electrode was pre-cleaned NF pieces with an exposed area of 1x1 cm, while platinum wire and an Ag/AgCl/saturated KCl electrode served as the counter and reference electrodes, respectively. The Ni-S deposition was performed by dissolving 0.05M of $NiCl_2$. $4H_2O$ and 1.5M of CH_4N_2S in 20 mL of DI water and using the obtained solution as the electrolyte. The deposition was carried out at a constant potential of -1V vs. Ag/AgCl for a specific deposition time, following a modification of a previously reported method (Yihui Wu et al., 2021). The resulting black film was subjected to washing with ethanol and deionized water, followed by drying at a temperature of 60 °C. Additional electrodeposition experiments were conducted on 1 cm × 3 cm pieces of Fluorine-doped tin oxide (FTO) films for XRD analysis. All HER experiments were performed using NF electrodes.

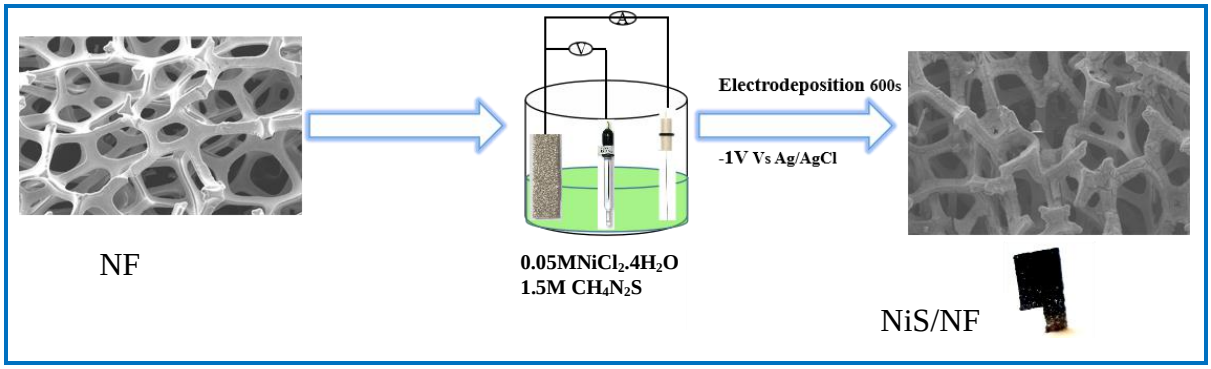

Figure 3.2 Schematic illustration of the fabrication of NiS/NF

3.4 Electrodeposition of Ni-S /CuO heterostructures electrocatalyst

In order to create a heterostructure, a two-step electrodeposition was carried out using a three-electrode system with a BioLogic SP300 electrochemical workstation (Won-A-Tech Co. Ltd, South Korea) at ambient temperature. Pre-cleaned pieces of nickel foam (NF), along with Ag/AgCl/saturated KCl and platinum wire, were utilized as the working, reference, and auxiliary electrodes, respectively for the initial deposition (CuO/NF) and the Copper oxide-modified NF acted as the working electrode for the second deposition (other electrodes being the same). About 0.1 M of $CuSO_4.5H_2O$ and 0.1 M of Na_2SO_4 were dissolved in 20 mL of DI water and the obtained solution acted as the electrolyte for the first deposition. The NF piece was partially dipped in the electrolyte in such a way that the effective area for electrodeposition was 1 × 1 cm^2 and then chronoamperometry was performed at − 1.0 V for 200s. The Copper oxide modified NF was thoroughly washed with DI water and ethanol and then dried at 60 ◦C for 6 h. The electrodeposited copper on nickel foam underwent a calcination process in an air atmosphere at a temperature of 400 °C for 2 hours. Approximately 0.05M of $NiCl_2$. $4H_2O$ and 1.5M of CH_4N_2S were dissolved in 20 mL of DI water and the obtained solution acted as the electrolyte for the second deposition. For the second electrodeposition, the copper oxide-deposited region of the nickel foam (NF) was exposed, and chronoamperometry was conducted at a potential of -1V for a specific duration. Subsequently, the heterostructure-modified NF was extensively washed and dried at a temperature of 60 °C inside an oven for 6 hours. The resulting heterostructures were denoted as CNSy, with "y" indicating the duration of the second electrodeposition in seconds. For example, the heterostructure obtained after the second depositions for 600s is designated as CNS_{600}. Some electrodeposition experiments were

also performed on FTO films for XRD analysis. All HER experiments were carried out with the materials on an NF electrode.

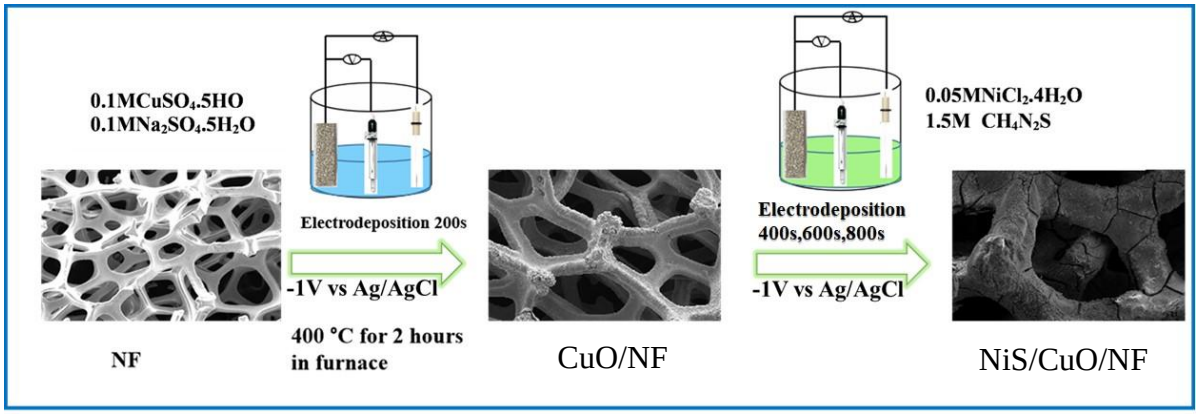

Figure 3.3 Schematic illustration of the fabrication of NiS/CuO/NF

3.5 Materials Characterization techniques

The phase composition and crystallinity of prepared samples were determined by x-ray diffraction (XRD) (ShimadzuXRD-7000) with CuK α radiation. The morphologies of the samples were examined by Field-emission scanning electron microscopy (FESEM, JSM 6500F, and JEOL).

3.6 Electrochemical performance test

The BioLogic SP300 potentiostat electrochemical workstation (Won-A-Tech Co. Ltd, South Korea) was used for voltammetric measurements. A standard three-electrode cell was used, with the as-prepared electrode (NF, CuO/NF, NiS/NF, NiS/CuO/NF) serving as the working electrode, Pt wire as the counter electrode, and Ag/AgCl as the reference electrode in both acidic and basic solutions. All potentials were determined relative to the Reversible Hydrogen Electrode (RHE) and calculated using Eq. 3.1, where E(RHE) represents the potential relative to the RHE, E(Ag/AgCl) is the measured potential relative to the Ag/AgCl electrode, pH is the pH of the electrolyte, and E_0(Ag/AgCl) is the standard potential of the Ag/AgCl electrode at 25°C, which is 0.1976 V (Gicha, Tufa, Choi, & Lee, 2021). The data was collected without iR compensation.

$$E_{RHE} = E_{Ag/AgCl} + 0.059\ pH + E_{oAg/AgCl} \qquad 3.1$$

Before conducting LSV, a stabilization process was carried out which involved performing up to 50 cycles of CV scans within the range of -0.25 V to 0.25 V vs RHE until a stable

polarization curve was obtained. LSV curves were then conducted in acid and basic electrolytes at a scan rate of 2 mV s^{-1} to obtain polarization curves.

The value of overpotential was calculated by using equation 3.2

$$\eta = E_{RHE} - E_o \qquad 3.2$$

where η is overpotential, and E_o is the thermodynamic potential to evolve hydrogen.

The polarization curves were used to create Tafel plots, which display overpotential versus log (current density), and the linear region at low overpotential was fit to the Tafel equation (Equation 3.3)(Yuhan Wu et al., 2020).

$$\eta = b\log j + a \qquad 3.3$$

where j is current density, b is the Tafel slope and a is constant

EIS was conducted over a frequency range of 100 kHz to 10 Hz with a 10 mV amplitude. Data were fitted with the electrochemical workstation inbuilt Z-fit EIS analysis software. To assess the long-term durability, galvanostatic experiments were conducted at 25°C in 0.5 M H_2SO_4 and 1.0 M KOH by applying a fixed potential to the working electrode until maintaining its catalytic activity with no decline.

Electrochemical active surface area

Capacitive currents are recorded in a potential range where there is no involvement of faradic processes (J. Xie et al., 2017). To evaluate the double layer capacitance (C_{dl}) values, cyclic voltammetry (CV) was recorded for different scan rates (10, 20, 40, 60, 80, 100, 120, and 140 mV s^{-1}) at a fixed potential window. The differences in current density variation (Δj= ja - jc) at a half potentialwere plotted against the scan rate, resulting in a linear relationship. The slope of the line obtained by the linear fit of this graph is twice the value of the double-layer capacitance (C_{dl}) as given in Eq. (3.4), which is used to estimate the electrochemical surface area (ECSA) using eqn 3.5 (Gupta et al., 2018).

$$\Delta j = v * 2 * C_{dl} \qquad 3.4$$

Where Δj is the anodic–cathodic current difference and v is the scan rate.

$$ECSA = C_{dl} / C_s \qquad 3.5$$

where Cs is the specific capacitance and the value was reported to be 0.040 mF cm^{-2} (McCrory, Jung, Peters, & Jaramillo, 2013).

Turnover Frequency

Turnover frequency (TOF) can be defined as either the rate at which molecules evolve per active site per unit of time or the rate at which electrons are provided per surface metal atom per second (Popczun et al., 2013). The number of molecules transformed per active site in a given amount of time is a measure of a catalyst's effectiveness.

TOF was estimated from Eq. 3.6 (Chinnadurai, Rajendiran, Li, & Prabakar, 2021).

$$TOF = j * \frac{NA}{n.F.C} s^{-1} \qquad 3.6$$

$$C = \frac{\int \text{area of reduction peak/Scan rate}}{\text{charge of one electron}}$$

where,

j− current density

NA− Avogadro's number

n− number of electrons transferred (2 in case of HER)

F− Faraday constant

C− Surface concentration of active sites.

The surface concentration of surface-active sites or electrochemically accessible active sites was determined by analyzing the reduction region of the cyclic voltammogram (CV) obtained at a scan rate of 50 mV/s in a 1 M KOH electrolyte (Sengeni Anantharaj, Sugime, & Noda, 2020).

CHAPTER FOUR

4. Results and Discussion

4.1 Structural Characterization by XRD

To verify the crystal structures of electrochemically deposited electrocatalysts, XRD was utilized. XRD patterns of the prepared CuO, NiS, and NiS/CuO heterostructure are shown in Fig. 4.1. It can be observed that the XRD of CuO (Figure 4.1a) shows that it exhibits diffraction peaks having 2θ values of 32.4, 35.4, 38.7, 48.7,53.2 58.3,66.4, 67.9, 72 and 75° which correspond to the planes (110), (002), (111), (20-2), (112), (202) (11-3), (022), (311) and (31-1) planes, respectively. The obtained diffraction peaks are assigned to the monoclinic structure of CuO and are well-matched with JCPD card number 045-0937 (Roy et al., 2019). The absence of additional diffraction peaks in CuO's XRD pattern amply demonstrates the purity of the CuO layer on FTO. The pure FTO substrate is responsible for all other prominent peaks.

The diffraction peaks of NiS (Figure 4.1b) at 30.3º 45.5º, and 53.5º correspond to (100), (102), and (110) diffraction planes of NiS, as per the observation. Observed diffraction peaks at 45.5º, and 53.5º correspond to (102), and (110) are in agreement with the standard hexagonal NiS data (α-NiS JCPDS No. 75-0613) (Murthy, Theerthagiri, Premnath, Madhavan, & Murugan, 2017) and at 30.3º correspond to (101), diffraction planes of rhombohedral NiS phase (β-NiS, JCPDS no. 86-2281) (Guan, Fu, Zhang, & Peng, 2018).

The XRD patterns of CuO, NiS, and prepared NiS/CuO composite catalyst with different deposition times of NiS on CuO are shown in Figure 4.1(c). The characteristic diffraction peaks of both CuO and NiS are observed in the XRD pattern of NiS/CuO heterostructure, as shown in Figure 4.1 (c). FTO was used as the substrate for electrodepositions, and as a result, all of the sample's XRD patterns showed strong peaks associated with the SnO_2 (Theerthagiri et al., 2016). Furthermore, no additional peak is seen in the samples for any possible impurities or phases.

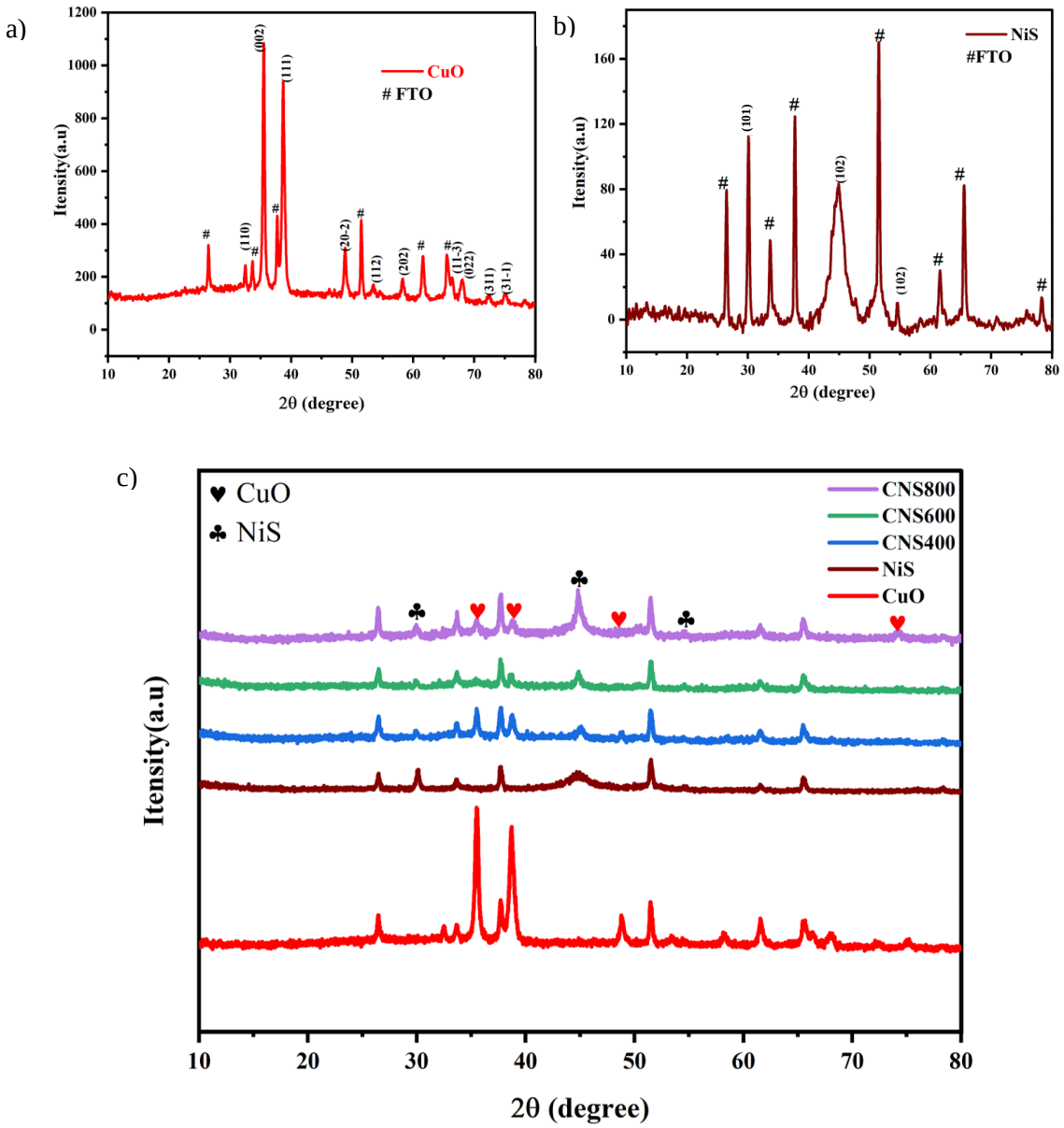

Figure 4.1 XRD pattern of a) CuO b) NiS c) CuO, NiS, CNS_{400}, CNS_{600}, CNS_{800}

4.2 Morphology analysis by Scanning Electron Microscope

Scanning electron microscopy (SEM) is a widely used technique to examine the surface morphology of electrocatalysts. In this study, SEM analysis was performed on CuO, NiS, and CNS_{600} electrocatalysts, and the results are presented in Figure 4.2. The SEM images clearly show that CuO particles (Figure 4.2b) have a spherical shape and are randomly dispersed. The NiS particles shown in Figure 4.2c exhibit significant clustering, leading to the formation of larger particles with numerous interconnected porous spaces. These serve as reservoirs for electrolytes, potentially enhancing the electrocatalytic activity (Edison et

al., 2020). In Figure 4.2d, the scanning electron microscope (SEM) image of NiS/CuO reveals that spherical CuO nanoparticles are covered with the porous spaces of NiS. The surface of the nickel foam substrate is observed to be covered with these particles, without any visible cracks or spalling. This indicates that the NiS/CuO composite exhibit strong mechanical adhesion to the nickel foam substrate. Moreover, the heterostructure possesses a porous configuration that allows for the exposure of abundant active sites and facilitates rapid diffusion of ions and efficient conduction of charges during electrochemical reactions (Liu, Cao, & Cheng, 2021). This advantageous structure renders it highly suitable for catalytic purposes. The examination of the scanning electron microscopy (SEM) image verified the successful creation of a hierarchical NiS/CuO heterostructure.

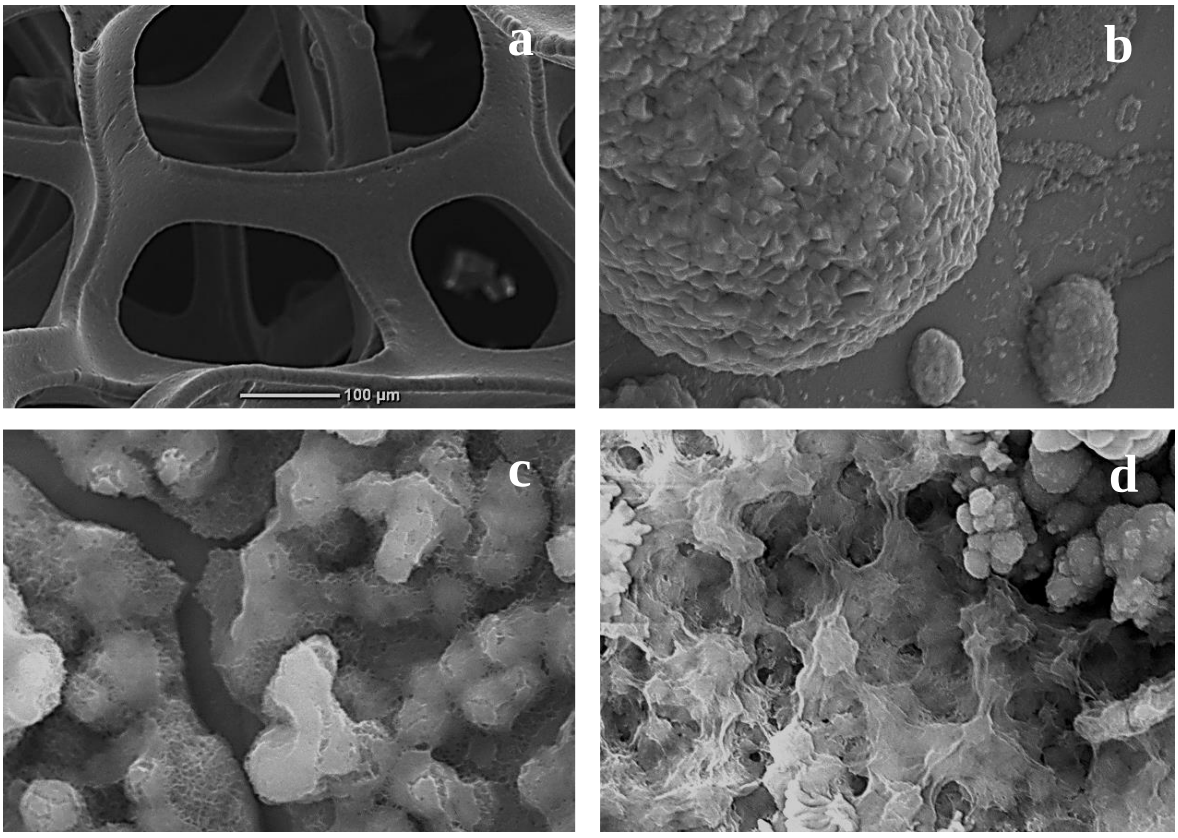

Figure 4.2 Scanning electron microscopy images a) NF b) CuO c) NiS d) CNS_{600}

4.3 Electrochemical analysis in acidic electrolyte

4.3.1 Catalytic Activity for HER

The electrocatalytic performance of CNS_{600} was evaluated in an acidic environment using 0.5 M H_2SO_4 at a scan rate of 2 mV/s. Contrastive samples, including NF, CuO, NiS, CNC_{400}, and CNS_{800}, were also tested. All potentials were determined relative to the RHE and calculated using Equation 3.1. The electrocatalytic activity of CuO, NiS, CNS_{400}, CNS_{600}, and CNS_{800} toward HER was analyzed using LSV in an acid electrolyte. The LSV curves for all materials were obtained, and the results indicated that all catalysts displayed cathodic current increase with potentials, indicating HER occurrence. Figure 4.3 a) shows the polarization curves for CuO, NiS, and CNS_{400}, CNS_{600}, and CNS_{800} electrocatalysts in acidic media. The CNS_{600} composite for HER exhibits a low overpotential of about 260mV at 10 mA/cm^2 compared to the pristine CuO and NiS electrocatalysts. The overpotentials of other samples to attain the geometrical current density of 10 mA/cm^2 were 300, 310, 290,270 mV CuO, NiS, CNS_{400}, and CNS_{800}, respectively. Figure 4.3(b) presents the recorded overpotentials at various current densities. The analysis of the results revealed that CNS_{600} had the highest catalytic activity for HER followed by CNS_{800} and CNS_{400}, indicating that the addition of more nickel sulfide (NiS) to copper oxide (CuO) enhances the catalytic activity of the resulting electrocatalyst. The voltage required for catalytic activity decreased as the amount of NiS increased, with CNS_{600} showing the lowest overpotential. The study also revealed that CNS_{600} had better HER performance compared to pure copper oxide (CuO) and nickel sulfide (NiS), suggesting the synergistic effect of the CuO and NiS combination in HER catalysis.

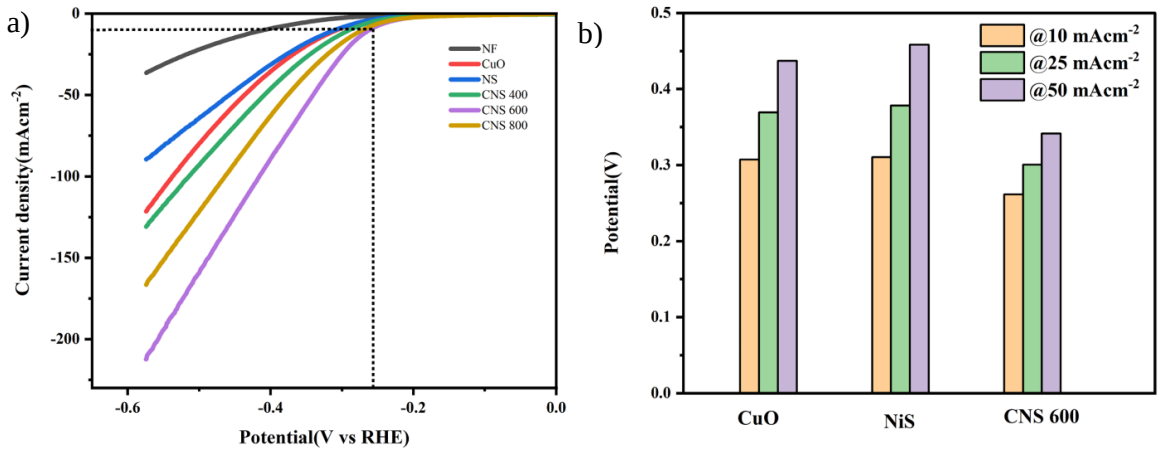

Figure 4.3 (a) HER Polarization curves obtained through linear sweep voltammetry (LSV). (b) Comparison of overpotentials at various geometrical current densities.

Furthermore, the assessment of the electrochemical active surface area (ECSA), a crucial factor for evaluating the effectiveness of electrocatalysts, was carried out by employing C_{dl}. These capacitances were obtained from cyclic voltammetry (CV) measurements within a non-Faradaic process range (illustrated in Figure 4.4a - e), which exhibit a linear relationship with the ECSA. Figure 4.3f illustrates a linear correlation between scan rates and current densities, where C_{dl} is half of the slope value (S Anantharaj et al., 2018). By using the measured C_{dl} value, the corresponding ECSA was calculated using Equation 3.5.

Typically, the specific capacitance (Cs) of a flat surface is estimated to be 40 μF cm^{-2}, based on previous literature (Wenjuan Zhang et al., 2019; Zhou et al., 2018). As shown in Figure 4.3, CNS_{600} exhibits a higher Cdl value (8.35 μF cm^{-2}) compared to CNS_{400}(4.4 μF cm^{-2}), CNS_{800}(5.33 μF cm^{-2}) CuO/NF (2.2 μF cm^{-2}) and NiS/NF (4.2 μF cm^{-2}), indicating that CNS_{600} possesses the largest ECSA among the synthesized electrocatalysts. The ECSA of CNS_{600} is 0.208 cm^2 which is greater than that of CNS_{800}(0.133 cm^2), CNS_{400}(0.11 cm^2) CuO/NF (0.055 cm^2), and NiS/NF (0.105 cm^2) indicating a vast number of exposed active sites. This implies that CNS_{600} has a greater number of exposed active sites on its surface, demonstrating that the fabricated heterostructures are advantageous for generating a higher quantity of electrochemically accessible active sites (Ying Wang et al., 2021).

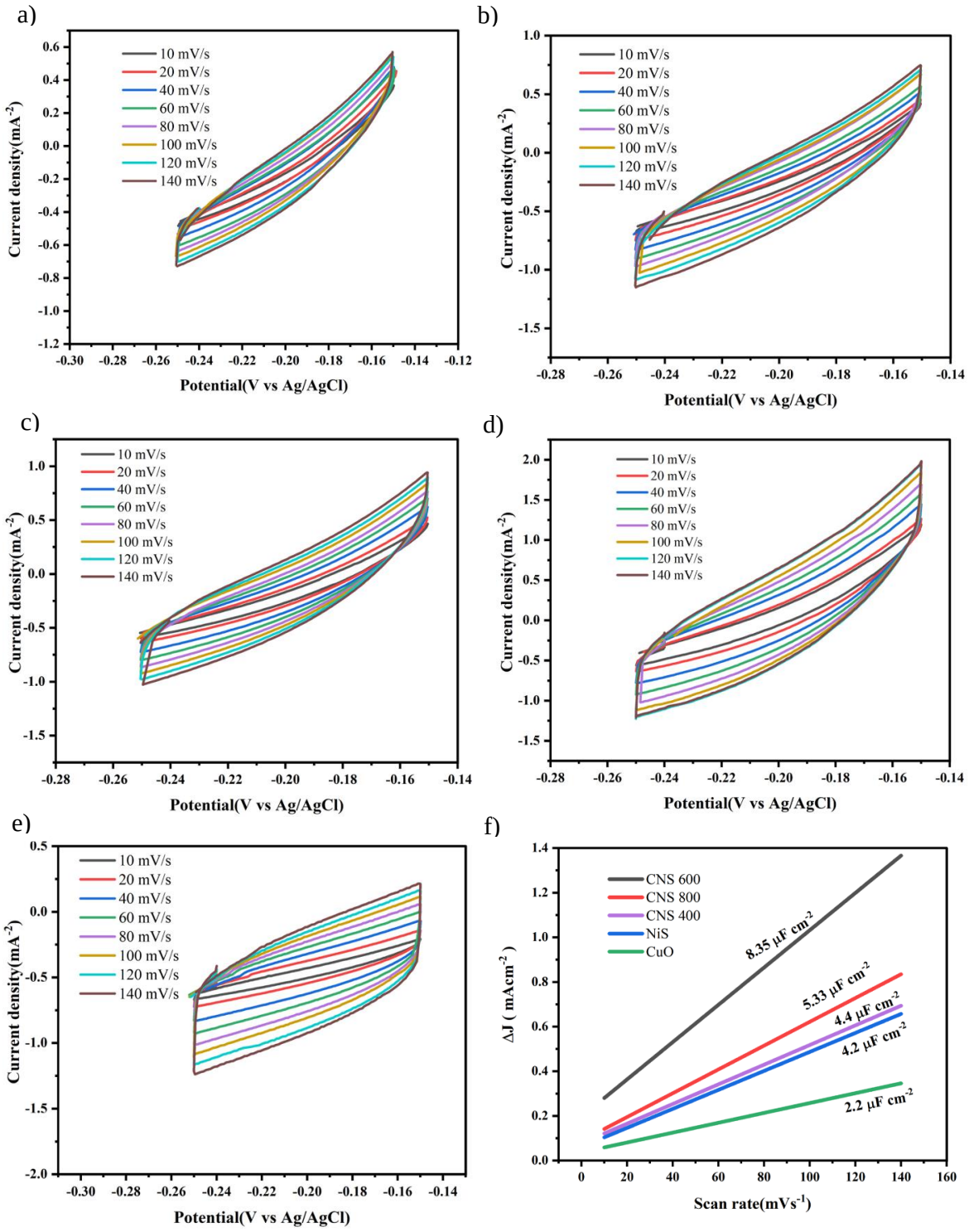

Figure 4.4 Cyclic voltammograms recorded for samples (a)CuO, (b)NiS, (c)CNS_{400}, (d)CNS_{600}, and (e) CNS_{800} in 0.5 M H_2SO_4 at various scan rates in the double layer charging region. (f) The plot of capacitive current obtained at -0.2V against sweep rate.

4.3.2 HER kinetics and Tafel-slopes

In order to examine the rate at which charge transfers occur during HER, EIS was utilized. Fig. 4.5 displays the Nyquist plots obtained at a fixed HER potential of 200 mV vs RHE. The collected data were then analyzed using the built-in Z-fit EIS analysis software of the electrochemical workstation where a constant phase element (CPE) represents the departure from ideal capacitance behavior, which exhibits a dependence on frequency, a series resistance (Rs), and charge transfer resistance (Rct). Among the as-prepared catalysts, CNS_{600} exhibits the lowest charge transfer resistance (R_{ct}, 28.96 $\Omega \cdot cm^2$) suggesting a fast charge transfer for HER. The charge transfer resistance of CNS_{600} is significantly lower than that of CuO, NiS, CNS_{400}, and CNS_{800} indicating that the incorporated NiS improves the electrical conductivity.

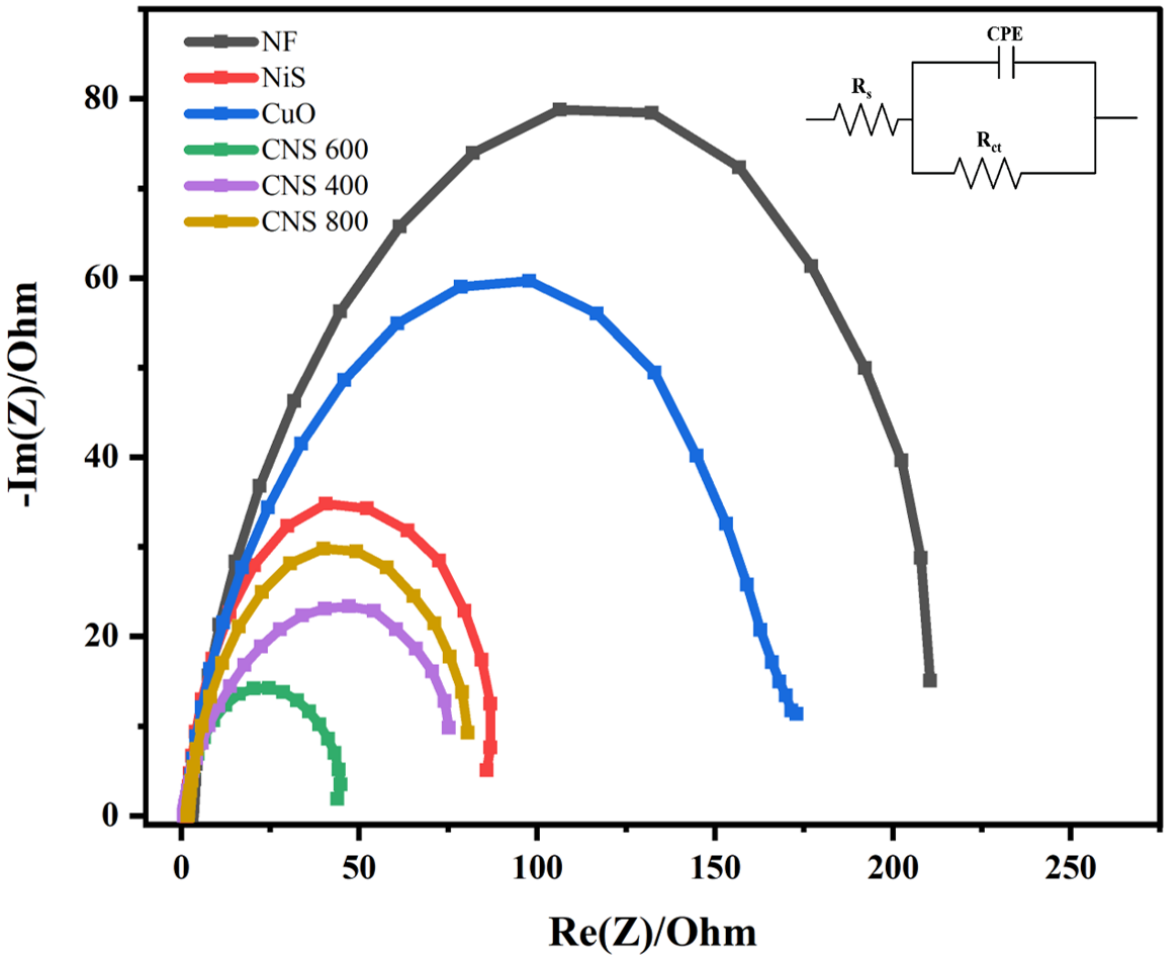

Figure 4.5 EIS characterization of samples. (a) Nyquist plots of different samples at a current density of 10 mA cm^{-2} in 0.5 M H_2SO_4. (b) Simulated equivalent circuit

Table 4-1 Data from fitting the impedance data to an equivalent circuit in acidic medium

Catalyst	**Solution Resistance (Rs, Ω)**	**Charge Transfer resistance (Rct, Ω)**	**Constant Phase Element (CPE, F)**
NF	3.013	189.5	0.203
CuO/NF	4.115	143	0.00189
NiS/NF	1.517	76.56	0.00315
CNS/NF 400	1.297	35.07	0.0026
CNS/NF 600	1.624	28.96	0.00663
CNS/NF 800	1.735	49.69	0.00348

The Tafel slope, which is an inherent property of electrocatalysts, can be utilized to determine the elementary steps involved in the process of hydrogen evolution reaction (HER). The overall reaction in the acid solution for HER consists of three principal steps as given in eqn. 2.6, 2.8, and 2.10 (D. J. Li et al., 2014).

The HER elementary reaction steps can be described as a three-state process comprising the initial state (H^+), adsorbed intermediate state (H*), and terminal product ($1/2H_2$). The rate-limiting step of HER can be inferred from the Tafel slope, which indicates different reaction mechanisms via Volmer-Heyrovsky or Volmer-Tafel reaction. The Tafel slopes derived from the linear portion of the corresponding polarization curves presented in Figure 4.6, the CNS_{600} shows small Tafel slope of 47.4 $mV \cdot dec^{-1}$, which is lower than those of the CNS_{400} (98.8 $mV \cdot dec^{-1}$), CNS_{800} (53.7 $mV \cdot dec^{-1}$), CuO/NF (117.7 $mV \cdot dec^{-1}$), NiS/NF(56.5 $mV \cdot dec^{-1}$) and NF (119.2 $mV \cdot dec^{-1}$) which implies that the fast electron transfer (better kinetics) (Sengeni Anantharaj, Sugime, & Noda, 2021). In addition, the Tafel slope for CNS_{600} is within the range between 40 and 120 mV dec^{-1}, indicating that the HER process may follow the Volmer-Heyrovsky mechanism on the electrode surface (C. Dong et al., 2017). The low Tafel slope suggests that the initial step of HER happens rapidly, known as the Volmer step, followed by a slower electrochemical desorption step, known as the Heyrovsky step and the rate-limiting step for the HER is the desorption of hydrogen (Solomon et al., 2019; Tong et al., 2017).

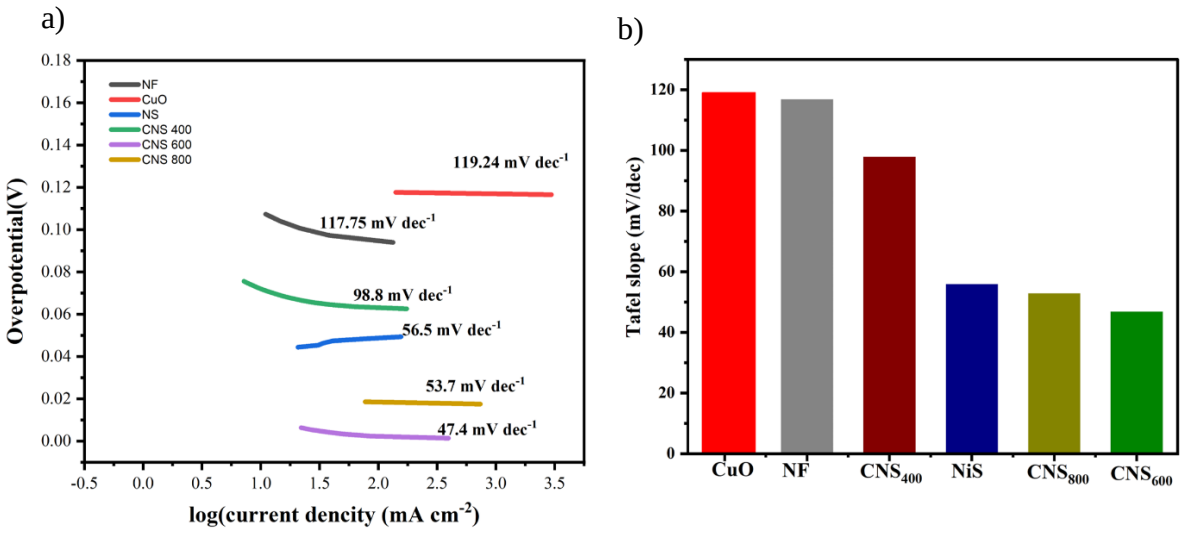

Figure 4.6 (a) Tafel plots of NF, CuO, NiS, CNS_{400}, CNS_{600}, CNS_{800} and (b) comparison of Tafel slope values

4.4 Electrochemical analysis in alkaline electrolyte

4.4.1 Investigating Catalytic Activity for HER

Apart from the acidic medium, the electrocatalytic activity of samples towards the hydrogen evolution reaction (HER) was also examined using a three-electrode setup in a 1.0 M KOH solution. The results were compared to experiments carried out using CuO and NiS. The obtained polarization curves for CuO, NiS, CNS_{400}, CNS_{600}, and CNS_{800} are presented in Figure 4.7a. The CNS_{600} exhibited a current density of 10 mA cm^{-2} at an overpotential (η_{10}) of 170 mV, which is comparable to and better than some recently reported non-noble metal electrocatalysts. CuO, NiS, $CNC_{400,}$ and CNS_{800} achieved 10 $mAcm^{-2}$ current density at overpotentials of 370, 240, 216, and 240 mV respectively. Figure 4.7b demonstrates the recorded overpotentials for various current densities. CuO achieved a current density of j = 50 $mAcm^{-2}$ at an overpotential of 570mV, whereas NiS achieved j = 50 mA cm^{-2} at overpotentials of 430mV, whereas CNS_{600} achieved j = 50 mA cm^{-2} at overpotentials of 320mV.

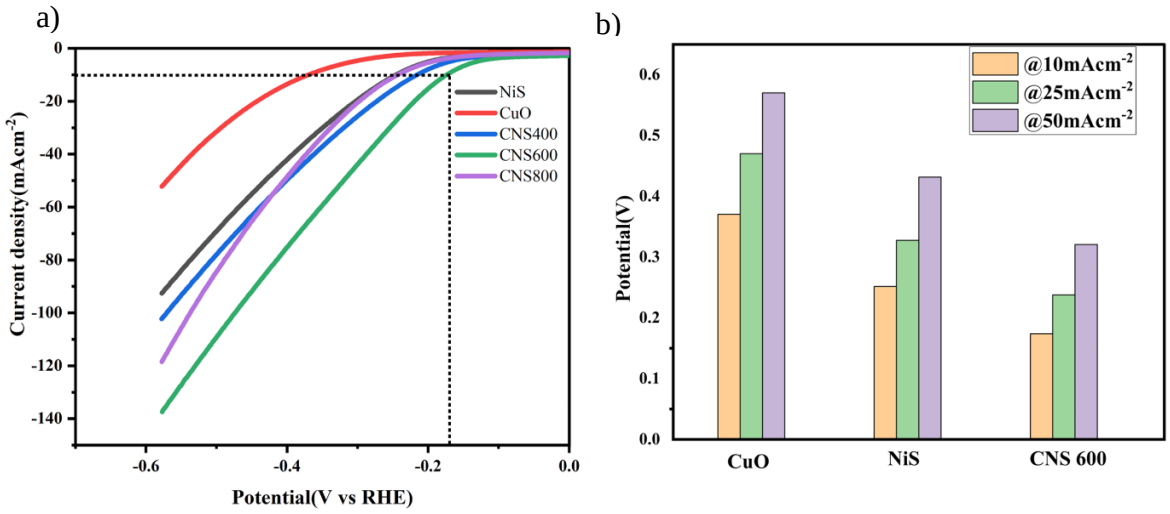

Figure 4.7 (a) The polarization curves of the LSV for HER. (b) Contrasting overpotentials at varying geometric current densities.

The ECSA was evaluated by calculating the C_{dl} at the solid/liquid interface using cyclic voltammetry (CV) scans at different scan rates in the non-faradic region (Xinyi Li et al., 2020). Figures 4.8 exhibit the CV obtained in the non-faradic region by sweeping the scan rates from 10 to 140 mV/s, where the current response solely results from double-layer charging (Y. Wang et al., 2020). The C_{dl} was determined by calculating the slope of the linear polynomial plot of the difference between anodic and cathodic current versus the scan rate, as shown in Fig. (4.8). The values of C_{dl} for CNS_{600} sample is higher, 33.89 ηF/cm^{-2}, compared to CNS_{400}(19.2 μF cm^{-2}), CNS_{800}(18.54 μF cm^{-2}), NiS/NF (16.6 μF cm^{-2}) and CuO/NF (13.17 μF cm^{-2}). The ECSA of CNS_{600} is 0.847 cm^2 which is greater than that of CNS_{400}(0.48 cm^2), CNS_800(0.463 cm^2) CuO/NF (0.329 cm^2), and NiS/NF (0.415 cm^2) indicating a vast number of exposed active sites. These values indicate a greater surface roughness, resulting in more active sites being exposed, ultimately leading to higher activity for HER (Q. Liu et al., 2018).

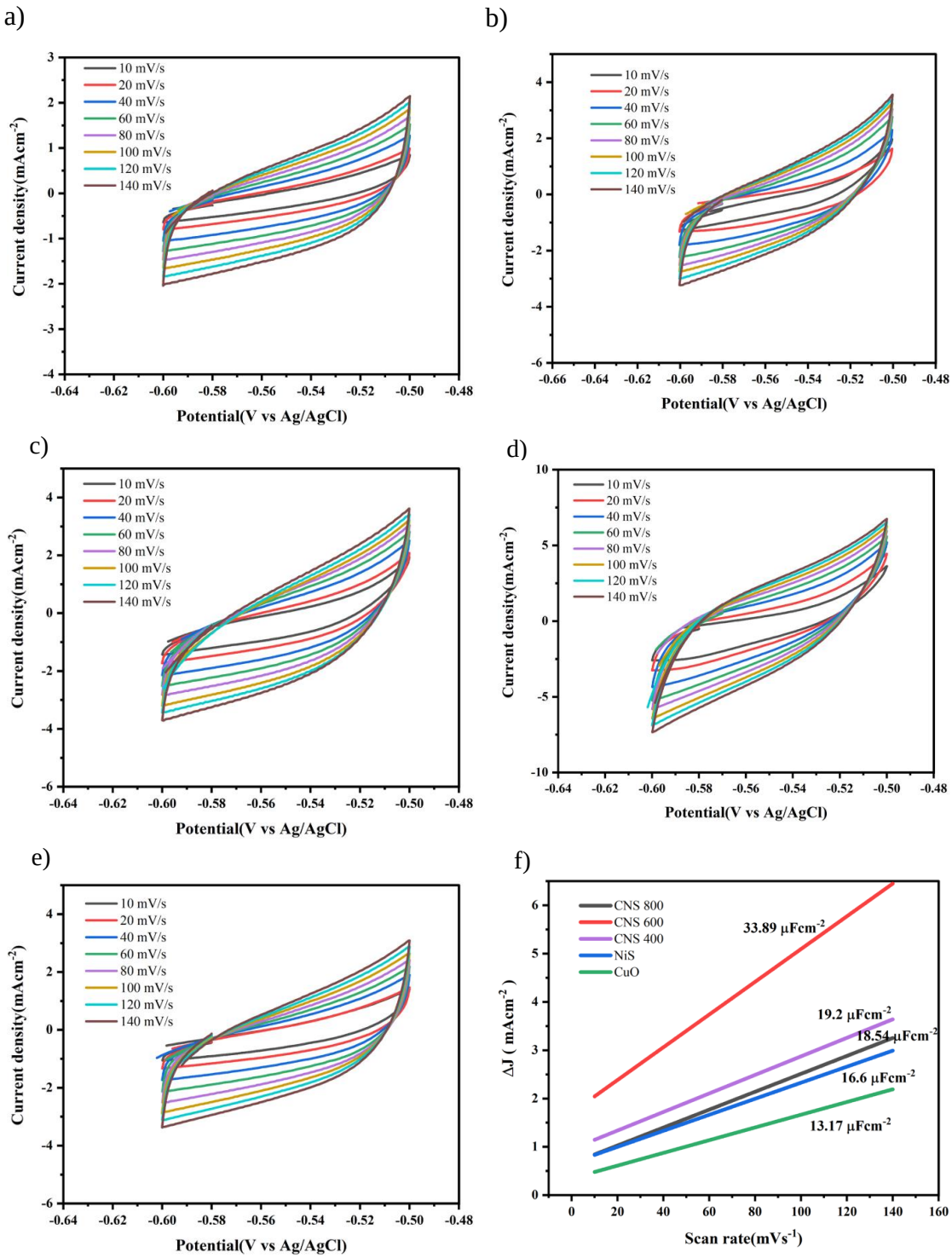

Figure 4.8 Cyclic voltammograms recorded for samples (a)CuO, (b)NiS, (c)CNS_{400}, (c)CNS_{600}, and (d)CNS_{800} in 1.0 M KOH at various scan rates in the double layer charging region. (d) A plot of capacitive current obtained at -0.55V against sweep rate.

4.4.2 HER kinetics and Tafel-slopes

The HER electrocatalytic performance is significantly impacted by the rate of charge transfer occurring at the surface of the catalyst (Ding et al., 2019). (EIS) was used to analyze the electrode resistance and charge transfer capacity and the resulting Nyquist plots were depicted in Figure 4.9. The equivalent circuit diagram shown in Figure 4.9 was used to fit the Nyquist plots within inbuilt Z fit software, which included a series resistance (Rs), charge transfer resistance (Rct), and Constant Phase Element (CPE). In order to make a comparison between the results, electrochemical impedance spectroscopy (EIS) experiments were conducted for the hydrogen evolution reaction (HER) at a fixed potential of -0.170 V vs RHE. Among the tested samples, CNS_{600} exhibited the smallest semicircle in the lower frequency region as shown in Table 4.2, indicating the lowest charge transfer resistance (Rct) when compared to CuO, NiS, $CNC_{400,}$ and CNS_{800}. This suggests that CNS_{600} has a better ability to combine electrons and H_{ads}, as well as reduce ohmic losses (Z. Peng, Jia, Al-Enizi, Elzatahry, & Zheng, 2015).

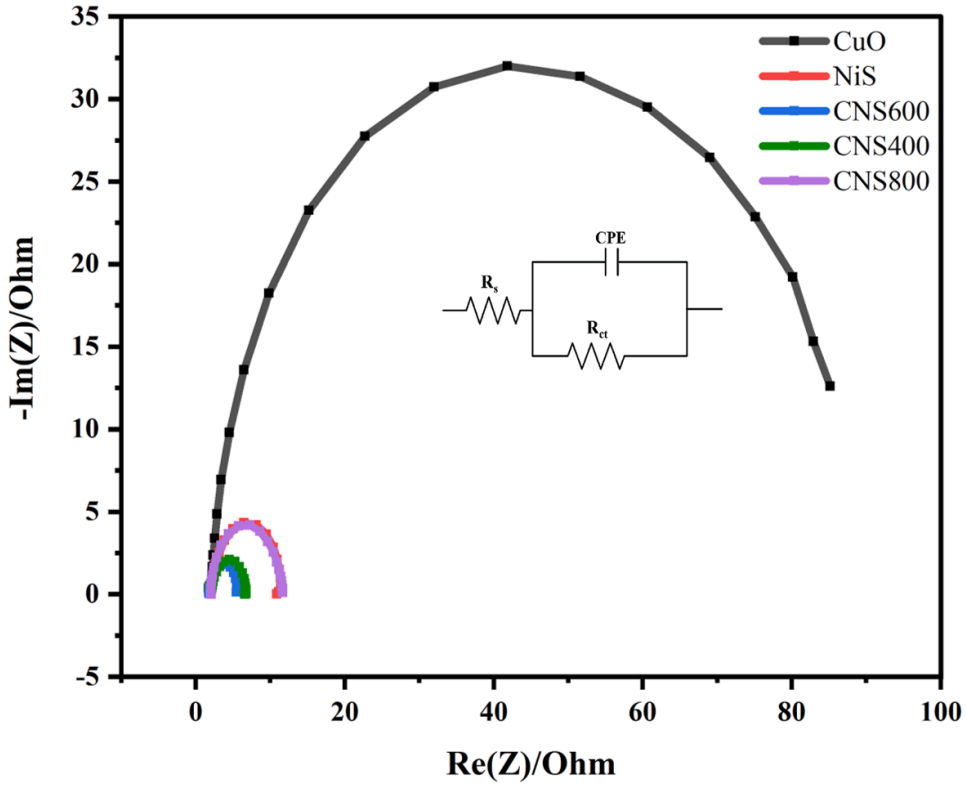

Figure 4.9 Nyquist plots of different samples reflecting the charge transfer resistance at a current density of 10 mA cm^{-2} from 1 MHz to 10 mHz in 1 M KOH.

Table 4-2 Data from fitting the impedance data to an equivalent circuit in basic medium

Catalyst	**Solution Resistance (Rs, Ω)**	**ChargeTransfer resistance (Rct, Ω)**	**Constant Phase Element (CPE, F)**
CuO/NF	2.036	74.37	0.00306
NiS/NF	1.994	8.246	0.933
CNS/NF 400	2.434	4.465	0.0038
CNS/NF 600	1.81	3.467	0.00631
CNS/NF 800	1.712	9.13	0.0057

The Tafel slopes derived from the respective LSV curves are provided in Figure 4.10 revealing that the Tafel slope of CNS $_{600}$ was 117 mV dec^{-1}, which is lower than that of CuO (200 mV dec^{-1}), NiS(161 mV dec^{-1}), CNC_{400} (136 mV dec^{-1}) and CNS_{800} (158 mV dec^{-1}) which demonstrates that the CNS_{600} tend to have a good catalytic ability and high conductivity and hence results in more rapid charge and kinetic gas transfer compared to CuO, NiS, $CNC_{400,}$ and CNS_{800}. It is commonly recognized that HER in alkaline conditions involves the dissociation of water, followed by the adsorption of H (Volmer step), and then either the chemical (Tafel) or electrochemical (Heyrovsky) desorption of H_{ads}. The Tafel slope can be employed for identifying the rate-determining step in an electrochemical reaction. The Tafel slope of CNS_{600} falls within the range of 40 to 120 mV dec^{-1}, suggesting that the hydrogen evolution reaction (HER) on the electrode surface likely proceeds through the Volmer-Heyrovsky mechanism (C. Dong et al., 2017). In this, the obtained findings indicated that the Volmer step served as the rate-determining step (eqn 2.7).The observed small Tafel slope values suggest that the CNS_{600} tends to have faster kinetics (Chinnadurai, Rajendiran, & Kandasamy, 2022).

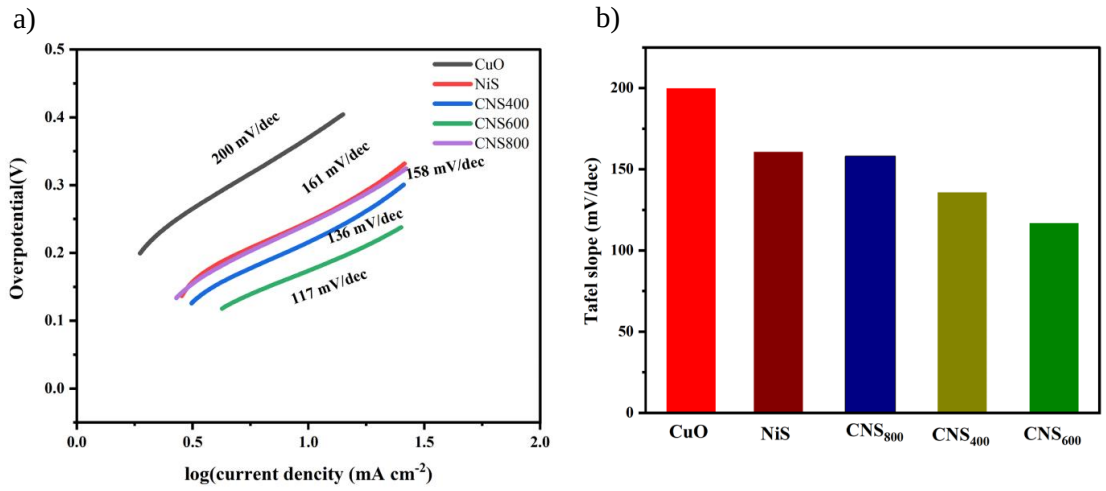

Figure 4.10 (a)Tafel plots of CuO, NiS, CNS_{400}, CNS_{600}, CNS_{800} and (b) comparison of Tafel slope values

4.5 The turnover frequencies of HER for catalysts

In order to strengthen the evidence of the HER intrinsic catalytic activity of samples, additional calculations were performed to determine the TOF. Turnover frequency is calculated by measuring the active sites from the integrated charges obtained from cyclic voltammograms in a pH=14 KOH solution. The surface-active site concentrations were calculated from the reduction region of CV curves measured at 50 mV/s and are found to be 0.02225×10^{19}. atoms cm^{-2}, 0.1052×10^{19}. atoms cm^{-2},$0. 33199 \times 10^{19}$. atoms cm^{-2}, 0.3615×10^{19}. atoms cm^{-2}, and 0.3418×10^{19}. atoms cm^{-2} active component CuO, NiS, CNC_{400}, $CNS_{600,}$ and CNS_{800} respectively. The addition of more nickel sulfide (NiS) to copper oxide (CuO) results in a slight increase in the concentrations number of active sites. The measured TOF at different overpotentials from Figure 4.11 ensures that sample CNS_{600} is having excellent intrinsic activity and higher hydrogen turnover per active site. The calculated TOF for CNS_{600} is found to be 0.2314 s^{-1} at 200 mV, which is higher than those of CuO(0.0144 s^{-1}), NiS(0.0672 s^{-1}), CNS_{400}(0.2126 s^{-1}), and CNS_{800}(0.21889 s^{-1}), indicating the superior intrinsic HER activity of CNS_{600} (N. Zhang et al., 2019).

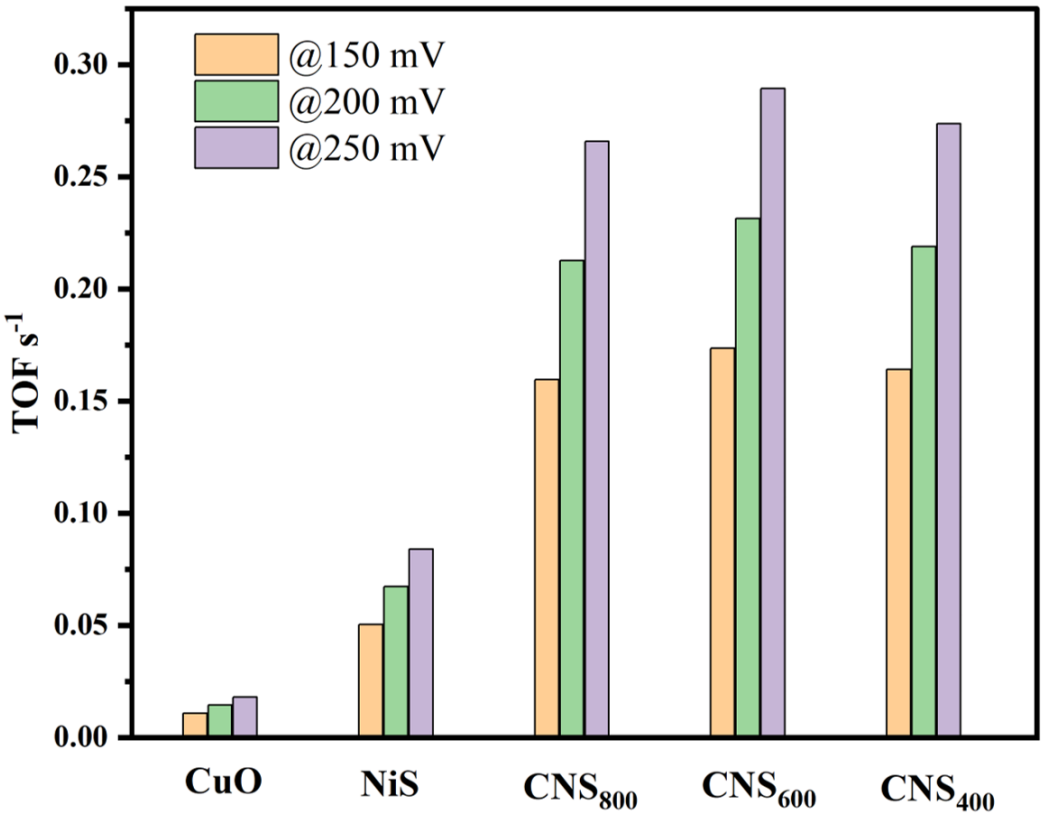

Figure 4.11 TOF values measured at various overpotential

4.6 Long-term Durability

Long-term stability in water electrolysis is a crucial prerequisite for electrocatalysts intended for industrial applications. The stability of the CNS_{600} composite electrocatalyst was evaluated using Chronoamperometry, as shown in Figure 4.12 Significantly, it is noteworthy that the electrocatalyst exhibits a sustained current at a constant potential of 0.26V and 0.17V vs RHE in acidic and basic medium respectively after a certain duration. These observations suggest that the composite electrode demonstrates high stability for a minimum of 8 hours in acidic conditions and at least 18 hours in alkaline environments. No current drop was observed beyond these time intervals, indicating the excellent mass transport, conductivity, and mechanical robustness of the electrode material leading to the conclusion that the CNS_{600} electrocatalyst possesses considerable long-term stability (M. Guo et al., 2020).

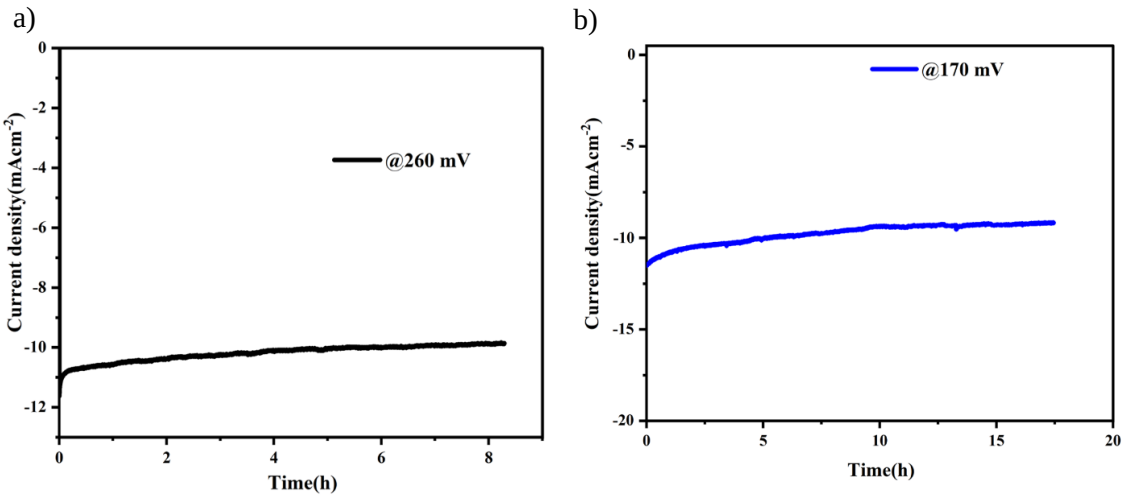

Figure 4.12 (a) Chronoamperometry stability test for CNS_{600} in acidic medium (b) Chronoamperometry stability test for CNS_{600} in alkaline medium

Table 4-3 Comparison of the electrocatalytic activity of the as-prepared NiS/CuO (current density of 10 mA cm^{-2}) heterostructure toward HER with previously reported electrocatalysts.

Catalysts	**Electrolyte**	**η (mV)**	**Tafel slope (mV dec^{-1})**	**Stability**	**Refs.**
NiS/CuO	1 KOH	170	47.4	18h	This work
NiS/CuO	0.5H_2SO_4	260	117	8h	This work
Co_3O_4-CuO	1 KOH	288	65	2000cycle	(Tahira et al., 2019)
Cu_2O/Co_3O_4	0.5H_2SO_4	160	73	10,000s	(Jin & Chen, 2018)
NiO/Co_3O_4	1 KOH	170	119	20h	(Wei et al., 2019)
$Ni_xS_y@MnO_xH_y$	1 KOH	179	95.1	100h	(P. Wang et al., 2022)
WS_2/WO_3	0.5H_2SO_4	395	50	2000cycle	(Shang, Rao, et al., 2017)
$MoSe_2/MoO_3$	0.5H_2SO_4	221	56	7000s	(Xia et al., 2018)
MoS_2/Co_3O_4	1 KOH	205	98	14hr	(Muthurasu et al., 2019)
MoS_2/Ti_4O_7	0.5H_2SO_4	287	48	1000cycle	(J. Zhao et al., 2020)
CoO/Fe_3O_4	1 KOH	220	73	10hr	(Adamson et al., 2020)
Co_3O_4/Fe_3O_4	1 KOH	370	117	14hr	(Ng et al., 2017)

5. CONCLUSION AND RECOMMENDATIONS

5.1 Conclusions

In summary, this study successfully synthesized a heterostructure-based electrocatalyst CNS_{600} through a two-step electrochemical deposition for HER. The synthesized electrocatalyst exhibited tolerable stability, efficiency, and cost-effectiveness. Crystal structure characterization and morphology analysis were conducted using FE-SEM and XRD techniques. Polarization curves were measured at a scan rate of 2 mV/s in 0.5 M H_2SO_4 and 1 M KOH solutions and the optimized CNS_{600} electrode achieved remarkable results, with low overpotentials of 170 mV and 260 mV required to reach a cathodic current density of 10 mA cm^{-2} in 1 M KOH and 0.5 M H_2SO_4 electrolytes, respectively. The corresponding Tafel slopes in acidic and basic medium were found to be 47.4 mV dec^{-1} and 117 mV dec^{-1}, respectively. The excellent electrocatalytic activity of the prepared catalyst can be attributed to the elimination of a binder during electrode fabrication, the formation of a NiS/CuO heterostructure that enhances charge transfer efficiency, and an increase in the number of active sites. Furthermore, the composite system displayed good stability, maintaining its integrity for at least 8 hours in acidic media and 18 hours in alkaline media during operation. The results also demonstrated the effectiveness and simplicity of the two-step electrodeposition process in creating heterostructure electrocatalysts and adjusting their activity.

5.2 Recommendations

To enhance the electrocatalytic performance of NiS/CuO in the practical application of the HER, several avenues can be explored. The following recommendations can be implemented to ensure the completion of the research work. Additionally, there are further recommendations for utilizing NiS/CuO in the oxygen evolution reaction (OER) and supercapacitor applications.

1) Active Site Engineering: explore methods to engineer and enhance the number of active sites in the NiS/CuO/NF catalyst. Investigate approaches such as introducing defects, doping, or surface modification to increase the density of active sites and improve the catalyst's performance for HER.
2) Mechanistic Understanding: conduct in-depth mechanistic studies to gain a comprehensive understanding of the reaction kinetics and catalytic mechanisms involved in the NiS/CuO/NF electrocatalysis. Employ advanced characterization techniques and theoretical modeling to elucidate the active sites, charge transfer processes, and reaction pathways. Employ techniques like in-situ spectroscopy or density functional theory (DFT) calculations to elucidate the underlying processes and identify the rate-determining steps.
3) Comparative Studies: conduct comparative studies with other commonly used catalysts such as Pt.
4) OER Application: to expand the application of NiS/CuO, it is advisable to explore its potential in the oxygen evolution reaction (OER).
5) Supercapacitor Application: further investigations should be conducted to assess the suitability of NiS/CuO as an electrode material for supercapacitors.

REFERENCES

Adamson, W., Bo, X., Li, Y., Suryanto, B. H., Chen, X., & Zhao, C. (2020). Co-Fe binary metal oxide electrocatalyst with synergistic interface structures for efficient overall water splitting. *Catalysis Today, 351*, 44-49.

Albonetti, S., Perathoner, S., & Quadrelli, E. A. (2019). *Horizons in sustainable industrial chemistry and catalysis*: Elsevier.

Albu, Z., Al Abass, N., & AlOtaibi, B. (2023). Electrodeposition of Hierarchical Nanosheet of NiCo 2 O 4/CC as Highly Active and Stable Electrode for Water Oxidation. *International Journal of Energy Research, 2023*.

An, L., Huang, L., Zhou, P., Yin, J., Liu, H., & Xi, P. (2015). A self-standing high-performance hydrogen evolution electrode with nanostructured NiCo2O4/CuS heterostructures. *Advanced Functional Materials, 25*(43), 6814-6822.

An, L., Huang, L., Zhou, P., Yin, J., Liu, H., & Xi, P. s. h. h. N. h. (2015). Adv. Funct. *Mater., 25*, 6814-6822.

Anantharaj, S., Ede, S., Karthick, K., Sankar, S. S., Sangeetha, K., Karthik, P., & Kundu, S. (2018). Precision and correctness in the evaluation of electrocatalytic water splitting: revisiting activity parameters with a critical assessment. *Energy & Environmental Science, 11*(4), 744-771.

Anantharaj, S., Ede, S. R., Sakthikumar, K., Karthick, K., Mishra, S., & Kundu, S. (2016). Recent trends and perspectives in electrochemical water splitting with an emphasis on sulfide, selenide, and phosphide catalysts of Fe, Co, and Ni: a review. *Acs Catalysis, 6*(12), 8069-8097.

Anantharaj, S., Sugime, H., & Noda, S. (2020). Ultrafast growth of a Cu (OH) 2–CuO nanoneedle array on Cu foil for methanol oxidation electrocatalysis. *ACS Applied Materials & Interfaces, 12*(24), 27327-27338.

Anantharaj, S., Sugime, H., & Noda, S. (2021). Surface amorphized nickel hydroxy sulphide for efficient hydrogen evolution reaction in alkaline medium. *Chemical Engineering Journal, 408*, 127275.

Anwar, S., Khan, F., Zhang, Y., & Djire, A. (2021). Recent development in electrocatalysts for hydrogen production through water electrolysis. *International Journal of Hydrogen Energy, 46*(63), 32284-32317.

Askari, M. B., & Salarizadeh, P. (2019). Superior catalytic performance of NiCo2O4 nanorods loaded rGO towards methanol electro-oxidation and hydrogen evolution reaction. *Journal of Molecular Liquids, 291*, 111306.

Bockris, J. O. M., & Appleby, A. (1972). Hydrogen economy-an ultimate economy. Practical answer to the problem of energy supply and pollution. *Environ. This Mon.;(United Kingdom), 1*(1).

Cammack, R., Frey, M., & Robson, R. (2001). *Hydrogen as a fuel: learning from nature*: CRC Press.

Chen, D., Chen, C., Baiyee, Z. M., Shao, Z., & Ciucci, F. (2015). Nonstoichiometric oxides as low-cost and highly-efficient oxygen reduction/evolution catalysts for low-temperature electrochemical devices. *Chemical reviews, 115*(18), 9869-9921.

Chen, G., Wang, T., Zhang, J., Liu, P., Sun, H., Zhuang, X., . . . Feng, X. (2018). Accelerated hydrogen evolution kinetics on NiFe-layered double hydroxide electrocatalysts by tailoring water dissociation active sites. *Advanced Materials, 30*(10), 1706279.

Chen, J., Yu, D., Liao, W., Zheng, M., Xiao, L., Zhu, H., . . . Yao, J. (2016). WO3–x nanoplates grown on carbon nanofibers for an efficient electrocatalytic hydrogen evolution reaction. *ACS Applied Materials & Interfaces, 8*(28), 18132-18139.

Chen, L., Zhang, J., Ren, X., Ge, R., Teng, W., Sun, X., & Li, X. (2017). A Ni (OH) 2–CoS 2 hybrid nanowire array: a superior non-noble-metal catalyst toward the hydrogen evolution reaction in alkaline media. *Nanoscale, 9*(43), 16632-16637.

Chen, Z., Duan, X., Wei, W., Wang, S., & Ni, B.-J. (2019). Recent advances in transition metal-based electrocatalysts for alkaline hydrogen evolution. *Journal of Materials Chemistry A, 7*(25), 14971-15005.

Chinnadurai, D., Rajendiran, R., & Kandasamy, P. (2022). Bimetallic copper nickel sulfide electrocatalyst by one step chemical bath deposition for efficient and stable overall water splitting applications. *Journal of Colloid and Interface Science, 606*, 101-112.

Chinnadurai, D., Rajendiran, R., Li, O. L., & Prabakar, K. (2021). Mn-Co bimetallic phosphate on electrodeposited PANI nanowires with composition modulated structural morphology for efficient electrocatalytic water splitting. *Applied Catalysis B: Environmental, 292*, 120202.

Curie, M. (2013). Renewable Hydrogen Technologies: Production. *Purification, Storage, Applications and Safety, 43*.

Dai, J., Zhu, Y., Zhong, Y., Miao, J., Lin, B., Zhou, W., & Shao, Z. (2019). Enabling high and stable electrocatalytic activity of iron-based perovskite oxides for water splitting by combined bulk doping and morphology designing. *Advanced Materials Interfaces, 6*(1), 1801317.

Dalai, N., Mohanty, B., Mitra, A., & Jena, B. (2019). Highly active ternary nickel–iron oxide as bifunctional catalyst for electrochemical water splitting. *ChemistrySelect, 4*(27), 7791-7796.

De Luna, P., Hahn, C., Higgins, D., Jaffer, S. A., Jaramillo, T. F., & Sargent, E. H. (2019). What would it take for renewably powered electrosynthesis to displace petrochemical processes? *Science, 364*(6438), eaav3506.

Deng, S., Zhong, Y., Zeng, Y., Wang, Y., Wang, X., Lu, X., . . . Tu, J. (2018). Hollow TiO2@ Co9S8 core–branch arrays as bifunctional electrocatalysts for efficient oxygen/hydrogen production. *Advanced Science, 5*(3), 1700772.

Dincer, I., & Acar, C. (2018). Smart energy solutions with hydrogen options. *International Journal of Hydrogen Energy, 43*(18), 8579-8599.

Ding, J., Wang, P., Ji, S., Wang, H., Brett, D. J., & Wang, R. (2019). Mesoporous nickel selenide N-doped carbon as a robust electrocatalyst for overall water splitting. *Electrochimica Acta, 300*, 93-101.

Doman, L. (2017). TODAY IN ENERGY. *U.S.Energy information Administration*. Retrieved from https://www.eia.gov/todayinenergy/detail.php?id=32912#

Dong, C., Liu, X., Wang, X., Yuan, X., Xu, Z., Dong, W., . . . Huang, F. (2017). Hierarchical Ni/NiTiO 3 derived from NiTi LDHs: a bifunctional electrocatalyst for overall water splitting. *Journal of Materials Chemistry A, 5*(47), 24767-24774.

Dong, W., Zhang, Y., Xu, J., Yin, J.-W., Nong, S., Dong, C., . . . Si, R. (2020). Subnano ruthenium species anchored on tin dioxide surface for efficient alkaline hydrogen evolution reaction. *Cell Reports Physical Science, 1*(3), 100026.

Draz, M. A., El-Maghrabi, H. H., Soliman, F. S., Selim, H., Razik, A. A., Amin, A. E.-s., . . . Nada, A. A. (2021). Large scale hybrid magnetic ZnFe 2 O 4/TiO 2 nanocomposite with highly photocatalytic activity for water splitting. *Journal of Nanoparticle Research, 23*, 1-10.

Dresselhaus, M. S., & Thomas, I. (2001). Alternative energy technologies. *Nature, 414*(6861), 332-337.

Du, X., Wang, Q., Li, Y., & Zhang, X. (2018). Oxide/sulfide-based hybrid arrays as robust electrocatalysts for water splitting. *Dalton Transactions, 47*(30), 10273-10280.

Du, X., Wang, Q., & Zhang, X. (2018). Controllable synthesis of NiO/Ni 3 S 2 hybrid arrays as efficient electrocatalysts for water splitting. *New Journal of Chemistry, 42*(22), 18201-18207.

Ebbinghaus, S. G. (2002). Ln1-xAxCoO3 (Ln= Er, La; A= Ca, Sr)/Carbon Nanotube composite materials applied for rechargeable Zn/Air batteries.

Edison, T. N. J. I., Atchudan, R., Karthik, N., Ganesh, K., Xiong, D., & Lee, Y. R. (2020). A novel binder-free electro-synthesis of hierarchical nickel sulfide nanostructures on nickel foam as a battery-type electrode for hybrid-capacitors. *Fuel*, *276*, 118077.

Elumeeva, K., Masa, J., Sierau, J., Tietz, F., Muhler, M., & Schuhmann, W. (2016). Perovskite-based bifunctional electrocatalysts for oxygen evolution and oxygen reduction in alkaline electrolytes. *Electrochimica acta*, *208*, 25-32.

Feng, J. X., Xu, H., Dong, Y. T., Lu, X. F., Tong, Y. X., & Li, G. R. (2017). Efficient hydrogen evolution electrocatalysis using cobalt nanotubes decorated with titanium dioxide nanodots. *Angewandte Chemie International Edition*, *56*(11), 2960-2964.

Gao, D., Liu, R., Biskupek, J., Kaiser, U., Song, Y. F., & Streb, C. (2019). Modular design of noble-metal-free mixed metal oxide electrocatalysts for complete water splitting. *Angewandte Chemie International Edition*, *58*(14), 4644-4648.

Gao, X., Zhang, H., Li, Q., Yu, X., Hong, Z., Zhang, X., . . . Lin, Z. (2016). Hierarchical NiCo2O4 hollow microcuboids as bifunctional electrocatalysts for overall water-splitting. *Angewandte Chemie International Edition*, *55*(21), 6290-6294.

Geng, S., Liu, Y., Yu, Y. S., Yang, W., & Li, H. (2020). Engineering defects and adjusting electronic structure on S doped MoO 2 nanosheets toward highly active hydrogen evolution reaction. *Nano Research*, *13*, 121-126.

Ghosh, S., & Basu, R. N. (2018). Multifunctional nanostructured electrocatalysts for energy conversion and storage: current status and perspectives. *Nanoscale*, *10*(24), 11241-11280.

Gicha, B. B., Tufa, L. T., Choi, Y., & Lee, J. (2021). Amorphous Ni1–x Fe x Oxyhydroxide Nanosheets with Integrated Bulk and Surface Iron for a High and Stable Oxygen Evolution Reaction. *ACS Applied Energy Materials*, *4*(7), 6833-6841.

Gileadi, E. (2011). Intermediates in Electrode Reactions. *Physical Electrochemistry, Fundamentals, Techniques and Applications; Wiley-VCH Verlag GmbH & Co. KGaA: Weinheim*, 151-164.

Gong, M., & Dai, H. (2015). A mini review of NiFe-based materials as highly active oxygen evolution reaction electrocatalysts. *Nano Research*, *8*(1), 23-39.

Gray, H. B. (2009). Powering the planet with solar fuel. *Nature chemistry*, *1*(1), 7-7.

Guan, S., Fu, X., Zhang, Y., & Peng, Z. (2018). β-NiS modified CdS nanowires for photocatalytic H 2 evolution with exceptionally high efficiency. *Chemical Science*, *9*(6), 1574-1585.

Guo, B., Sun, J., Hu, X., Wang, Y., Sun, Y., Hu, R., . . . Zhu, J. (2018). Fe3O4-CoP x Nanoflowers Vertically Grown on TiN Nanoarrays as Efficient and Stable Electrocatalysts for Overall Water Splitting. *ACS Applied Nano Materials*, *2*(1), 40-47.

Guo, J.-X., Yan, D.-Y., Qiu, K.-W., Mu, C., Jiao, D., Mao, J., . . . Ling, T. (2019). High electrocatalytic hydrogen evolution activity on a coupled Ru and CoO hybrid electrocatalyst. *Journal of Energy Chemistry*, *37*, 143-147.

Guo, M., Song, S., Zhang, S., Yan, Y., Zhan, K., Yang, J., & Zhao, B. (2020). Fe-Doped Ni–Co phosphide nanoplates with planar defects as an efficient bifunctional electrocatalyst for overall water splitting. *ACS Sustainable Chemistry & Engineering*, *8*(19), 7436-7444.

Guo, Y., Park, T., Yi, J. W., Henzie, J., Kim, J., Wang, Z., . . . Tang, J. (2019). Nanoarchitectonics for transition-metal-sulfide-based electrocatalysts for water splitting. *Advanced Materials*, *31*(17), 1807134.

Gupta, S., Yadav, A., Bhartiya, S., Singh, M., Miotello, A., Sarkar, A., & Patel, N. (2018). Co oxide nanostructures for electrocatalytic water-oxidation: effects of dimensionality and related properties. *Nanoscale*, *10*(18), 8806-8819.

Hao, Z., Yang, S., Niu, J., Fang, Z., Liu, L., Dong, Q., . . . Zhao, Y. (2018). A bimetallic oxide Fe 1.89 Mo 4.11 O 7 electrocatalyst with highly efficient hydrogen evolution reaction activity in alkaline and acidic media. *Chemical Science, 9*(25), 5640-5645.

Haque, F., Zavabeti, A., Zhang, B. Y., Datta, R. S., Yin, Y., Yi, Z., . . . Syed, N. (2019). Ordered intracrystalline pores in planar molybdenum oxide for enhanced alkaline hydrogen evolution. *Journal of Materials Chemistry A, 7*(1), 257-268.

Hassall, G., & van den Belt, M. (2017). Global sustainability: policy networks for the Sustainable Development Goals. *Policy Quarterly, 13*(1).

Hou, Y., Zhuang, X., & Feng, X. (2017). Recent advances in earth-abundant heterogeneous electrocatalysts for photoelectrochemical water splitting. *Small Methods, 1*(6), 1700090.

Hu, G., Li, J., Liu, P., Zhu, X., Li, X., Ali, R. N., & Xiang, B. (2019). Enhanced electrocatalytic activity of WO3@ NPRGO composite in a hydrogen evolution reaction. *Applied Surface Science, 463*, 275-282.

Hu, J., Zhang, C., Jiang, L., Lin, H., An, Y., Zhou, D., . . . Yang, S. (2017). Nanohybridization of MoS2 with layered double hydroxides efficiently synergizes the hydrogen evolution in alkaline media. *Joule, 1*(2), 383-393.

Hu, J., Zhang, C., Zhang, Y., Yang, B., Qi, Q., Sun, M., . . . Huang, B. (2020). Interface modulation of MoS2/metal oxide heterostructures for efficient hydrogen evolution electrocatalysis. *Small, 16*(28), 2002212.

Hua, B., Li, M., Pang, W., Tang, W., Zhao, S., Jin, Z., . . . Luo, J.-L. (2018). Activating p-blocking centers in perovskite for efficient water splitting. *Chem, 4*(12), 2902-2916.

Hua, B., Li, M., Sun, Y.-F., Zhang, Y.-Q., Yan, N., Chen, J., . . . Luo, J.-L. (2017). A coupling for success: controlled growth of Co/CoOx nanoshoots on perovskite mesoporous nanofibres as high-performance trifunctional electrocatalysts in alkaline condition. *Nano Energy, 32*, 247-254.

Hua, B., Li, M., Zhang, Y. Q., Sun, Y. F., & Luo, J. L. (2017). All-in-one perovskite catalyst: smart controls of architecture and composition toward enhanced oxygen/hydrogen evolution reactions. *Advanced Energy Materials, 7*(20), 1700666.

Huan, T. N., Rousse, G., Zanna, S., Lucas, I. T., Xu, X., Menguy, N., . . . Fontecave, M. (2017). A dendritic nanostructured copper oxide electrocatalyst for the oxygen evolution reaction. *Angewandte Chemie, 129*(17), 4870-4874.

Huang, C., Huang, X., Hu, C., Wang, J., Liu, H., Ma, Z., . . . Ding, W. (2021). Materials Today Energy. *Materials Today, 19*, 100613.

Huang, J., Han, J., Wang, R., Zhang, Y., Wang, X., Zhang, X., . . . Jin, S. (2018). Improving electrocatalysts for oxygen evolution using Ni x Fe3–x O4/Ni hybrid nanostructures formed by solvothermal synthesis. *ACS Energy Letters, 3*(7), 1698-1707.

Huang, L., Chen, D., Luo, G., Lu, Y. R., Chen, C., Zou, Y., . . . Wang, S. (2019). Zirconium-regulation-induced bifunctionality in 3D cobalt–iron oxide nanosheets for overall water splitting. *Advanced Materials, 31*(28), 1901439.

Huang, X., Zheng, H., Lu, G., Wang, P., Xing, L., Wang, J., & Wang, G. (2018). Enhanced water splitting electrocatalysis over MnCo2O4 via introduction of suitable Ce content. *ACS Sustainable Chemistry & Engineering, 7*(1), 1169-1177.

Huang, Z. F., Song, J., Du, Y., Dou, S., Sun, L., Chen, W., . . . Wang, X. (2019). Optimizing interfacial electronic coupling with metal oxide to activate inert polyaniline for superior electrocatalytic hydrogen generation. *Carbon Energy, 1*(1), 77-84.

Ibupoto, Z. H., Tahira, A., Tang, P., Liu, X., Morante, J. R., Fahlman, M., . . . Vomiero, A. (2019). MoSx@ NiO composite nanostructures: an advanced nonprecious catalyst for hydrogen evolution reaction in alkaline media. *Advanced Functional Materials, 29*(7), 1807562.

Islam, M. S., Kim, M., Jin, X., Oh, S. M., Lee, N.-S., Kim, H., & Hwang, S.-J. (2018). Bifunctional 2D superlattice electrocatalysts of layered double hydroxide–transition metal dichalcogenide active for overall water splitting. *ACS Energy Letters, 3*(4), 952-960.

Jain, I. (2009). Hydrogen the fuel for 21st century. *International journal of hydrogen energy, 34*(17), 7368-7378.

Ji, Q., Bi, L., Zhang, J., Cao, H., & Zhao, X. S. (2020). The role of oxygen vacancies of ABO 3 perovskite oxides in the oxygen reduction reaction. *Energy & Environmental Science, 13*(5), 1408-1428.

Jiang, Y., Yang, M., Qu, M., Wang, Y., Yang, Z., Feng, Q., . . . He, R. (2020). In situ confinement of Pt within three-dimensional MoO 2@ porous carbon for efficient hydrogen evolution. *Journal of Materials Chemistry A, 8*(20), 10409-10418.

Jin, W., & Chen, J. (2018). Electrochemically activated Cu 2 O/Co 3 O 4 nanocomposites on defective carbon nanotubes for the hydrogen evolution reaction. *New Journal of Chemistry, 42*(24), 19400-19406.

Kale, M. B., Borse, R. A., Gomaa Abdelkader Mohamed, A., & Wang, Y. (2021). Electrocatalysts by electrodeposition: recent advances, synthesis methods, and applications in energy conversion. *Advanced Functional Materials, 31*(25), 2101313.

Kang, B., Hussain, M. B., Cheng, X., Peng, C., & Wang, Z. (2022). Green electrodeposition synthesis of NiFe-LDH/MoOx/BiVO4 for efficient photoelectrochemical water splitting. *Journal of colloid and interface science, 626*, 146-155.

Kang, H., Youn, J.-S., Oh, I., Manavalan, K., & Jeon, K.-J. (2020). Controllable atomic-ratio of CVD-grown MoS2-MoO2 hybrid catalyst by soft annealing for enhancing hydrogen evolution reaction. *International Journal of Hydrogen Energy, 45*(3), 1399-1408.

Khan, N. A., Rashid, N., Junaid, M., Zafar, M. N., Faheem, M., & Ahmad, I. (2019). NiO/NiS heterostructures: an efficient and stable electrocatalyst for oxygen evolution reaction. *ACS Applied Energy Materials, 2*(5), 3587-3594.

Kim, J. H., Yoo, S., Murphy, R., Chen, Y., Ding, Y., Pei, K., . . . Liu, M. (2021). Promotion of oxygen reduction reaction on a double perovskite electrode by a water-induced surface modification. *Energy & Environmental Science, 14*(3), 1506-1516.

Kim, J. S., Kim, B., Kim, H., & Kang, K. (2018). Recent progress on multimetal oxide catalysts for the oxygen evolution reaction. *Advanced Energy Materials, 8*(11), 1702774.

Kim, Y., Jun, S. E., Lee, G., Nam, S., Jang, H. W., Park, S. H., & Kwon, K. C. (2023). Recent Advances in Water-Splitting Electrocatalysts Based on Electrodeposition. *Materials, 16*(8), 3044.

Kuang, M., Han, P., Wang, Q., Li, J., & Zheng, G. (2016). CuCo hybrid oxides as bifunctional electrocatalyst for efficient water splitting. *Advanced Functional Materials, 26*(46), 8555-8561.

Kudo, A., & Miseki, Y. (2009). Heterogeneous photocatalyst materials for water splitting. *Chemical Society Reviews, 38*(1), 253-278.

Lee, W., Muhammad, S., Sergey, C., Lee, H., Yoon, J., Kang, Y. M., & Yoon, W. S. (2020). Advances in the cathode materials for lithium rechargeable batteries. *Angewandte Chemie International Edition, 59*(7), 2578-2605.

Lewis, N. S., & Nocera, D. G. (2006). Powering the planet: Chemical challenges in solar energy utilization. *Proceedings of the National Academy of Sciences, 103*(43), 15729-15735.

Li, C., & Baek, J.-B. (2019). Recent advances in noble metal (Pt, Ru, and Ir)-based electrocatalysts for efficient hydrogen evolution reaction. *ACS omega, 5*(1), 31-40.

Li, C., Zhao, S., Zhu, K., Wang, B., Wang, E., Luo, Y., . . . Fan, S. (2020). Flexible and free-standing hetero-electrocatalyst of high-valence-cation doped MoS 2/MoO 2/CNT foam with synergistically enhanced hydrogen evolution reaction catalytic activity. *Journal of Materials Chemistry A, 8*(30), 14944-14954.

Li, D. J., Maiti, U. N., Lim, J., Choi, D. S., Lee, W. J., Oh, Y., . . . Kim, S. O. (2014). Molybdenum sulfide/N-doped CNT forest hybrid catalysts for high-performance hydrogen evolution reaction. *Nano letters, 14*(3), 1228-1233.

Li, H., Chen, S., Lin, H., Xu, X., Yang, H., Song, L., & Wang, X. (2017). Nickel diselenide ultrathin nanowires decorated with amorphous nickel oxide nanoparticles for enhanced water splitting electrocatalysis. *Small, 13*(37), 1701487.

Li, S., Sirisomboonchai, S., Yoshida, A., An, X., Hao, X., Abudula, A., & Guan, G. (2018). Bifunctional CoNi/CoFe 2 O 4/Ni foam electrodes for efficient overall water splitting at a high current density. *Journal of Materials Chemistry A, 6*(39), 19221-19230.

Li, S., Wang, J., Wang, J., Chen, C., Guo, Z., Cai, N., . . . Yu, F. (2021). CoFe2O4 nanoparticles@ N-doped carbon coupled with N-doped graphene toward efficient electrochemical water oxidation. *Colloids and Surfaces A: Physicochemical and Engineering Aspects, 626*, 126898.

Li, T., Niu, K., Yang, M., Shrestha, N. K., Gao, Z., & Song, Y.-Y. (2017). Ultrathin CoS2 shells anchored on Co3O4 nanoneedles for efficient hydrogen evolution electrocatalysis. *Journal of power sources, 356*, 89-96.

Li, X., Hao, X., Abudula, A., & Guan, G. (2016). Nanostructured catalysts for electrochemical water splitting: current state and prospects. *Journal of Materials Chemistry A, 4*(31), 11973-12000.

Li, X., Liu, P. F., Zhang, L., Zu, M. Y., Yang, Y. X., & Yang, H. G. (2016). Enhancing alkaline hydrogen evolution reaction activity through Ni–Mn 3 O 4 nanocomposites. *Chemical Communications, 52*(69), 10566-10569.

Li, X., Wang, Y., Wang, J., Da, Y., Zhang, J., Li, L., . . . Hu, W. (2020). Sequential electrodeposition of bifunctional catalytically active structures in MoO3/Ni–NiO composite electrocatalysts for selective hydrogen and oxygen evolution. *Advanced Materials, 32*(39), 2003414.

Li, X., Zhang, R., Luo, Y., Liu, Q., Lu, S., Chen, G., . . . Sun, X. (2020). A cobalt–phosphorus nanoparticle decorated N-doped carbon nanosheet array for efficient and durable hydrogen evolution at alkaline pH. *Sustainable Energy & Fuels, 4*(8), 3884-3887.

Li, Y., Sun, Y., Qin, Y., Zhang, W., Wang, L., Luo, M., . . . Guo, S. (2020). Recent advances on water-splitting electrocatalysis mediated by noble-metal-based nanostructured materials. *Advanced Energy Materials, 10*(11), 1903120.

Li, Y. H., Liu, P. F., Pan, L. F., Wang, H. F., Yang, Z. Z., Zheng, L. R., . . . Yang, H. G. (2015). Local atomic structure modulations activate metal oxide as electrocatalyst for hydrogen evolution in acidic water. *Nature communications, 6*(1), 1-7.

Liu, D., Zhang, C., Yu, Y., Shi, Y., Yu, Y., Niu, Z., & Zhang, B. (2018). Hydrogen evolution activity enhancement by tuning the oxygen vacancies in self-supported mesoporous spinel oxide nanowire arrays. *Nano Research, 11*, 603-613.

Liu, J., Zheng, Y., Jiao, Y., Wang, Z., Lu, Z., Vasileff, A., & Qiao, S. Z. (2018). NiO as a bifunctional promoter for RuO2 toward superior overall water splitting. *Small, 14*(16), 1704073.

Liu, Q., Tang, C., Lu, S., Zou, Z., Gu, S., Zhang, Y., & Li, C. M. (2018). Rationally tuning the atomic ratio of electrodeposited NiP for greatly enhanced hydrogen evolution in alkaline media. *Chemical Communications, 54*(87), 12408-12411.

Liu, S.-Q., Wen, H.-R., Zhu, Y.-W., Fu, X.-Z., Sun, R., & Wong, C.-P. (2018). Amorphous Ni (OH) 2 encounter with crystalline CuS in hollow spheres: a mesoporous nano-

shelled heterostructure for hydrogen evolution electrocatalysis. *Nano Energy, 44*, 7-14.

Liu, W., Cao, D., & Cheng, D. (2021). Review on synthesis and catalytic coupling mechanism of highly active electrocatalysts for water splitting. *Energy Technology, 9*(2), 2000855.

Lu, K., Liu, Y., Lin, F., Cordova, I. A., Gao, S., Li, B., . . . Coliz, D. (2020). Li x NiO/Ni heterostructure with strong basic lattice oxygen enables electrocatalytic hydrogen evolution with Pt-like activity. *Journal of the American Chemical Society, 142*(29), 12613-12619.

Lu, S.-S., Zhang, L.-M., Fan, K., Xie, J.-Y., Shang, X., Zhang, J.-Q., . . . Chai, Y.-M. (2019). In situ formation of ultrathin C3N4 layers on metallic WO2 nanorods for efficient hydrogen evolution. *Applied Surface Science, 487*, 945-950.

Luo, Z., Miao, R., Huan, T. D., Mosa, I. M., Poyraz, A. S., Zhong, W., . . . He, J. (2016). Mesoporous MoO3–x material as an efficient electrocatalyst for hydrogen evolution reactions. *Advanced Energy Materials, 6*(16), 1600528.

Lv, C., Xu, S., Yang, Q., Huang, Z., & Zhang, C. (2019). Promoting electrocatalytic activity of cobalt cyclotetraphosphate in full water splitting by titanium-oxide-accelerated surface reconstruction. *Journal of Materials Chemistry A, 7*(20), 12457-12467.

Manoharan, R., & Goodenough, J. (1990). Hydrogen Evolution on Sr x NbO3− δ (0.7≤ x≤ 0.95) in Acid. *Journal of The Electrochemical Society, 137*(3), 910.

McCrory, C. C., Jung, S., Peters, J. C., & Jaramillo, T. F. (2013). Benchmarking heterogeneous electrocatalysts for the oxygen evolution reaction. *Journal of the American Chemical Society, 135*(45), 16977-16987.

Mettenbörger, A., Gönüllü, Y., Fischer, T., Heisig, T., Sasinska, A., Maccato, C., . . . Mayrhofer, L. (2016). Interfacial insight in multi-junction metal oxide photoanodes for water-splitting applications. *Nano Energy, 19*, 415-427.

Mishra, A., Basu, S., Shetti, N. P., Reddy, K. R., & Aminabhavi, T. M. (2019). Photocatalysis of graphene and carbon nitride-based functional carbon quantum dots. In *Nanoscale materials in water purification* (pp. 759-781): Elsevier.

Morales-Guio, C. G., Stern, L.-A., & Hu, X. (2014). Nanostructured hydrotreating catalysts for electrochemical hydrogen evolution. *Chemical Society Reviews, 43*(18), 6555-6569.

Murthy, A. P., Theerthagiri, J., Premnath, K., Madhavan, J., & Murugan, K. (2017). Single-step electrodeposited molybdenum incorporated nickel sulfide thin films from low-cost precursors as highly efficient hydrogen evolution electrocatalysts in acid medium. *The Journal of Physical Chemistry C, 121*(21), 11108-11116.

Muthurasu, A., Maruthapandian, V., & Kim, H. Y. (2019). Metal-organic framework derived Co3O4/MoS2 heterostructure for efficient bifunctional electrocatalysts for oxygen evolution reaction and hydrogen evolution reaction. *Applied Catalysis B: Environmental, 248*, 202-210.

Ng, K.-L., Kok, K.-Y., & Ong, B.-H. (2017). Facile synthesis of self-assembled cobalt oxide supported on iron oxide as the novel electrocatalyst for enhanced electrochemical water electrolysis. *ACS Applied Nano Materials, 1*(1), 401-409.

Nikolaidis, P., & Poullikkas, A. (2017). A comparative overview of hydrogen production processes. *Renewable and sustainable energy reviews, 67*, 597-611.

Nwogu, N. C., Alkali, A., & Gobina, E. (2015). Hydrogen transport through dense and porous membranes for fuel cell applications.

Oh, N. K., Kim, C., Lee, J., Kwon, O., Choi, Y., Jung, G. Y., . . . Park, H. (2019). In-situ local phase-transitioned MoSe2 in La0. 5Sr0. 5CoO3-δ heterostructure and stable overall water electrolysis over 1000 hours. *Nature Communications, 10*(1), 1723.

Ou, G., Fan, P., Zhang, H., Huang, K., Yang, C., Yu, W., . . . Li, Y. (2017). Large-scale hierarchical oxide nanostructures for high-performance electrocatalytic water splitting. *Nano Energy, 35*, 207-214.

Panda, C., Menezes, P. W., Zheng, M., Orthmann, S., & Driess, M. (2019). In situ formation of nanostructured core–shell Cu3N–CuO to promote alkaline water electrolysis. *ACS Energy Letters, 4*(3), 747-754.

Pant, K., & Gupta, R. B. (2008). Fundamentals and use of hydrogen as a fuel. In *Hydrogen Fuel* (pp. 15-44): CRC Press.

Park, H. W., Lee, D. U., Park, M. G., Ahmed, R., Seo, M. H., Nazar, L. F., & Chen, Z. (2015). Perovskite–nitrogen-doped carbon nanotube composite as bifunctional catalysts for rechargeable lithium–air batteries. *ChemSusChem, 8*(6), 1058-1065.

Pawar, S. M., Pawar, B. S., Babar, P. T., Ahmed, A. T. A., Chavan, H. S., Jo, Y., . . . Inamdar, A. I. (2019). Nanoporous CuCo2O4 nanosheets as a highly efficient bifunctional electrode for supercapacitors and water oxidation catalysis. *Applied Surface Science, 470*, 360-367.

Peng, S., Gong, F., Li, L., Yu, D., Ji, D., Zhang, T., . . . Du, Y. (2018). Necklace-like multishelled hollow spinel oxides with oxygen vacancies for efficient water electrolysis. *Journal of the American Chemical Society, 140*(42), 13644-13653.

Peng, Z., Jia, D., Al-Enizi, A. M., Elzatahry, A. A., & Zheng, G. (2015). From water oxidation to reduction: homologous Ni–Co based nanowires as complementary water splitting electrocatalysts. *Advanced Energy Materials, 5*(9), 1402031.

Phuruangrat, A., Ham, D. J., Hong, S. J., Thongtem, S., & Lee, J. S. (2010). Synthesis of hexagonal WO 3 nanowires by microwave-assisted hydrothermal method and their electrocatalytic activities for hydrogen evolution reaction. *Journal of Materials Chemistry, 20*(9), 1683-1690.

Popczun, E. J., McKone, J. R., Read, C. G., Biacchi, A. J., Wiltrout, A. M., Lewis, N. S., & Schaak, R. E. (2013). Nanostructured nickel phosphide as an electrocatalyst for the hydrogen evolution reaction. *Journal of the American Chemical Society, 135*(25), 9267-9270.

Ragupathi, V., Raja, M. A., Panigrahi, P., & Subramaniam, N. G. (2020). CuO/g-C3N4 nanocomposite as promising photocatalyst for photoelectrochemical water splitting. *Optik, 208*, 164569.

Rincon, P. (2021). Climate change. *Global carbon dioxide emissions*. Retrieved from https://www.bbc.com/news/science-environment-59148520

Roger, I., Shipman, M. A., & Symes, M. D. (2017). Earth-abundant catalysts for electrochemical and photoelectrochemical water splitting. *Nature Reviews Chemistry, 1*(1), 1-13.

Roy, A., Jadhav, H. S., Cho, M., & Seo, J. G. (2019). Electrochemical deposition of self-supported bifunctional copper oxide electrocatalyst for methanol oxidation and oxygen evolution reaction. *Journal of Industrial and Engineering Chemistry, 76*, 515-523.

Sabir, A. S., Pervaiz, E., Khosa, R., & Sohail, U. (2023). An inclusive review and perspective on Cu-based materials for electrochemical water splitting. *RSC Advances, 13*(8), 4963-4993.

Sahoo, P. K., Bisoi, S. R., Huang, Y.-J., Tsai, D.-S., & Lee, C.-P. (2021). 2D-layered non-precious electrocatalysts for hydrogen evolution reaction: fundamentals to applications. *Catalysts, 11*(6), 689.

Scholz, W. H. (1993). Processes for industrial production of hydrogen and associated environmental effects. *Gas separation & purification, 7*(3), 131-139.

Seh, Z. W., Kibsgaard, J., Dickens, C. F., Chorkendorff, I., Nørskov, J. K., & Jaramillo, T. F. (2017). Combining theory and experiment in electrocatalysis: Insights into materials design. *Science, 355*(6321), eaad4998.

Shang, X., Chi, J.-Q., Lu, S.-S., Dong, B., Liu, Z.-Z., Yan, K.-L., . . . Liu, C.-G. (2017). Hierarchically three-level Ni3 (VO4) 2@ NiCo2O4 nanostructure based on nickel foam towards highly efficient alkaline hydrogen evolution. *Electrochimica Acta*, *256*, 100-109.

Shang, X., Rao, Y., Lu, S.-S., Dong, B., Zhang, L.-M., Liu, X.-H., . . . Liu, C.-G. (2017). Novel WS2/WO3 heterostructured nanosheets as efficient electrocatalyst for hydrogen evolution reaction. *Materials Chemistry and Physics*, *197*, 123-128.

Sharma, L., Kumar, P., & Halder, A. (2019). Phase and vacancy modulation in tungsten oxide: electrochemical hydrogen evolution. *ChemElectroChem*, *6*(13), 3420-3428.

Shit, S., Bolar, S., Murmu, N. C., & Kuila, T. (2021). Tailoring the bifunctional electrocatalytic activity of electrodeposited molybdenum sulfide/iron oxide heterostructure to achieve excellent overall water splitting. *Chemical Engineering Journal*, *417*, 129333.

Shu, C., Kang, S., Jin, Y., Yue, X., & Shen, P. K. (2017). Bifunctional porous non-precious metal WO 2 hexahedral networks as an electrocatalyst for full water splitting. *Journal of Materials Chemistry A*, *5*(20), 9655-9660.

Si, C., Zhang, W., Lu, Q., Guo, E., Yang, Z., Chen, J., . . . Luo, J. (2022). Recent Advances in Perovskite Catalysts for Efficient Overall Water Splitting. *Catalysts*, *12*(6), 601.

Sinha, S., Kim, H., & Robertson, A. (2021). Materials Today Advances.

Sivakumar, P., Vikraman, D., Raj, C. J., Hussain, S., Park, J., Kim, H. S., & Jung, H. (2021). Hierarchical NiCo/NiO/NiCo2O4 composite formation by solvothermal reaction as a potential electrode material for hydrogen evolutions and asymmetric supercapacitors. *International Journal of Energy Research*, *45*(14), 19947-19961.

Solomon, G., Mazzaro, R., You, S., Natile, M. M., Morandi, V., Concina, I., & Vomiero, A. (2019). Ag2S/MoS2 nanocomposites anchored on reduced graphene oxide: Fast interfacial charge transfer for hydrogen evolution reaction. *ACS applied materials & interfaces*, *11*(25), 22380-22389.

Song, C., Zhao, Z., Sun, X., Zhou, Y., Wang, Y., & Wang, D. (2019). In situ growth of Ag nanodots decorated Cu2O porous nanobelts networks on copper foam for efficient HER electrocatalysis. *Small*, *15*(29), 1804268.

Subbaraman, R., Tripkovic, D., Strmcnik, D., Chang, K.-C., Uchimura, M., Paulikas, A. P., . . . Markovic, N. M. (2011). Enhancing hydrogen evolution activity in water splitting by tailoring Li+-Ni (OH) 2-Pt interfaces. *Science*, *334*(6060), 1256-1260.

Suryanto, B. H., Wang, Y., Hocking, R. K., Adamson, W., & Zhao, C. (2019). Overall electrochemical splitting of water at the heterogeneous interface of nickel and iron oxide. *Nature communications*, *10*(1), 5599.

Swaminathan, J., Subbiah, R., & Singaram, V. (2016). Defect-Rich Metallic Titania (TiO1. 23) • An Efficient Hydrogen Evolution Catalyst for Electrochemical Water Splitting. *ACS Catalysis*, *6*(4), 2222-2229.

Tahir, M., Pan, L., Zhang, R., Wang, Y.-C., Shen, G., Aslam, I., . . . Wang, L. (2017). High-valence-state NiO/Co3O4 nanoparticles on nitrogen-doped carbon for oxygen evolution at low overpotential. *ACS Energy Letters*, *2*(9), 2177-2182.

Tahira, A., Ibupoto, Z. H., Willander, M., & Nur, O. (2019). Advanced Co3O4–CuO nano-composite based electrocatalyst for efficient hydrogen evolution reaction in alkaline media. *International Journal of Hydrogen Energy*, *44*(48), 26148-26157.

Theerthagiri, J., Senthil, R., Buraidah, M., Madhavan, J., Arof, A., & Ashokkumar, M. (2016). One-step electrochemical deposition of Ni 1− x Mo x S ternary sulfides as an efficient counter electrode for dye-sensitized solar cells. *Journal of Materials Chemistry A*, *4*(41), 16119-16127.

Thiele, D., Colmenarejo, E. L.-C., Grobéty, B., & Züttel, A. (2009). Synthesis of carbon nanotubes on La0. 6Sr0. 4CoO3 as substrate. *Diamond and related materials*, *18*(1), 34-38.

Tong, J., Li, Q., Li, W., Wang, W., Ma, W., Su, B., & Bo, L. (2017). MoS2 thin sheet growing on nitrogen self-doped mesoporous graphic carbon derived from ZIF-8 with highly electrocatalytic performance on hydrogen evolution reaction. *ACS Sustainable Chemistry & Engineering, 5*(11), 10240-10247.

Vadakkekara, R., Illathvalappil, R., & Kurungot, S. (2018). Layered TiO2 Nanosheet-Supported NiCo2O4 Nanoparticles as Bifunctional Electrocatalyst for Overall Water Splitting. *ChemElectroChem, 5*(24), 4000-4007.

Veziro, T., & Barbir, F. (1992). Hydrogen: the wonder fuel. *International Journal of Hydrogen Energy, 17*(6), 391-404.

Wang, H., Fu, W., Yang, X., Huang, Z., Li, J., Zhang, H., & Wang, Y. (2020). Recent advancements in heterostructured interface engineering for hydrogen evolution reaction electrocatalysis. *Journal of Materials Chemistry A, 8*(15), 6926-6956.

Wang, J., Yue, X., Yang, Y., Sirisomboonchai, S., Wang, P., Ma, X., . . . Guan, G. (2020). Earth-abundant transition-metal-based bifunctional catalysts for overall electrochemical water splitting: A review. *Journal of Alloys and Compounds, 819*, 153346.

Wang, P., Luo, Y., Zhang, G., Chen, Z., Ranganathan, H., Sun, S., & Shi, Z. (2022). Interface engineering of NixSy@ MnOxHy nanorods to efficiently enhance overall-water-splitting activity and stability. *Nano-Micro Letters, 14*(1), 120.

Wang, W., Xu, M., Xu, X., Zhou, W., & Shao, Z. (2020). Perovskite oxide based electrodes for high-performance photoelectrochemical water splitting. *Angewandte Chemie International Edition, 59*(1), 136-152.

Wang, X., Gan, X., Hu, T., Fujisawa, K., Lei, Y., Lin, Z., . . . Terrones, M. (2017). Noble-Metal-Free Hybrid Membranes for Highly Efficient Hydrogen Evolution. *Advanced Materials, 29*(4), 1603617.

Wang, X., He, Y., Han, X., Zhao, J., Li, L., Zhang, J., . . . Hu, W. (2022). Engineering cobalt sulfide/oxide heterostructure with atomically mixed interfaces for synergistic electrocatalytic water splitting. *Nano Research, 15*(2), 1246-1253.

Wang, X., Zheng, Y., Sheng, W., Xu, Z. J., Jaroniec, M., & Qiao, S.-Z. (2020). Strategies for design of electrocatalysts for hydrogen evolution under alkaline conditions. *Materials Today, 36*, 125-138.

Wang, Y., Wang, T., Zhang, R., Liu, Q., Luo, Y., Cui, G., . . . Sun, X. (2020). CuO@ CoFe layered double hydroxide core–shell heterostructure as an efficient water oxidation electrocatalyst under mild alkaline conditions. *Inorganic Chemistry, 59*(14), 9491-9495.

Wang, Y., Yan, D., El Hankari, S., Zou, Y., & Wang, S. (2018). Recent progress on layered double hydroxides and their derivatives for electrocatalytic water splitting. *Advanced Science, 5*(8), 1800064.

Wang, Y., Yan, L., Dastafkan, K., Zhao, C., Zhao, X., Xue, Y., . . . Zhai, Q. (2021). Lattice matching growth of conductive hierarchical porous MOF/LDH heteronanotube arrays for highly efficient water oxidation. *Advanced Materials, 33*(8), 2006351.

Wang, Z., Wang, H., Ji, S., Wang, X., Pollet, B. G., & Wang, R. (2020). Multidimensional regulation of Ni3S2@ Co (OH) 2 catalyst with high performance for wind energy electrolytic water. *Journal of Power Sources, 446*, 227348.

Wei, X., Song, Y., Zhang, Q., Hu, B., Cen, Y., Gong, J., . . . Wan, Q. (2022). Metal-organic Frameworks Derived Electrocatalysts for Energy Conversion Reaction. In *Electrochemical Transformation of Renewable Compounds* (pp. 38-75): CRC Press.

Wei, X., Zhang, Y., He, H., Gao, D., Hu, J., Peng, H., . . . Xiao, P. (2019). Carbon-incorporated NiO/Co 3 O 4 concave surface microcubes derived from a MOF precursor for overall water splitting. *Chemical Communications, 55*(46), 6515-6518.

Worku, A. K., Ayele, D. W., Habtu, N. G., & Yemata, T. A. (2021). Engineering Co3O4/MnO2 nanocomposite materials for oxygen reduction electrocatalysis. *Heliyon, 7*(9), e08076.

Wu, H., Li, S., Lu, X., Toe, C. Y., Chung, H. Y., Tang, Y., . . . Ng, Y. H. (2018). Pulsed Electrodeposition of Co3O4 Nanocrystals on One-Dimensional ZnO Scaffolds for Enhanced Electrochemical Water Oxidation. *ChemPlusChem, 83*(10), 934-940.

Wu, J., Li, Z., Huang, X., & Lin, Y. (2013). Porous Co3O4/NiO core/shell nanowire array with enhanced catalytic activity for methanol electro-oxidation. *Journal of power sources, 224*, 1-5.

Wu, R., Zhang, J., Shi, Y., Liu, D., & Zhang, B. (2015). Metallic WO2–carbon mesoporous nanowires as highly efficient electrocatalysts for hydrogen evolution reaction. *Journal of the American Chemical Society, 137*(22), 6983-6986.

Wu, Y., Lian, J., Wang, Y., Sun, J., He, Z., & Gu, Z. (2021). Potentiostatic electrodeposition of self-supported NiS electrocatalyst supported on Ni foam for efficient hydrogen evolution. *Materials & Design, 198*, 109316.

Wu, Y., Yi, Y., Sun, Z., Sun, H., Guo, T., Zhang, M., . . . Sun, J. (2020). Bimetallic Fe-Ni phosphide carved nanoframes toward efficient overall water splitting and potassium-ion storage. *Chemical engineering journal, 390*, 124515.

Xia, X., Wang, C., Liu, L., Du, Y., & Ye, W. (2018). Synthesis of yolk–shell spheres based on molybdenum diselenide-encapsulated molybdenum oxide for efficient electrocatalytic hydrogen evolution. *Sustainable Energy & Fuels, 2*(2), 444-454.

Xiao, X., Wang, X., Jiang, X., Song, S., Huang, D., Yu, L., . . . Shen, Y. (2020). In situ growth of Ru nanoparticles on (Fe, Ni)(OH) 2 to boost hydrogen evolution activity at high current density in alkaline media. *Small Methods, 4*(6), 1900796.

Xie, C., Chen, W., Du, S., Yan, D., Zhang, Y., Chen, J., . . . Wang, S. (2020). In-situ phase transition of WO3 boosting electron and hydrogen transfer for enhancing hydrogen evolution on Pt. *Nano Energy, 71*, 104653.

Xie, J., Zhang, X., Zhang, H., Zhang, J., Li, S., Wang, R., . . . Xie, Y. (2017). Intralayered Ostwald Ripening to Ultrathin Nanomesh Catalyst with Robust Oxygen-Evolving Performance. *Advanced Materials (Deerfield Beach, Fla.), 29*(10).

Xing, Z., Han, C., Wang, D., Li, Q., & Yang, X. (2017). Ultrafine Pt nanoparticle-decorated Co (OH) 2 nanosheet arrays with enhanced catalytic activity toward hydrogen evolution. *ACS Catalysis, 7*(10), 7131-7135.

Xu, X., Chen, Y., Zhou, W., Zhu, Z., Su, C., Liu, M., & Shao, Z. (2016). A perovskite electrocatalyst for efficient hydrogen evolution reaction. *Advanced Materials, 28*(30), 6442-6448.

Yang, G., Jiao, Y., Yan, H., Xie, Y., Wu, A., Dong, X., . . . Fu, H. (2020). Interfacial engineering of MoO2-FeP heterojunction for highly efficient hydrogen evolution coupled with biomass electrooxidation. *Advanced Materials, 32*(17), 2000455.

Yang, L., Liu, R., & Jiao, L. (2020). Electronic redistribution: construction and modulation of interface engineering on CoP for enhancing overall water splitting. *Advanced Functional Materials, 30*(14), 1909618.

Yang, L., Zhou, H., Qin, X., Guo, X., Cui, G., Asiri, A. M., & Sun, X. (2018). Cathodic electrochemical activation of Co 3 O 4 nanoarrays: a smart strategy to significantly boost the hydrogen evolution activity. *Chemical Communications, 54*(17), 2150-2153.

Yang, M. Q., Wang, J., Wu, H., & Ho, G. W. (2018). Noble metal-free nanocatalysts with vacancies for electrochemical water splitting. *Small, 14*(15), 1703323.

Yang, Y., Wang, S., Jiang, C., Lu, Q., Tang, Z., & Wang, X. (2016). Controlled synthesis of hollow Co–Mo mixed oxide nanostructures and their electrocatalytic and lithium storage properties. *Chemistry of Materials, 28*(7), 2417-2423.

Yang, Y., Zhu, C., Zhang, Y., Xie, Y., Lv, L., Chen, W., . . . Hu, Z. (2021). Construction of Co3O4/Fe2O3 nanosheets on nickel foam as efficient electrocatalyst for the oxygen evolution reaction. *Journal of Physics and Chemistry of Solids, 148*, 109680.

Ye, L., & Wen, Z. (2018). Self-supported three-dimensional Cu/Cu 2 O–CuO/rGO nanowire array electrodes for an efficient hydrogen evolution reaction. *Chemical Communications, 54*(49), 6388-6391.

Yin, H., Zhao, S., Zhao, K., Muqsit, A., Tang, H., Chang, L., . . . Tang, Z. (2015). Ultrathin platinum nanowires grown on single-layered nickel hydroxide with high hydrogen evolution activity. *Nature communications, 6*(1), 6430.

Yu, L., Zhou, H., Sun, J., Qin, F., Yu, F., Bao, J., . . . Ren, Z. (2017). Cu nanowires shelled with NiFe layered double hydroxide nanosheets as bifunctional electrocatalysts for overall water splitting. *Energy & Environmental Science, 10*(8), 1820-1827.

Yu, X., Wang, X., Wu, S., Bai, J., He, P., Qin, F., . . . Ren, L. (2023). Insight into the effect of P on Co3O4/NiO heterostructure for efficient alkaline oxygen evolution reaction. *Journal of Alloys and Compounds, 946*, 169383.

Yu, X., Yu, Z.-Y., Zhang, X.-L., Li, P., Sun, B., Gao, X., . . . Gao, M.-R. (2020). Highly disordered cobalt oxide nanostructure induced by sulfur incorporation for efficient overall water splitting. *Nano Energy, 71*, 104652.

Zeng, L., Zhou, K., Yang, L., Du, G., Liu, L., & Zhou, W. (2018). General approach of in situ etching and doping to synthesize a nickel-doped M x O y (M= Co, Mn, Fe) nanosheets array on nickel foam as large-sized electrodes for overall water splitting. *ACS Applied Energy Materials, 1*(11), 6279-6287.

Zhang, B., Liu, J., Wang, J., Ruan, Y., Ji, X., Xu, K., . . . Jiang, J. (2017). Interface engineering: the Ni (OH) 2/MoS2 heterostructure for highly efficient alkaline hydrogen evolution. *Nano Energy, 37*, 74-80.

Zhang, J., Cui, R., Gao, C., Bian, L., Pu, Y., Zhu, X., . . . Huang, W. (2019). Cation-modulated HER and OER activities of hierarchical VOOH hollow architectures for high-efficiency and stable overall water splitting. *Small, 15*(47), 1904688.

Zhang, J., Wang, T., Liu, P., Liao, Z., Liu, S., Zhuang, X., . . . Feng, X. (2017). Efficient hydrogen production on MoNi4 electrocatalysts with fast water dissociation kinetics. *Nature communications, 8*(1), 15437.

Zhang, L., Amiinu, I. S., Ren, X., Liu, Z., Du, G., Asiri, A. M., . . . Sun, X. (2017). Surface modification of a NiS2 nanoarray with Ni (OH) 2 toward superior water reduction electrocatalysis in alkaline media. *Inorganic Chemistry, 56*(22), 13651-13654.

Zhang, L., Liu, P. F., Li, Y. H., Zu, M. Y., Li, X., Jiang, Z., . . . Yang, H. G. (2018). N-Modified NiO Surface for Superior Alkaline Hydrogen Evolution. *ChemSusChem, 11*(6), 1020-1024.

Zhang, N., Gao, Y., Mei, Y., Liu, J., Song, W., & Yu, Y. (2019). CuS–Ni 3 S 2 grown in situ from three-dimensional porous bimetallic foam for efficient oxygen evolution. *Inorganic Chemistry Frontiers, 6*(1), 293-302.

Zhang, W., Li, H., Firby, C. J., Al-Hussein, M., & Elezzabi, A. Y. (2019). Oxygen-vacancy-tunable electrochemical properties of electrodeposited molybdenum oxide films. *ACS applied materials & interfaces, 11*(22), 20378-20385.

Zhang, W., Zheng, J., Gu, X., Tang, B., Li, J., & Wang, X. (2019). Facile synthesis, characterization and DFT studies of a nanostructured nickel–molybdenum–phosphorous planar electrode as an active electrocatalyst for the hydrogen evolution reaction. *Nanoscale, 11*(19), 9353-9361.

Zhao, H., Meng, Y., Yu, H., Li, Z., & Liu, Z. (2022). 1D/2D Co3O4/NiO composite film for high electrochromic performance. *Ceramics International, 48*(21), 32205-32212.

Zhao, J., Li, W., Wu, S., Xu, F., Du, J., Li, J., . . . Zhao, Y. (2020). Strong interfacial interaction significantly improving hydrogen evolution reaction performances of MoS2/Ti4O7 composite catalysts. *Electrochimica acta, 337*, 135850.

Zhao, S., Wang, L., & Fu, L. (2019). Precise vapor-phase synthesis of two-dimensional atomic single crystals. *Iscience, 20*, 527-545.

Zheng, S., Guo, X., Xue, H., Pan, K., Liu, C., & Pang, H. (2019). Facile one-pot generation of metal oxide/hydroxide@ metal–organic framework composites: highly efficient bifunctional electrocatalysts for overall water splitting. *Chemical Communications*, *55*(73), 10904-10907.

Zheng, T., Sang, W., He, Z., Wei, Q., Chen, B., Li, H., . . . Pan, B. (2017). Conductive tungsten oxide nanosheets for highly efficient hydrogen evolution. *Nano letters*, *17*(12), 7968-7973.

Zhong, C., Han, Z., Wang, T., Wang, Q., Shen, Z., Zhou, Q., . . . Li, S. (2020). Aliovalent fluorine doping and anodization-induced amorphization enable bifunctional catalysts for efficient water splitting. *Journal of Materials Chemistry A*, *8*(21), 10831-10838.

Zhong, X., Zhang, L., Tang, J., Chai, J., Xu, J., Cao, L., . . . Wang, S. (2017). Efficient coupling of a hierarchical V 2 O 5@ Ni 3 S 2 hybrid nanoarray for pseudocapacitors and hydrogen production. *Journal of Materials Chemistry A*, *5*(34), 17954-17962.

Zhou, Y., Li, T., Xi, S., He, C., Yang, X., & Wu, H. (2018). One-step synthesis of self-standing Ni3S2/Ni2P heteronanorods on nickel foam for efficient electrocatalytic hydrogen evolution over a wide pH range. *ChemCatChem*, *10*(23), 5487-5495.

Zhou, Y., Sun, S., Wei, C., Sun, Y., Xi, P., Feng, Z., & Xu, Z. J. (2019). Significance of engineering the octahedral units to promote the oxygen evolution reaction of spinel oxides. *Advanced Materials*, *31*(41), 1902509.

Zhou, Y., Wang, Z., Pan, Z., Liu, L., Xi, J., Luo, X., & Shen, Y. (2019). Exceptional performance of hierarchical Ni–Fe (hydr) oxide@ NiCu electrocatalysts for water splitting. *Advanced Materials*, *31*(8), 1806769.

Zhu, J., Hu, L., Zhao, P., Lee, L. Y. S., & Wong, K.-Y. (2019). Recent advances in electrocatalytic hydrogen evolution using nanoparticles. *Chemical reviews*, *120*(2), 851-918.

Zhu, K., Shi, F., Zhu, X., & Yang, W. (2020). The roles of oxygen vacancies in electrocatalytic oxygen evolution reaction. *Nano Energy*, *73*, 104761.

Zhu, Y., Lin, Q., Zhong, Y., Tahini, H. A., Shao, Z., & Wang, H. (2020). Metal oxide-based materials as an emerging family of hydrogen evolution electrocatalysts. *Energy & Environmental Science*, *13*(10), 3361-3392.

Zhu, Y., Zhou, W., Zhong, Y., Bu, Y., Chen, X., Zhong, Q., . . . Shao, Z. (2017). A perovskite nanorod as bifunctional electrocatalyst for overall water splitting. *Advanced Energy Materials*, *7*(8), 1602122.

Zong, R., Fang, Y., Zhu, C., Zhang, X., Wu, L., Hou, X., . . . Shao, J. (2021). Surface defect engineering on perovskite oxides as efficient bifunctional electrocatalysts for water splitting. *ACS Applied Materials & Interfaces*, *13*(36), 42852-42860.

Zong, Z., Qian, Z., Tang, Z., Liu, Z., Tian, Y., & Wang, S. (2019). Hydrogen evolution and oxygen reduction reactions catalyzed by core-shelled Fe@ Ru nanoparticles embedded in porous dodecahedron carbon. *Journal of Alloys and Compounds*, *784*, 447-455.

Zou, X., & Zhang, Y. (2015). Noble metal-free hydrogen evolution catalysts for water splitting. *Chemical Society Reviews*, *44*(15), 5148-5180.

Research Fund Acknowledgement

This research thesis was funded by Adama Science and Technology University under the grant number of ASTU/SM-R/747/23, Adama, Ethiopia.